Copy No 1

THE PHYSICAL PROPERTIES OF A GASPE SKARN

by

Tso-min Shih, B. Sc. (Mining)

A thesis submitted to the Faculty of Graduate Studies and Research in partial fulfillment of the requirements for the degree of Master of Engineering

Department of Mining Engineering
and Applied Geophysics
McGill University
Montreal, Que.

Feb. 10, 1965

CONTENTS

	Page
ACKNOWLEDGMENT	i
I. ABSTRACT	1
II. INTRODUCTION.	2
(1) Objective	2
(2) Treatment of Data	3
III. THE GASPE COPPER MINES LIMITED.	4
(1) Location of Mines	4
(2) Geology of Mines.	4
(3) Location of Specimen.	8
(4) Petrographic Description of Specimen. . .	8
IV. COMPRESSIVE TESTS	11
(1) Selection and Preparation of Specimens. .	11
(1-1) Uniaxial tests.	11
(1-2) Deformation tests	12
(1-3) Triaxial Tests.	14
(2) Testing Apparatus and Loading Procedure .	17
(2-1) Correction curve for 200,000 lbs. pressure gauge of Louis Small Compression Tester.	17
(2-2) Uniaxial test	17
(2-3) Deformation test.	20
(2-4) Triaxial tests.	21
(3) Testing Results	23
(3-1) Uniaxial compression.	23
(3-2) Deformation tests	27
(A) Modulus of Elasticity	27
(B) Poisson's Ratio	31
(C) Lateral deformation tests	61

Page

(3-3) Triaxial tests 77

V. TENSILE TESTS 82

(1) Selection and Preparation of Specimens. 82

(2) Testing Apparatus and Loading Procedures 84

(3) Testing Results 86

(3-1) Tensile Strength 86
(3-2) Splitting strength 90
(3-3) Flexural strength 96

VI. SHEARING TESTS. 102

(1) Selection and Preparation of Specimens. 102

(2) Testing Apparatus and Loading Procedures 102

(3) Testing Results 106

VII. DISCUSSION OF TESTING RESULTS 111

(1) Compressive Tests 111
(1-1) Effect of L/D ratio on compressive strength 111
(1-2) Effect of Cross-section on uniaxial compressive strength 112
(1-3) Effect of end lubrication on uniaxial compressive strength 114
(1-4) Elastic constant 114
(1-5) Effect of time on strain 116
(1-6) Lateral deformation. 116
(1-7) Effect of confining pressure on compressive strength 124
(1-8) Mohr's circle and internal friction angle. 124

(2) Tensile Tests 127

(2-1) Tensile strength and breaking angle 127
(2-2) Splitting strength 127
(2-3) Comparison of failure type between uniaxial compression and Brazilian tests 129
(2-4) Flexural strength. 133
(2-5) Reconciliation of tensile results. 134

(3) Shearing Tests. 135

Page

VIII. CONCLUSION 136

(8-1) Strength characteristics 136
(8-2) Deformation characteristics. . . . 137

BIBLIOGRAPHY 140

APPENDIX 143

ACKNOWLEDGMENT

The author wishes to express his appreciation and gratitude to Professor R. G. K. Morrison and Professor D. F. Coates of the Department of Mining Engineering and Applied Geophysics, McGill University, under whose direction and instruction, the laboratory tests and the thesis work were carried out.

The author is also indebted to Mr. J. E. Udd of this Department for his instruction in specimen preparations, testing procedures and his assistance in triaxial test.

It is also desired to thank Professor L. P. Geldart of this Department who gave his knowledge of statistical analysis of the testing data.

Gaspe Copper Mines Limited, Quebec, is to be thanked for supplying the cores used for the testing.

II. INTRODUCTION

(1) Objective

This thesis describes the various tests which were carried out on 492 specimens of a Gaspe skarn to determine a number of the physical properties for this particular rock type. The tests cover the following properties:

Strength properties:

- Uniaxial compressive strength
- Uniaxial tensile strength
- Flexural strength
- Splitting strength
- Shearing strength
- Angle of internal friction

Elastic properties:

- Young's modulus
- Poisson's ratio
- Modulus of rigidity (calculated)

A summary of testing results for each type of test is tabulated in separate chapters and the detailed data for each specimen can also be found in the Appendices.

A group of specimens for each testing project are given a code number in accordance with the physical properties and the distribution diagram has been prepared for each type of test, this diagram gives the mean value,

mode, maximum value, minimum value and the spread of testing results.

(2) Treatment of Data

Each type of test covered a number of specimens and each specimen has its own testing result, the maximum value sometimes is more than three times the minimum value because of the local variations in properties and experimental error for different specimens. In order to get a representative result for each group of testing data, a distribution diagram which indicates the mode and the spread of testing results is prepared for each case. The mean value, the standard deviation and the coefficient of variations are calculated from these distribution data.

The determination of mode, mean value, standard deviation and the coefficient of variation is based on the statistical theory.(1)

III. THE GASPE COPPER MINES LIMITED

(1) Location of Mines

The Gaspe Copper Mines [2] are located at the headwaters of the York River in the Gaspe Peninsula of the Province of Quebec (Figure 3-1). The town of Murdochville is maintained by the mining operation. The highway from Murdochville runs 60 miles east to Gaspe Harbour and 25 miles north to Mont Louis on the St. Lawrence River.

(2) Geology of Mines

The ore deposits of the Gaspe Copper Mines are located in the Grande Greve and Upper Cap Bon Ami formations of the lower Devonian period. This geological succession is shown in Table 3-1 and the relative location of the Needle Mountain A, B and C zones and the Copper Mountain ore bodies in cross section in Figure 3-2. For detailed geology, the literature can be referred to [2], [3]. This thesis is concerned with the skarn which is the host rock of the "C" zone or major ore body.

This ore body, averaging about 100 feet in thickness, extends down dip to the north for some 3,500 feet. It varies in dip from flattish at its upper or south end to an average of about 23° in the southern slope. It varies in breadth from about 800 feet at the south to about 1,800 feet at the

TABLE 3-1

Stratigraphic Column of Needle Mountain

Formation	Ore Zone	Unaltered equivalents	Thickness	Rock Horizons
GRANDE GREVE	A-zone	Calcareous siltstone	400'	Limy Quartzite
CAP BON AMI		Silicious shale	60'	1st chart
	B-zone		37'	1st porcelanite
		Silicious limestone	130'	Wollastone
		x	32'	2nd porcelanite
		Silicious shale	140'	2nd chart
	C-zone	Siltstone	17'	3rd porcelanite
		Limestone	129'	skarn
	D-zone	Siltstone and limestone		4th porcelanite

Scale = 1" = 2,000'

x = Alternating limestone and siltstones.

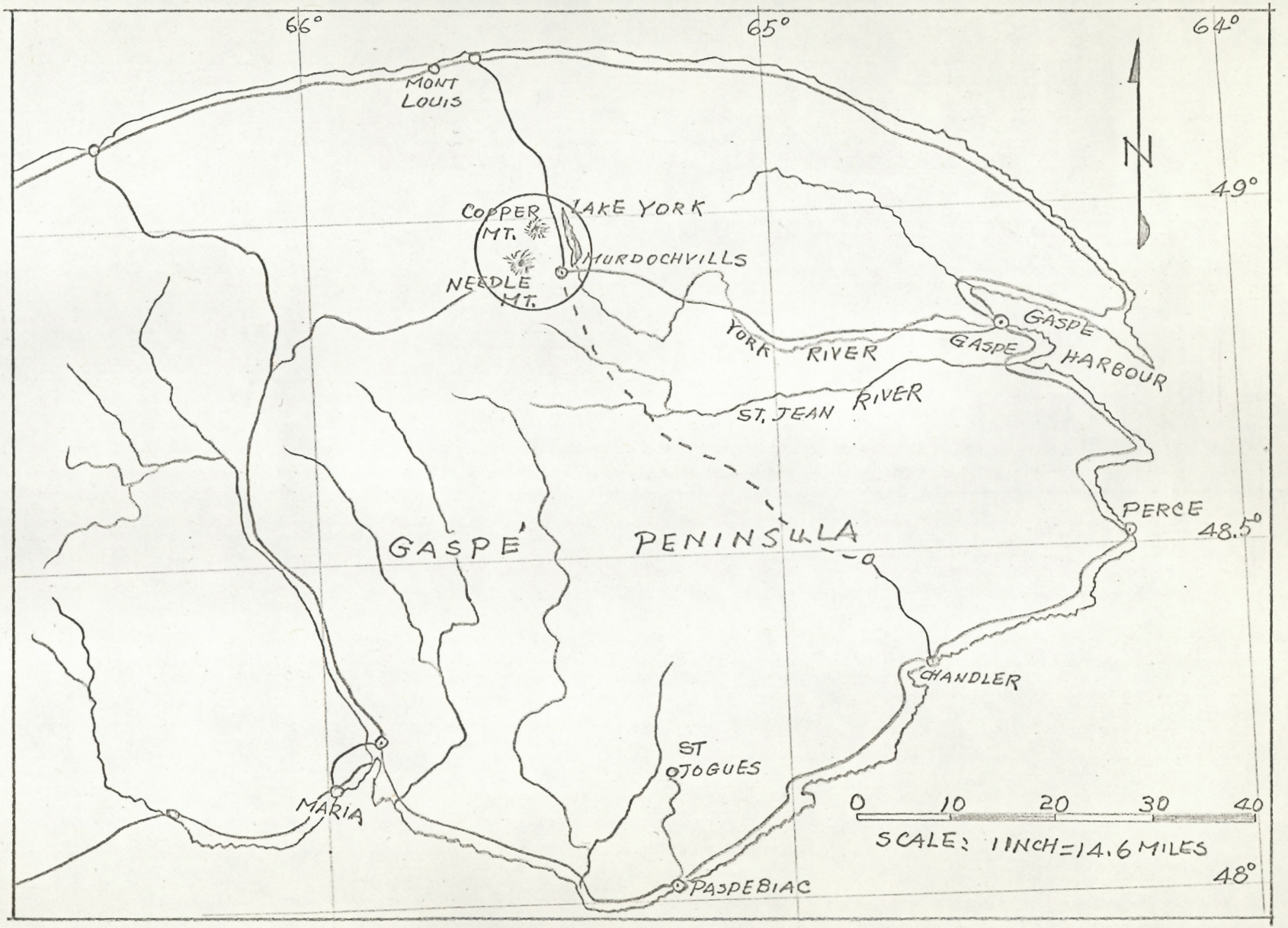

FIGURE 3-1 LOCATION OF GASPE COPPER MINES LTD.

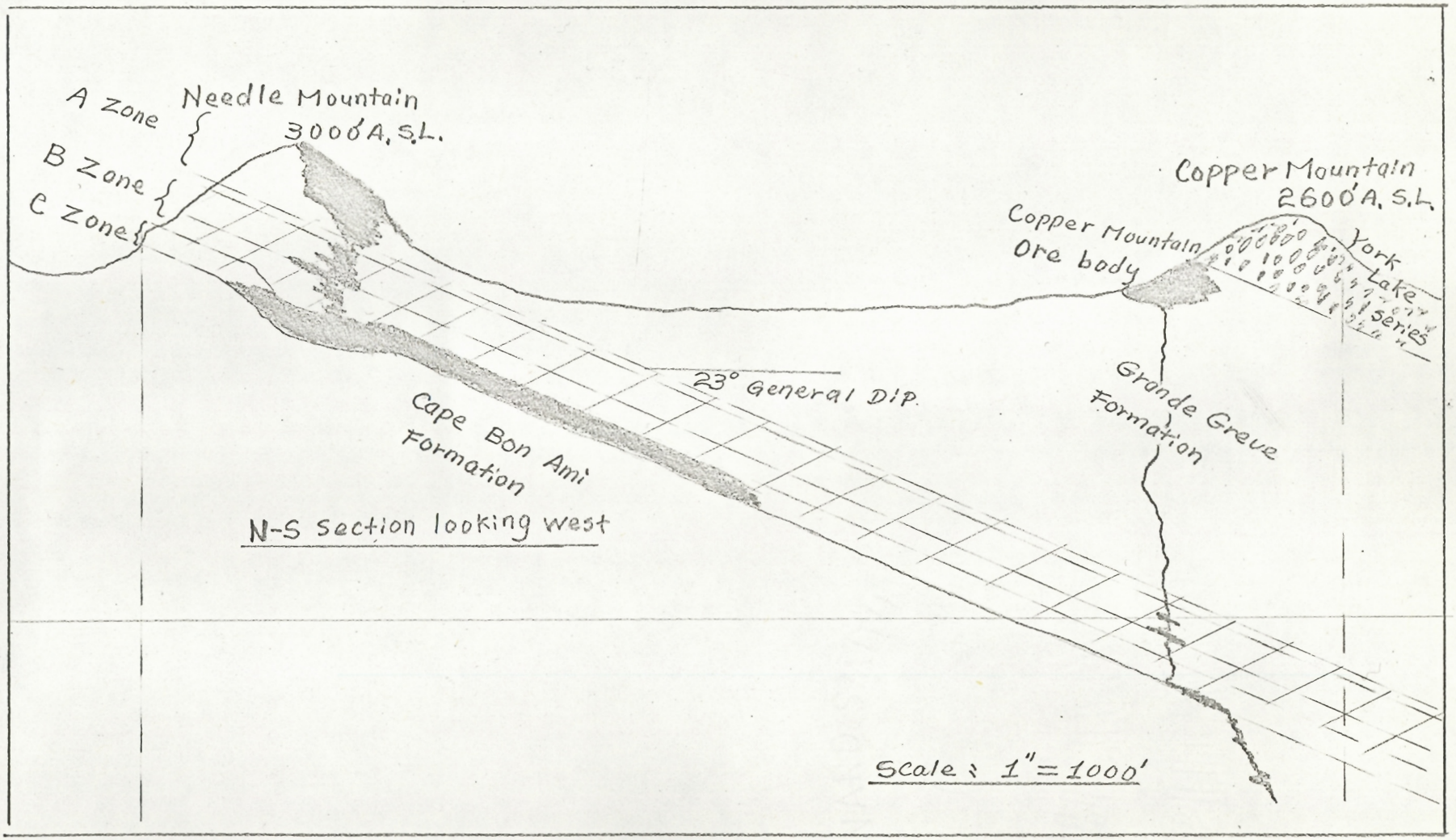

Figure: 3.2 SECTION OF GENERAL GEOLOGY AND ORE DEPOSITION

north. It represents a replacement within the skarn. The skarn, representing a silicified garnetized limestone, is in turn an alteration product of an original argillaceous limestone.

(3) Location of Specimen

All cores tested in this experiment were taken from the main production area of the Needle Mountain "C" zone ore body.

The EX-core of diamond drill hole U-1225 was taken from the back of the stope at the northern part of C-zone, Diamond drill hole U-1474 of NX-core is a vertical downhole which started from 50 feet below the back of C-zone and stopped 23 feet below the bottom of C-zone. The EX-core from diamond drill hole 1526 was also taken from a vertical downhole from 30 feet above the top to 10 feet below the bottom of C-zone.

As described previously, most of the cores were taken from vertical downholes which passed through the different phases of alteration with variations in colour, composition and grain size, etc. This was a factor contributing to variation in testing results.

(4) Petrographic Description of Specimen

The skarn altered from limestone is a silicious rock which is mainly composed of clino-pyroxene, cordierite, quartz, carbonate and some isotropic materials. Figure3-3 shows a petrographic section of this rock type. The

pyroxene is rather coarse grained and more or less idiomorphic. The cordierite usually appears as twinned in the rock. It grows between the pyroxene crystals and the grains are in the center of each grain, decomposed to an essentially isotropic material. Quartz and carbonate occur as fillings of the spaces between other minerals.

This petrographic section was taken from deformation testing specimen No. X-14, which was located at 128 feet in U-1225 diamond drill hole.

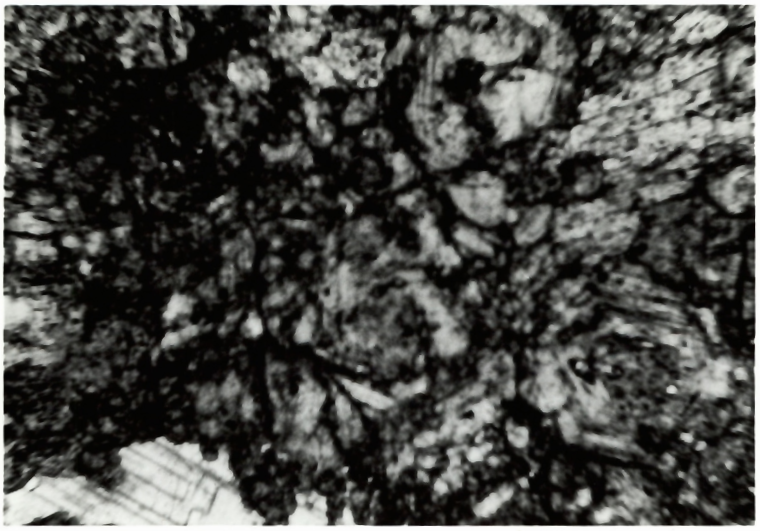

Figure 3-3 (a): Petrographic skarn, magnification 45x, single nicol. Deformation test, specimen No. X-14.

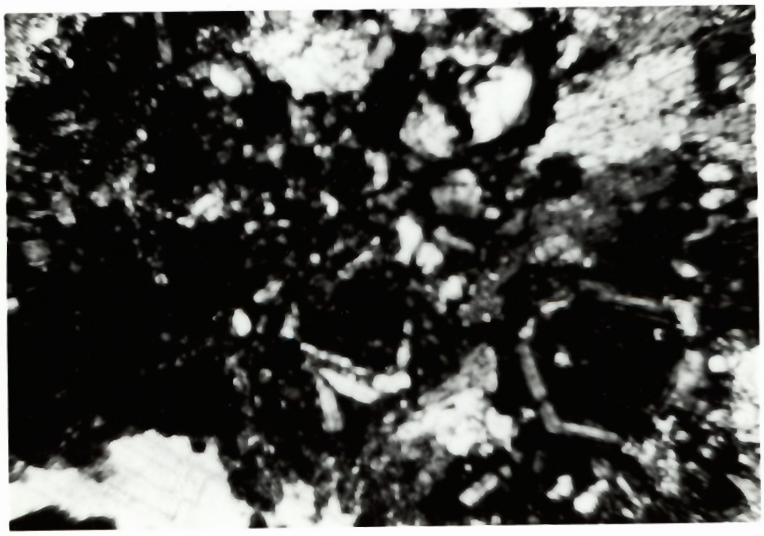

Figure 3-3 (b): Petrographic Skarn, magnification 45x, crossed nicol Deformation test, specimen No. X-14.

IV. COMPRESSIVE TESTS

(1) Selection and Preparation of Specimens

1-1. Uniaxial tests

All specimens tested in uniaxial compression were EX-core (7/8 inch in diameter), which were taken from U-1225 diamond drill hole in the Needle Mountain C-zone ore body of Gaspe Copper Mines Limited.

The sequence of selecting specimens for all tests was, as follows:

(a) Specimens with planes of weakness or fractures were rejected.

(b) The footage and location were marked on each piece of core.

(c) Specimens with similar visible physical characteristics, such as, colour, grain size and mineral composition were then chosen from each foot interval for each type of test when possible.

The preparation of specimens for compressive tests was, as follows:

(a) Using a diamond saw (Figure 4-1) lubricated and cooled with water, specimens were cut with L/D ratios as follows: 0.5, 0.7, 1.0. 1.5, 2.0, 2.5 and 3.0 (Figure 4-2).

(b) To ensure that the two bearing faces of the specimen were parallel, the specimen was rotated in a lathe and the ends were ground with a carborundum wheel, mounted on a tool post grinder (Figure 4-3).

(c) The length and the diameter of specimens were measured to an accuracy of 0.001 inches.

(d) The specimens were air dried, at room temperature, for at least 48 hours.

1-2. Deformation tests

The preparation of specimens for testing was, as follows, which departs somewhat from that suggested by the Department of Mines and Technical Surveys[4]:

(a) After grinding, center lines were drawn in both axial and lateral directions.

(b) Specimens were cleaned with acetone to remove all dirt and grease. Care must be taken to avoid subsequently touching the surfaces where the strain gauges will be placed.

(c) The SR-4 strain gauges, as required, are then cemented on the specimen with SR-4 cement. Any air beneath the gauges is removed by hand pressure.

(d) The strain gauges were then checked for orientation with respect to the loading axis.

(e) The prepared specimens were dried at room temperature for at least 24 hours prior to test.

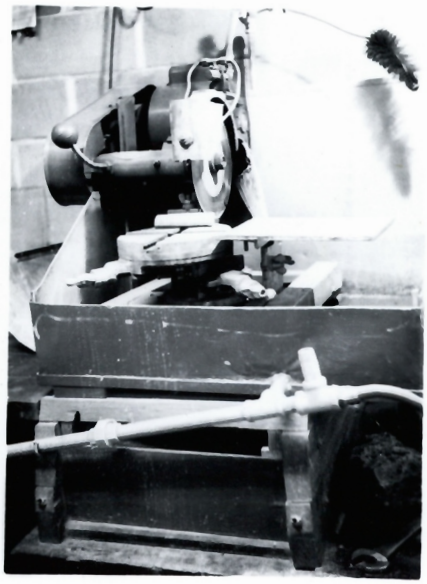

Figure 4-1:

Photograph showing the diamond saw.

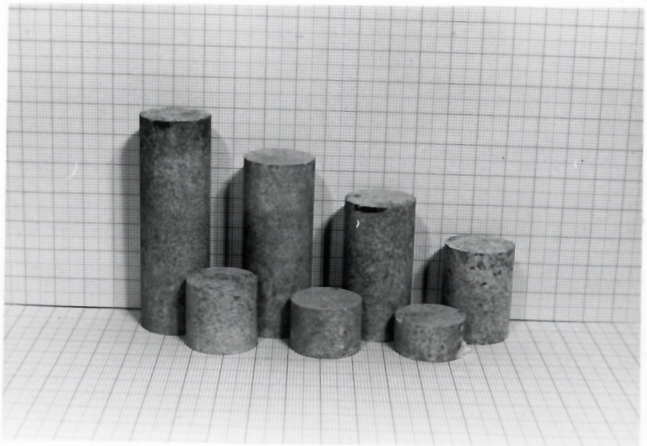

Figure 4-2: Photograph showing the prepared specimens with various L/D ratio for uniaxial compression test.

For lateral deformation tests with and without lubricated ends, seven gauges, two axial and five lateral, were placed on the NX-core specimens, as shown in Figure 4-4. For lubricating the ends, after attaching the strain gauges, specimens' ends were dipped in liquid paraffin.

1-3. Triaxial tests

Specimens for triaxial tests were prepared from drill hole U-1526 (EX-core). The preparation of specimens for this type of test is the same as for the uniaxial test, except for the following:
(a) A small rubber inner sleeve was drawn over the specimen to contain any fracturing and avoid puncturing an outer sleeve (b) described below.
(b) To seal the specimen from the hydraulic fluid, a larger outer rubber sleeve was drawn over the inner sleeve and clamped to the platten of the triaxial bomb (Figure 4-5).

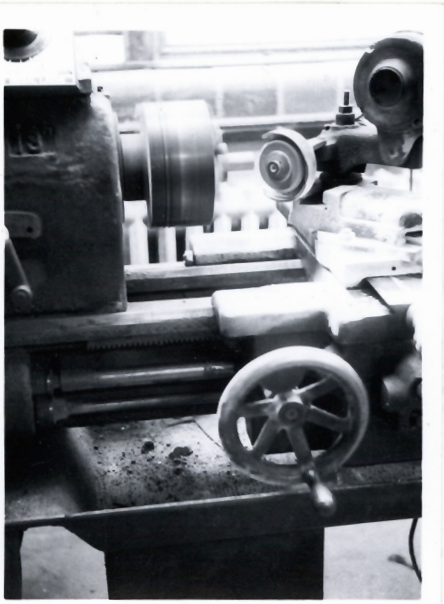

Figure 4-3:

Photograph showing the lathe and tool post grinder.

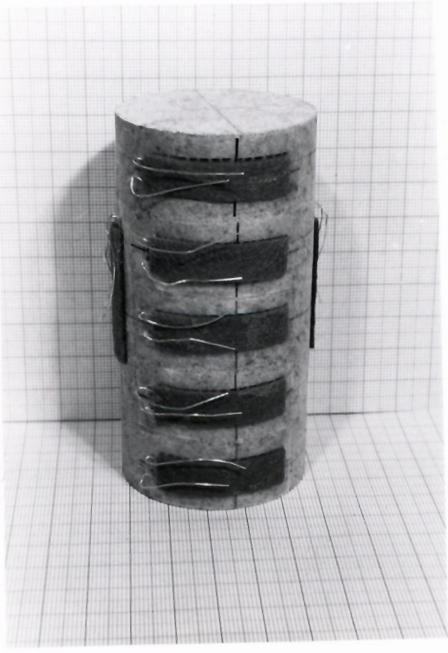

Figure 4-4:

Photograph showing the prepared specimen for lateral deformation test.

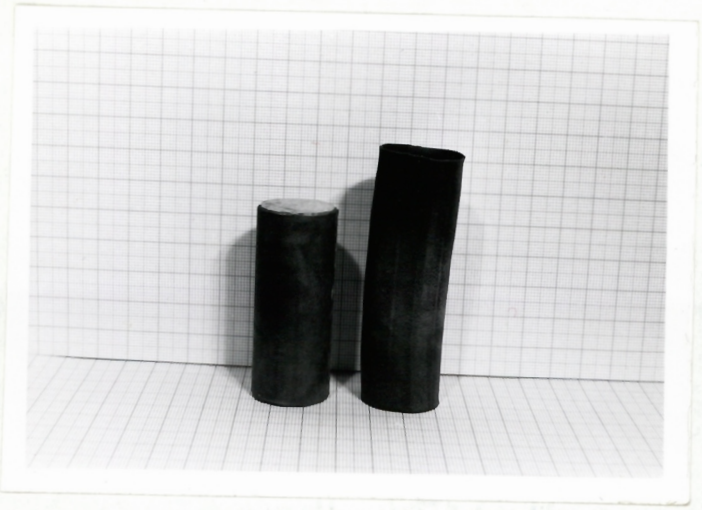

Figure 4-5: Photograph showing the rubber sleeves to cover the specimen for triaxial compression test.

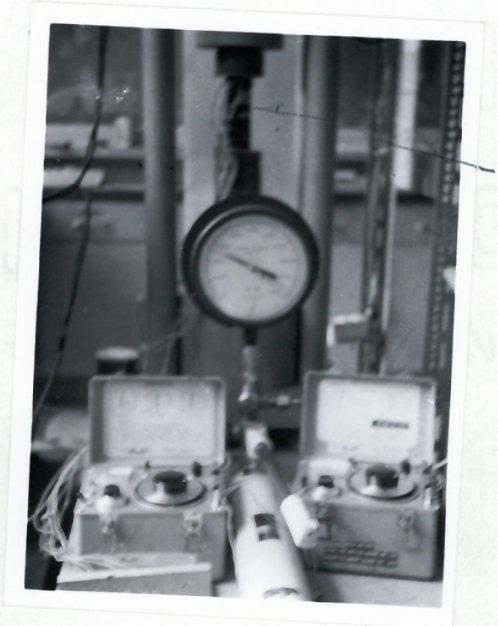

Figure 4-18:

Set up for lateral deformation test

(2) Testing Apparatus and Loading Procedure

2-1. Correction curve for 200,000 lbs. pressure gauge of Louis Small Compression Tester

A 200,000 lbs. Louis Small Compression Tester, with a dial pressure gauge, was used in the first deformation tests. Shortly, after this type of test was finished, an error was discovered in the pressure dial gauge readings for the loading and unloading cycle. A correction curve, based on the load cell reading for the pressure range, is shown in Figure 4-6.

2-2. Uniaxial test

The Louis Small Compression Tester with load cell reading taken by a strain gauge indicator was used for uniaxial compression tests (Figure 4-7 (a)).

The loading procedures are, as follows:

(a) The strain gauge indicator was connected with the load cell in full bridge circuit.

(b) The specimen was centered between the platens (Figure 4-7 (b)).

(c) A small load was applied slowly to adjust the spherical bearing block carrying the lower platen.

(d) Load was applied gradually to failure by the use of the oil pump.

(e) Load cell readings were taken from the strain gauge indicator when specimens fail.

(f) The readings of strain change were then converted

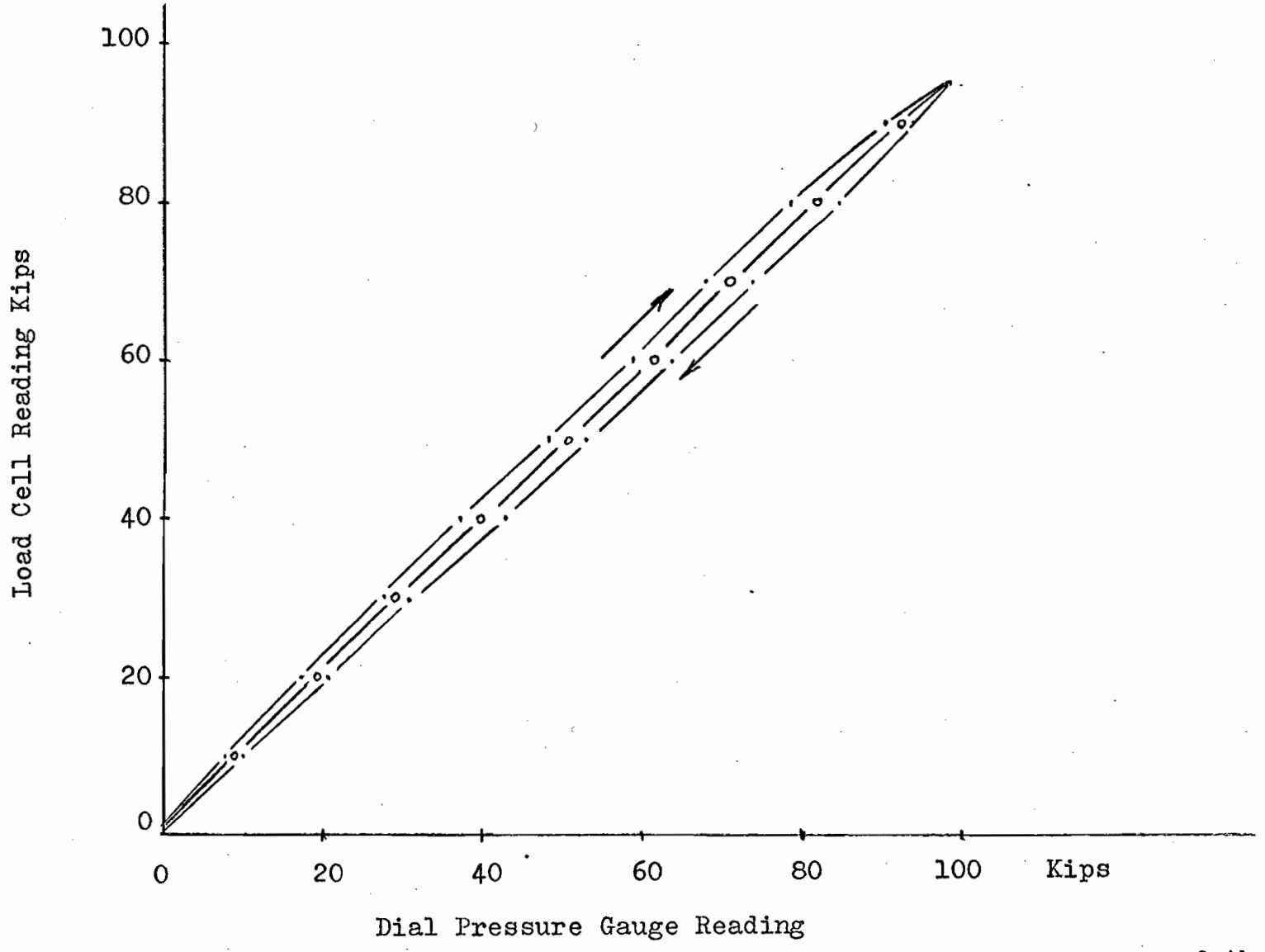

Figure 4-6: Correction curve for 200,000 lbs. compression pressure gauge of the Louis Small Machine

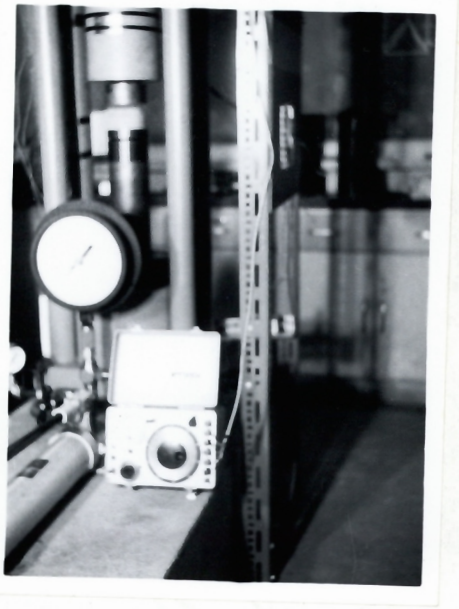

Figure 4-7 (a):

Photograph showing the Louis Small Compression tester and strain gauge indicator.

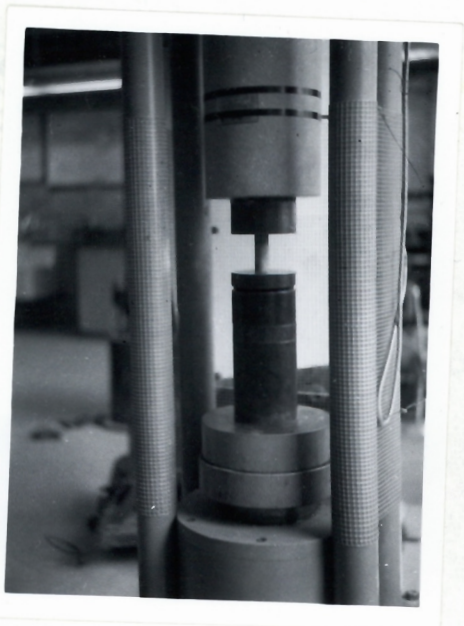

Figure 4-7 (b):

Set up for uniaxial compressive test.

into load units (1 micro in/in. = 50 lbs.).

2-3. Deformation tests

For simple stress-strain tests the following procedure was used:

(a) The uniaxial load was cycled between 0 and 3,000 lbs. to establish the zero load reading for the two strain gauges.

(b) The zero load reading on the longitudinal and lateral strain gauges was observed.

(c) The load was increased to failure with 3,000 lbs. loading intervals and readings of strain change were taken at each loading interval.

(d) For a hysteresis loop test, load was applied to 6,000 lbs. as in procedure (c) above, then reduced to zero also with a 3,000 lbs. loading interval. Readings of the strain change at each interval for each loading and unloading cycle were observed.

(e) The procedure (d) was repeated, over successively higher loading ranges, to failure.

(f) The difference in strain between loading and unloading for the same load is referred to as hysteresis. In the cycle it results in a loop.

For time-strain tests, loading and the time intervals for the constant load period for specimens No. X-20 and No. X-37 are recorded on Figure 4-37 and Figure 4-38, respectively.

For lateral deformation tests with and without lubricated ends on NX-core specimens, the loading procedures are described individually for each specimen.

2-4. Triaxial tests

The triaxial bomb used for these tests (Figure 4-8(a)) was designed by the Department of Mines and Technical Surveys, Ottawa, Canada. This apparatus provides an oil chamber surrounding the specimen for applying confining pressure (Figure 4-8(b)). The axial load was applied by the Louis Small Compression Tester.

Testing procedures are, as follows:

The specimen was mounted on the central piston and placed in the triaxial chamber which was then transferred to the loading machine. An initial axial load of 10,000 lbs. was applied to adjust the specimen on the spherical bearing block. A confining pressure was then applied on the specimen and maintained at a constant level. The axial load was then slowly increased to failure with the confining pressure kept constant.

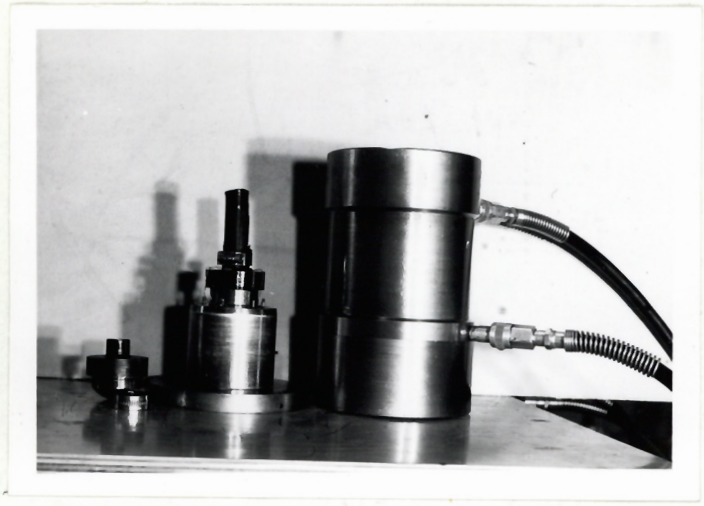

Figure 4-8 (a): Triaxial bomb

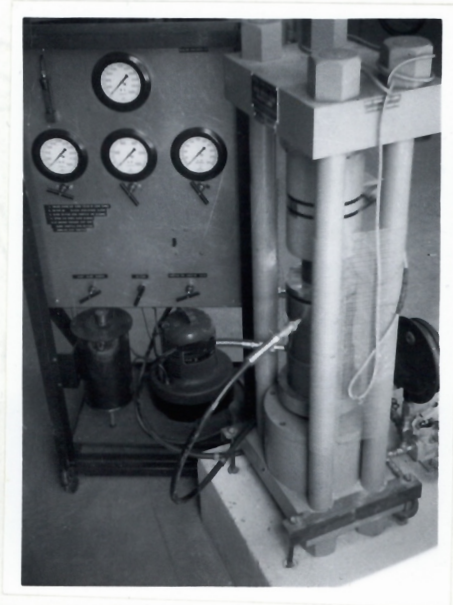

Figure 4-8 (b):

Triaxial testing apparatus.

(3) Testing Results

3-1. Uniaxial compression

Uniaxial compressive strength is defined as follows:

$$S = \frac{P}{A} ,$$

where S = Compressive strength of specimen, psi.

P = Rupture load, lbs.

A = Original cross-section area of specimen in. sq.

This assumes that the load applied is uniformly distributed over the whole cross-section of the specimen.

Table 4-1 summarizes the testing results of 148 compressive tests with L/D value varying from 0.528 to 2.871. These tests were carried out between steel platens. The supporting data are given in Tables 1A-1 to 1A-7.

The compressive strength from Table 4-1 was plotted as a function of the L/D ratio in Figure 4-9. The maximum and minimum values plotted here are an indication of the coefficient of variation.

The distribution diagram for the compressive strength of all specimens tested in uniaxial compression is shown in Figure 4-10. It suggests a random or Gaussian distribution.

TABLE 4-1

Summary of Uniaxial Compression Values with Free Ends and Varying L/D Ratios

No. of Specimen	L/D Ratio	Compressive Strength			Standard Deviation psi	Coeff. of Variation %
		Max.Value psi	Mean psi	Min.Value psi		
24	0.528	59.000	36.800	22.200	9160	24.7
21	0.667	56.200	34.800	23.200	9680	27.8
26	1.050	57.100	32.300	19.900	9320	28.8
24	1.532	54.200	30.900	18.200	9550	30.9
20	2.050	44.000	31.400	17.400	6560	20.9
21	2.591	43.000	28.900	17.700	6850	23.7
12	2.871	37.000	27.900	17.900	6780	24.8
Total 148			31.900		8160	25.6

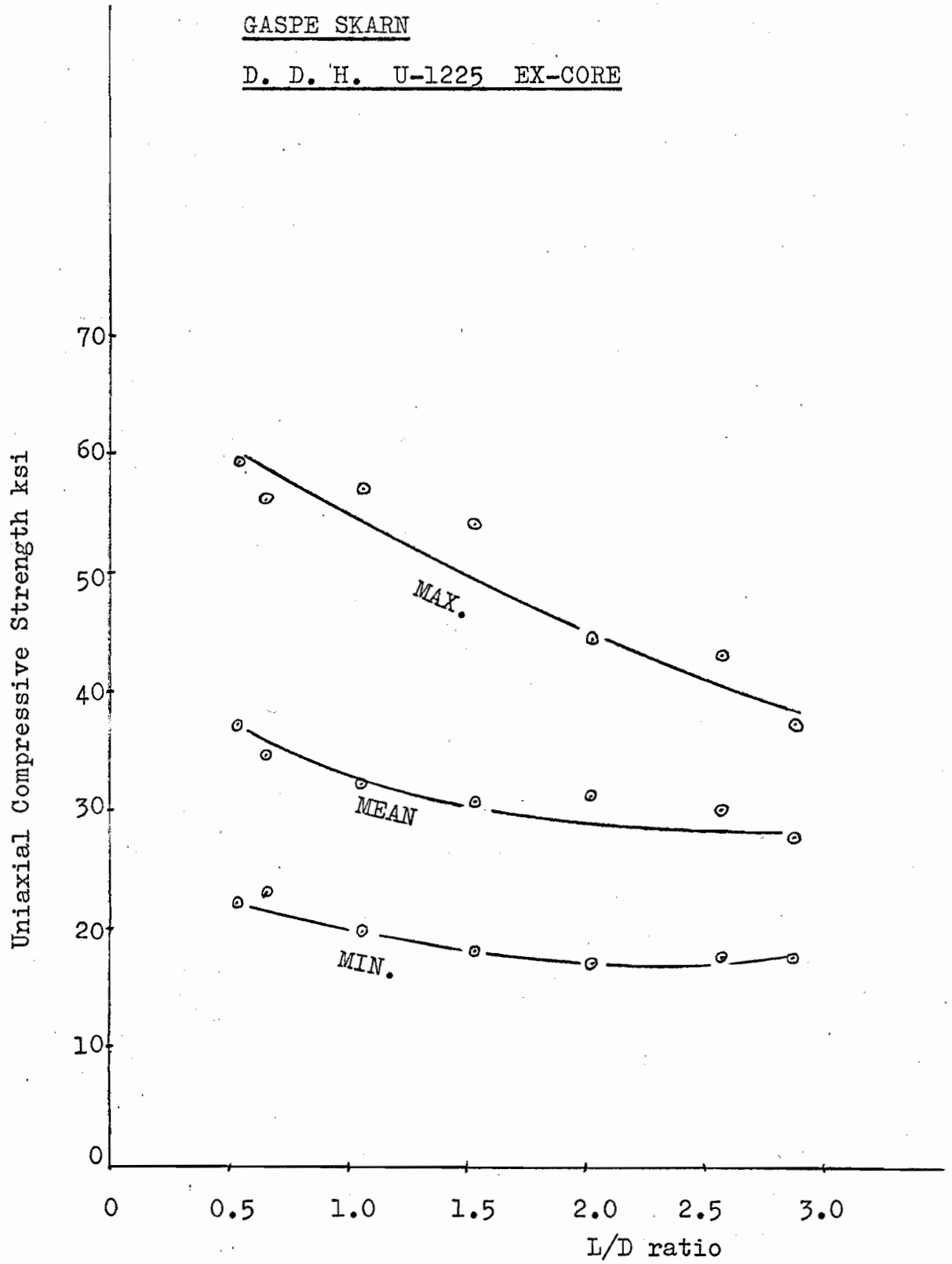

Figure 4-9: Relationship between L/D ratio and compressive strength.

Ref. Table 4-1

EX - U - 1225 GASPE SKARN

No. of Specimens	= 148
Mean Value	= 31,900 psi
Max. Value	= 59,000 psi
Min. Value	= 17,400 psi
Standard Deviation	= 8160 psi
Coefficient of Variation	= 25.6%

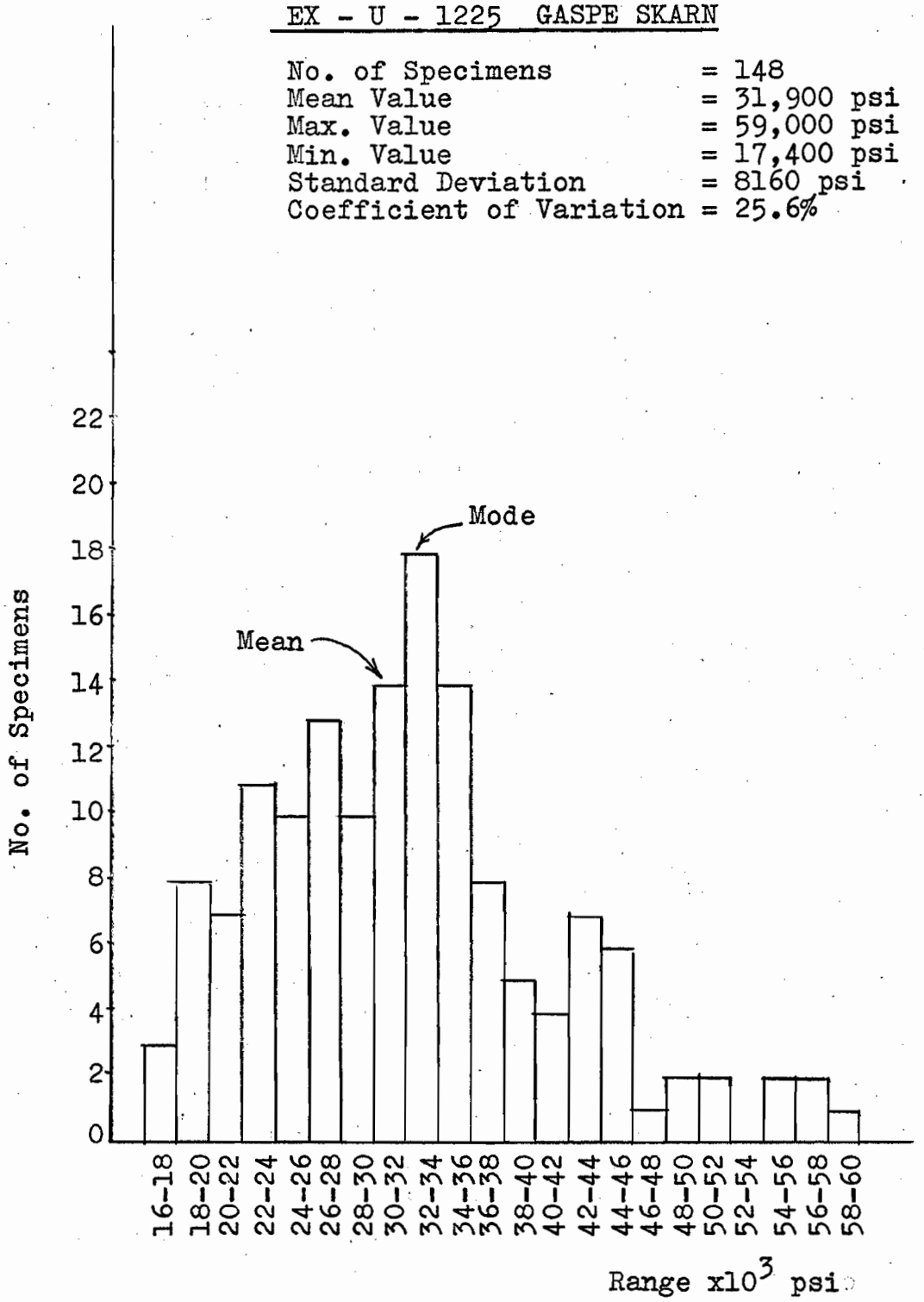

Figure 4-10: Distribution Diagram of Compressive Strength Value

Ref. Tables 1A-1 to 1A-7

Specimens subjected to uniaxial compression without lubricated ends generally failed with a cone or wedge, in shearing fracture (Figure 4-11, (a), (b), (c)). A characteristic of this type of failure is the grinding effect due to shear to be seen on the failure surfaces. Kvapil[5] has suggested that the conical fracture is due to the friction developed between the platens and the end surfaces of the specimen. Griggs[6] has suggested that a wedge will cause a tensile failure along the vertical axis.

3-2. Deformation tests

(A) Modulus of Elasticity

The modulus of elasticity, which is the ratio of applied stress to linear strain, is a measure of the stiffness or elasticity of a material and is defined by the following formula:

$$E = \frac{S}{e},$$

where E = Modulus of Elasticity, psi

S = Applied stress, psi

e = Linear strain, micro in/in.

The modulus of elasticity is the result of Hooke's Law -- Stress is proportional to strain. Within this relationship, the modulus of elasticity or Young's Modulus (E), the Modulus of Rigidity (G) and Poisson's ratio (u) are constants.

The methods of measurement of elastic moduli for rocks have been given by several

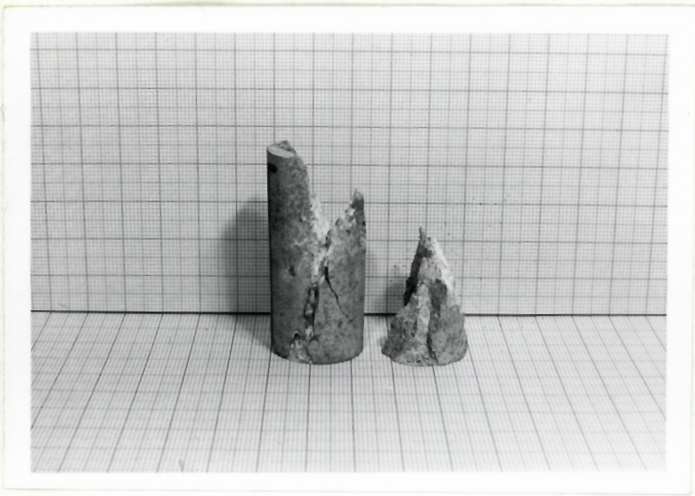

Figure 4-11 (a):

Shear failure with cone.

Uniaxial compression.

Specimen No. CF-20
L/D = 2.5

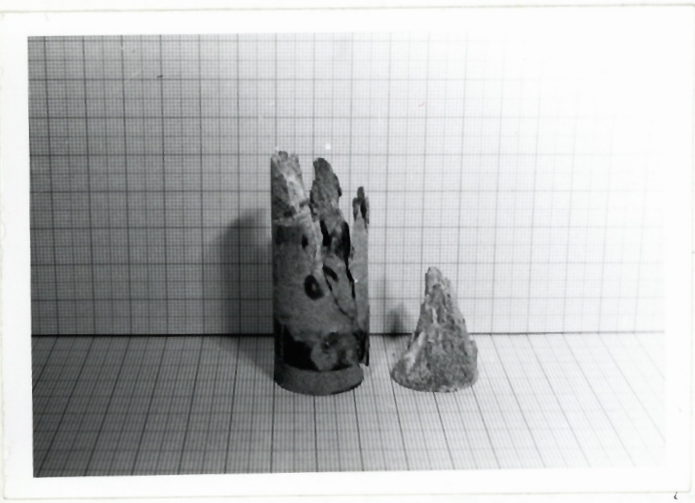

Figure 4-11 (b):

Shear failure with cone.

Deformation test.

Specimen No. X-26

L/D = 2.5

Figure 4-11 (c):

Shear failure with cone, wedging effect splitting the specimen.

Uniaxial compression.

Specimen No. CB-11
CB-15

L/D = 2.0

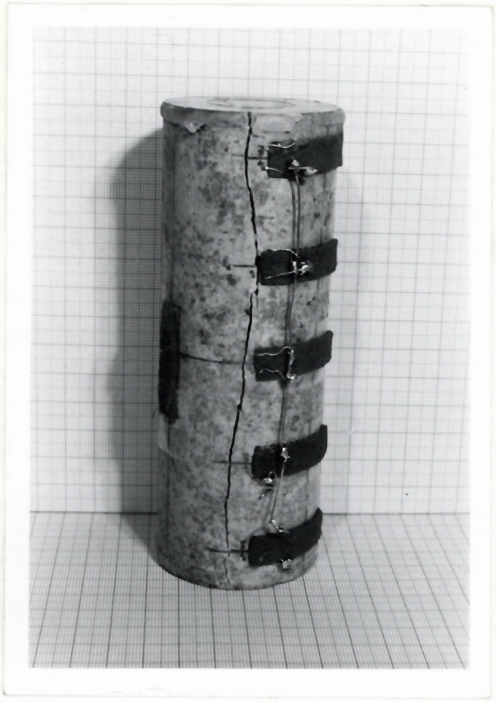

Figure 4-12 (a):

Tensile failure, splitting vertically into two pieces.

Lateral deformation test with lubricated ends.

Gaspe skarn

Specimen No. AB-3

L/D = 2.5

Figure 4-12 (b):

Tensile failure, splitting vertically into three pieces.

Lateral deformation test with lubricated ends.

Sigma porphyry

Specimen No. SPN-5

L/D = 2.0

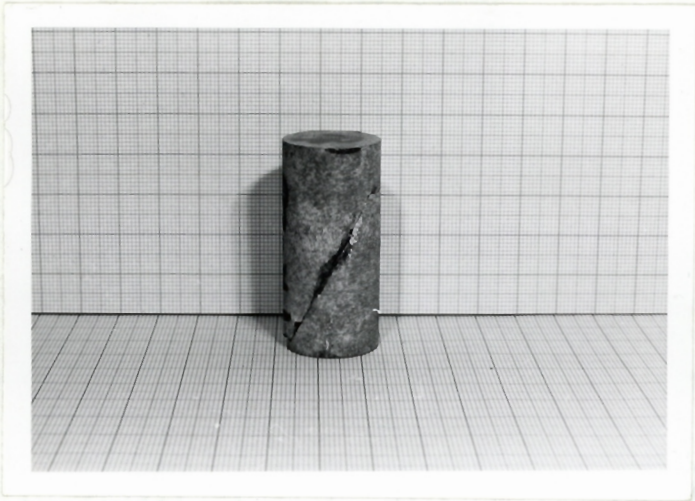

Figure 4-13 (a):

Shear failure with a diagonal curved plane through one end.

Triaxial compression

Confinement = 1.0 ksi

Specimen No. TR-5

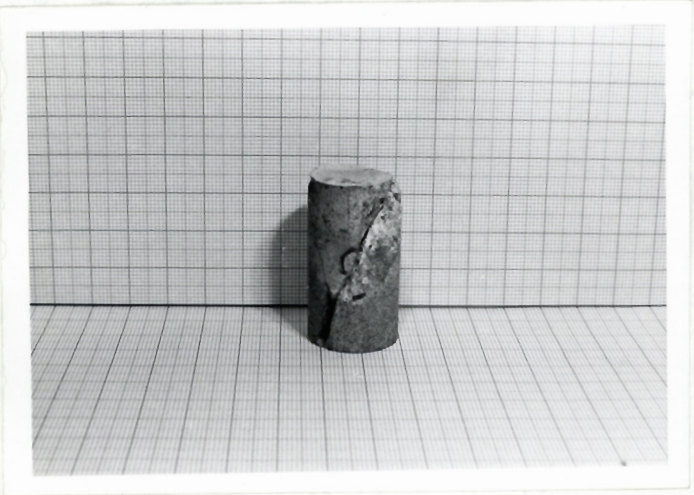

Figure 4-13 (b):

Shear failure with a diagonal curved plane through two ends

Triaxial compression

Confinement = 2.0 ksi

Specimen No. TR-12

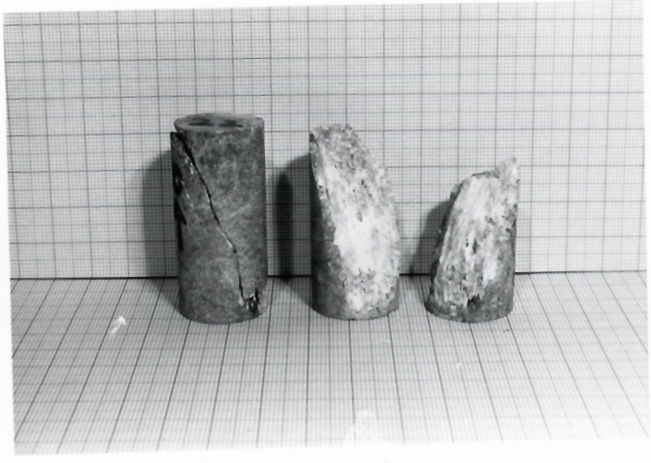

Figure 4-13 (c):

Shear failure with a diagonal curved plane.

Triaxial compression

Confinement = 3.0 ksi

Specimen Nos. TR-22
Tr-26

investigators.[7],[8],[9],[10] In this research, the L/D ratio of the specimen was 2.5, approximately. The modulus of elasticity was calculated from the Secant Method in successive sequence. The procedures are, as follows:

The applied load divided by the initial area of the specimen gives the corresponding stress for each loading level. The modulus was calculated at each loading level and the mean value for each specimen was determined, then the average for 21 specimens of this rock type was obtained from the mean value of each specimen. The standard deviation and the coefficient of variation were also determined for all specimens. The detailed data are shown in Table 1B-1 to Table 1B-21.

A summary of results for the modulus of elasticity for 21 specimens is listed in Table 4-2 and the distribution diagram is shown in Figure 4-14. A generalized curve of the variation of the modulus of elasticity with the applied load, for 21 specimens, appears in Figure 4-15. This curve indicates that the modulus increases with increasing load.

(B) Poisson's ratio

Poisson's ratio is the ratio of lateral strain to the longitudinal strain when the specimen is subjected to an axial load. This definition

TABLE 4-2*

Summary of Values for the Modulus of Elasticity and Poisson's Ratio, D.D.H. #U-1225

Code	Location ft.	Specimen Dia. in.	Specimen Length in.	Specimen Area in. sq.	Applied Load lbs.	Compressive Strength psi	Modulus of Elasticity psi	Poisson's Ratio	Modulus of Rigidity** psi
X- 1	106	0.896	2.319	0.631	19,600	31.000	6.43	0.125	2.86
X- 5	114	0.896	2.389	0.631	13,000	20.600	7.33	0.172	3.14
X- 6	120	0.898	2.318	0.634	21,000	33.100	9.72	0.161	4.19
X- 8	121	0.900	2.329	0.638	15,000	23.500	8.82	0.139	3.88
X-10	125	0.896	2.312	0.631	14,000	22.200	7.47	0.141	3.27
X-12	129	0.896	2.320	0.631	18,000	28.000	5.88	0.096	3.07
X-14	128	0.897	2.331	0.633	26,000	41.900	10.18	0.174	4.33
X-15	130	0.896	2.334	0.631	19,000	30.100	9.64	0.131	4.26
X-16	132	0.897	2.328	0.633	17,000	25.900	8.38	0.119	3.75
X-18	133	0.896	2.402	0.631	24,000	38.100	7.16	0.090	3.98
X-20	134	0.897	2.339	0.632	26,000	42.200	10.91	0.176	4.64
X-21	145	0.899	2.292	0.635	27,000	42.500	11.77	0.189	4.95
X-22	146	0.901	2.291	0.639	20,100	31.700	6.91	0.141	3.03
X-23	156	0.897	2.310	0.633	18,800	29.700	7.95	0.145	3.48
X-25	169	0.896	2.329	0.631	14,500	23.000	5.57	0.117	2.54
X-26	170	0.892	2.337	0.626	12,000	19.100	6.12	0.118	2.75
X-27	171	0.896	2.336	0.631	18,500	29.300	6.87	0.163	2.96
X-31	138	0.897	2.328	0.632	18,000	28.500	10.92	0.147	4.78
X-33	148	0.897	2.332	0.632	20,000	31.600	8.64	0.150	3.75
X-36	109	0.900	2.300	0.637	19,000	29.800	7.66	0.152	3.33
X-37	171	0.896	2.336	0.631	18,000	28.560	8.51	0.170	3.41
Mean Value		0.897	2.329	0.633		30,100	8.39 $\times 10^6$	0.148	3.68 $\times 10^6$
Standard Deviation						6.325	1.798	0.0262	0.668
Coefficient of Variation						21.1%	21.8%	17.4%	18.3%

* - Dial Pressure Reading
** - Calculated

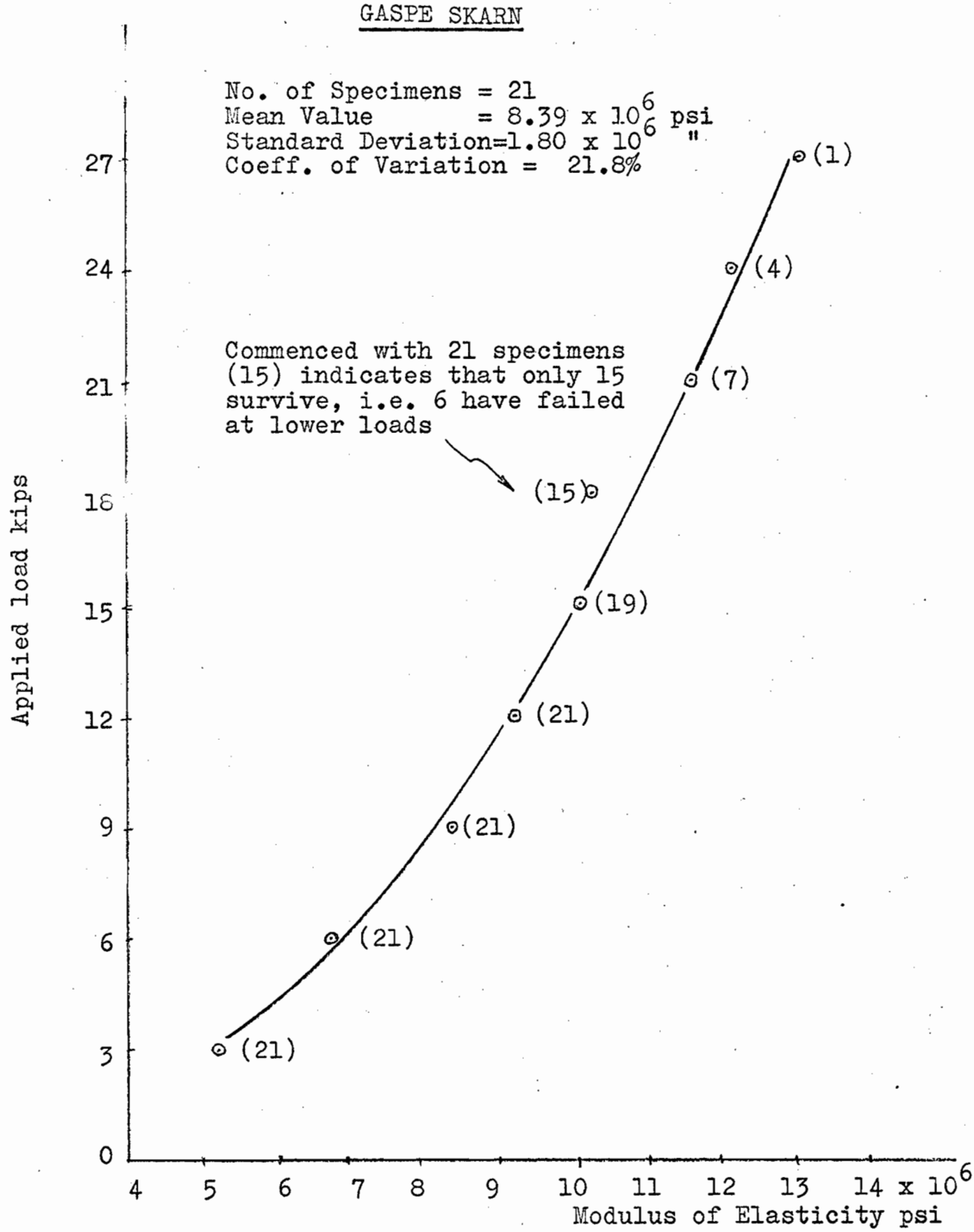

Figure 4-15: Variation of Modulus of Elasticity with Applied Load

EX-CORE D.D.H. U-1225 GASPE SKARN

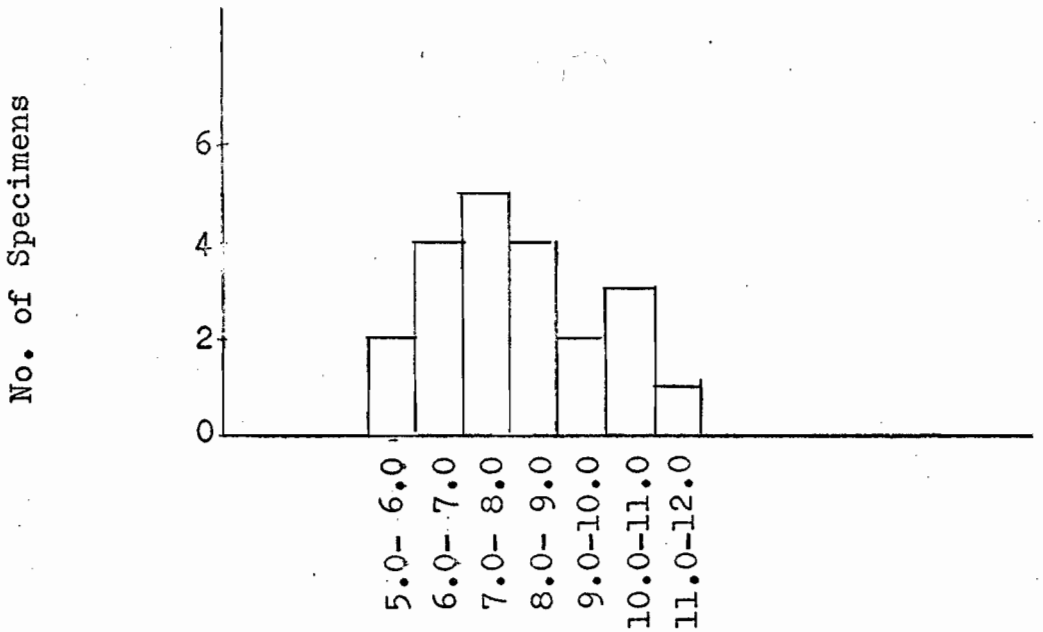

Figure 4-14: Distribution of Values for Modulus of Elasticity

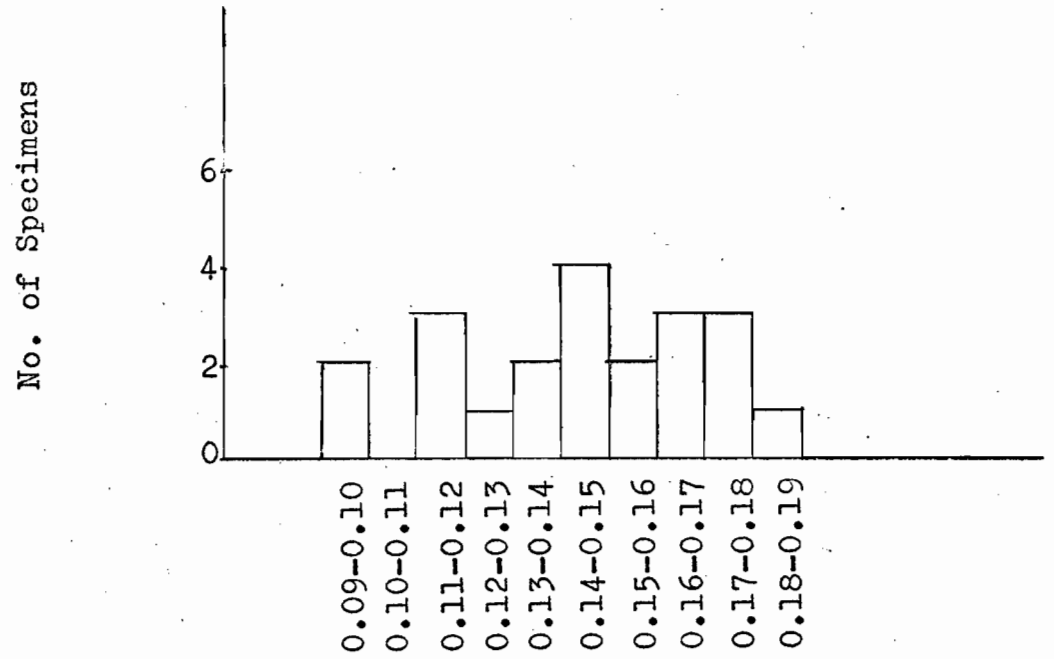

Figure 4-16: Distribution of Values for Poisson's Ratio.

Ref. Table 4-2

gives the following equation:

$$u = \frac{e_1}{e_2},$$

where u = Poisson's ratio

e_1 = Lateral strain observed for applied load P

e_2 = Longitudinal strain observed for applied load P

The following steps for determining Poisson's ratio were adopted:

(a) Readings of the increments or decrements in lateral and longitudinal strain at each loading level were taken.

(b) Lateral strain was divided by the longitudinal strain to get Poisson's ratio for each corresponding loading level.

(c) The mean value for each specimen was calculated from each loading level.

(d) The mean value of Poisson's ratio for 21 specimens was obtained from the mean value for each specimen.

(e) The standard deviation and coefficient of variation for 21 specimens were also calculated.

The value of Poisson's ratio for 21 specimens is given in Table 4-2 and the distribution diagram appears in Figure 4-16; this diagram shows a wide spread in value for Poisson's ratio. The relationship between Poisson's ratio and applied load was plotted in

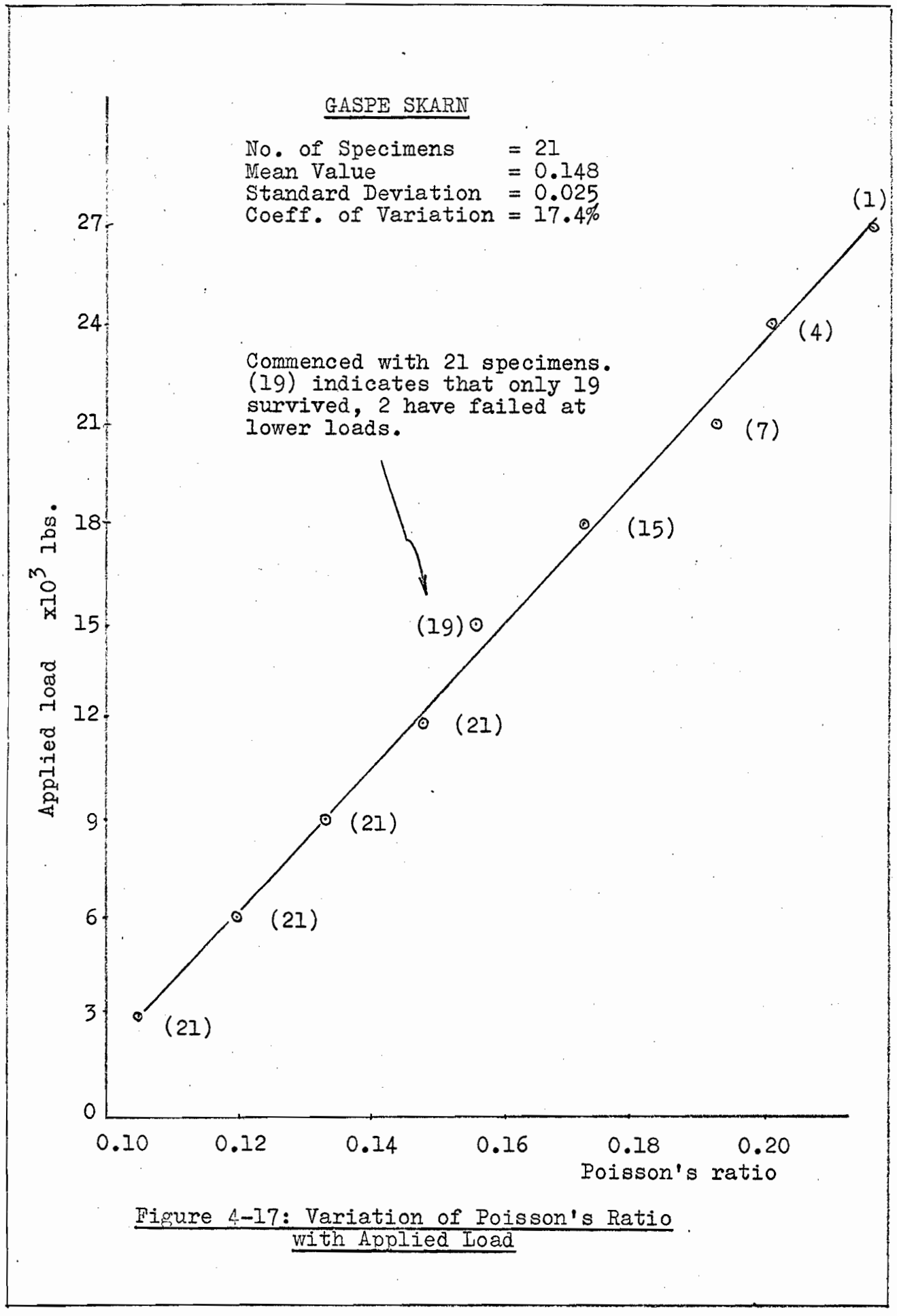

Figure 4-17: Variation of Poisson's Ratio with Applied Load

Figure 4-17. This curve shows that Poisson's ratio is approximately proportional to the applied load.

The stress-strain curves for each specimen were plotted as shown in Figure4-19 to Figure 4-38 (b).

The supporting data are listed in Table 1B-1 to Table 1B-21 in the Appendix.

For check reason, specimen No. AB-1 which was prepared from NX-core and tested with standard load cell reading taken from strain gauge indicator gives the results of 9.28×10^6 psi in modulus of elasticity and 0.256 in Poisson's ratio.

The stress-strain curve for this specimen was also plotted as shown in Figure 4-39.

The detailed data for this specimen is given in Table 1B-22 in the Appendix.

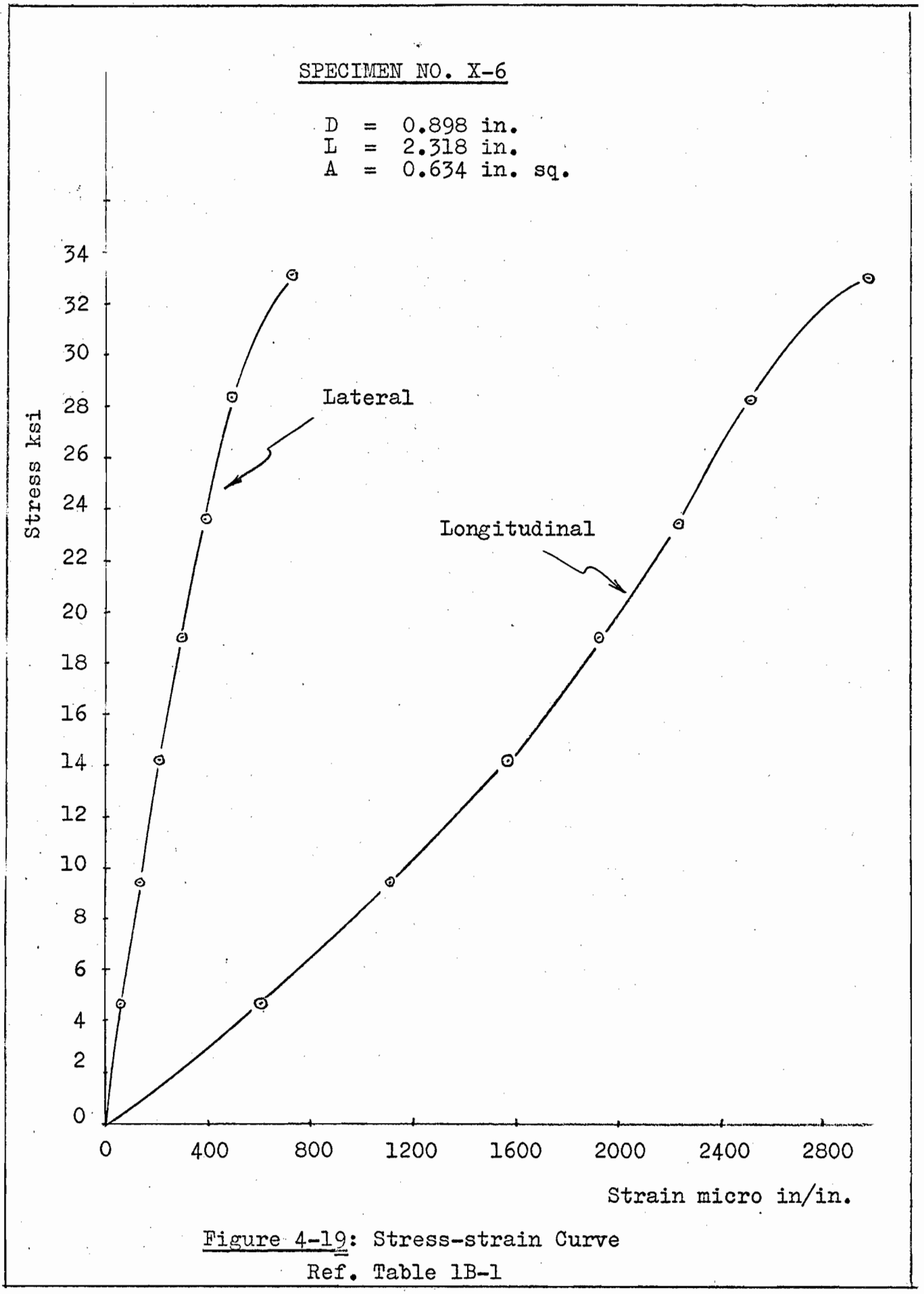

Figure 4-19: Stress-strain Curve
Ref. Table 1B-1

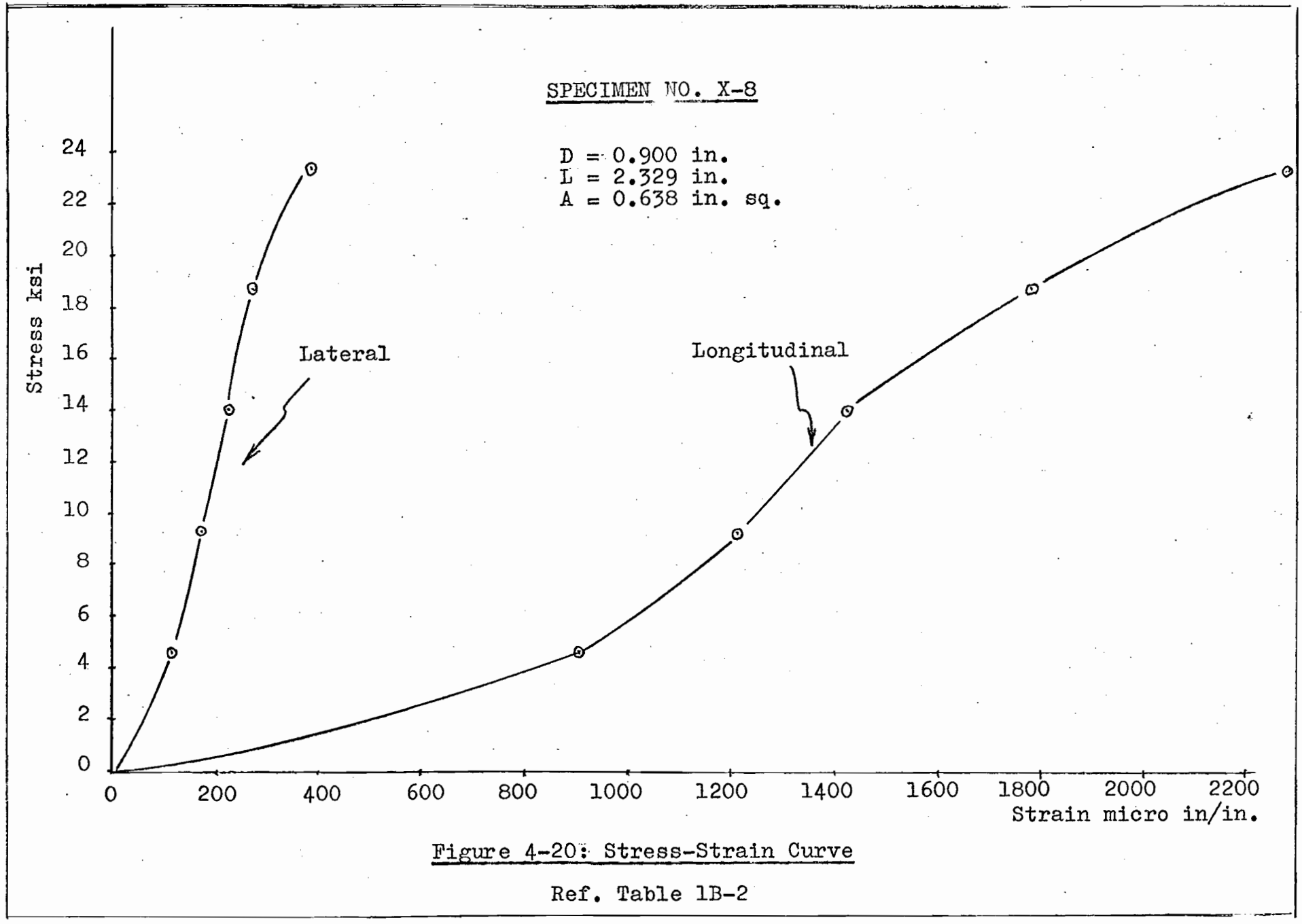

Figure 4-20: Stress-Strain Curve

Ref. Table 1B-2

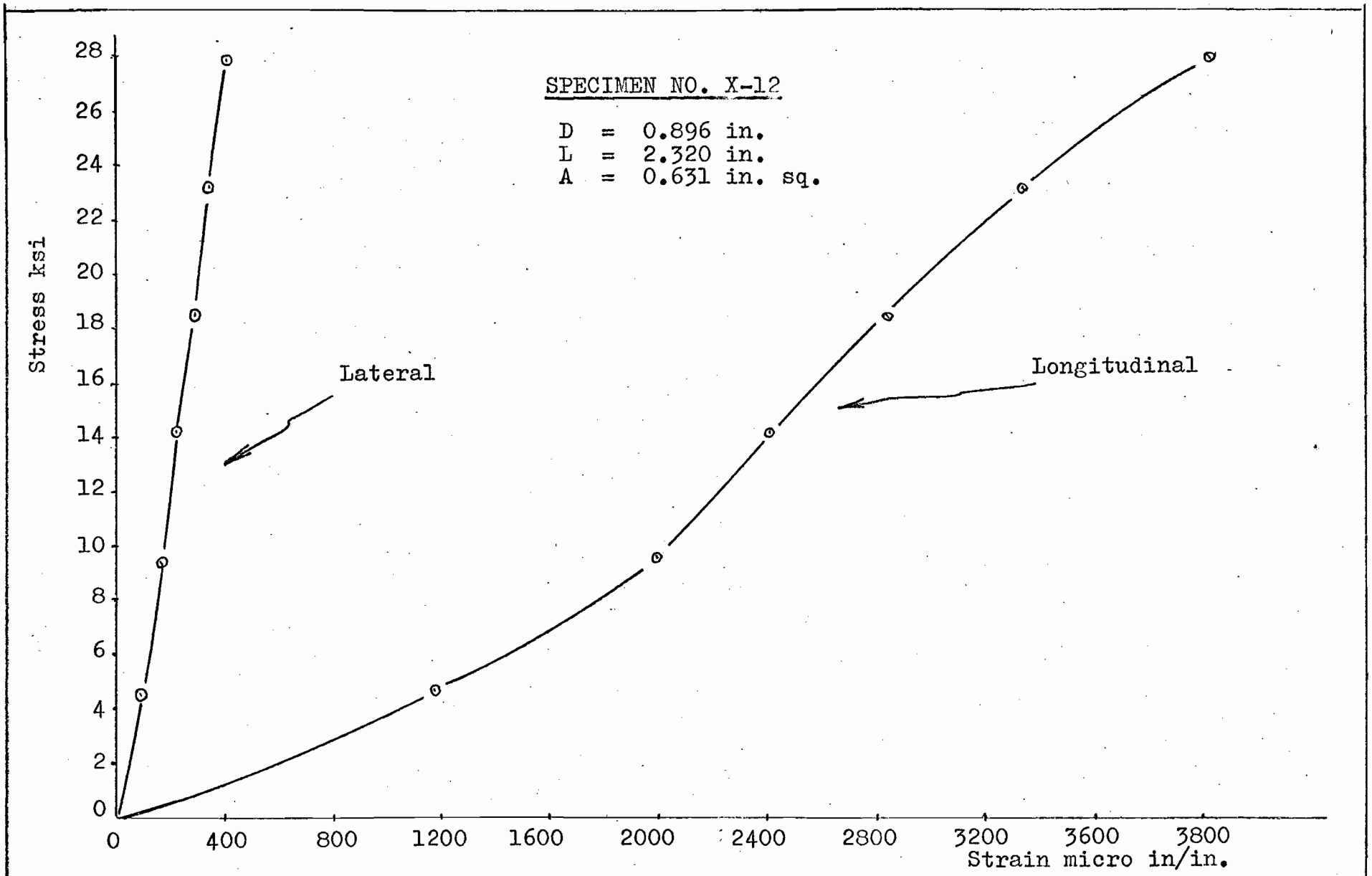

Figure 4-21: Stress-strain curve

Ref. Table 1B-3

SPECIMEN NO. X-15

D = 0.896 in.
L = 2.334 in.
A = 0.631 in. sq.

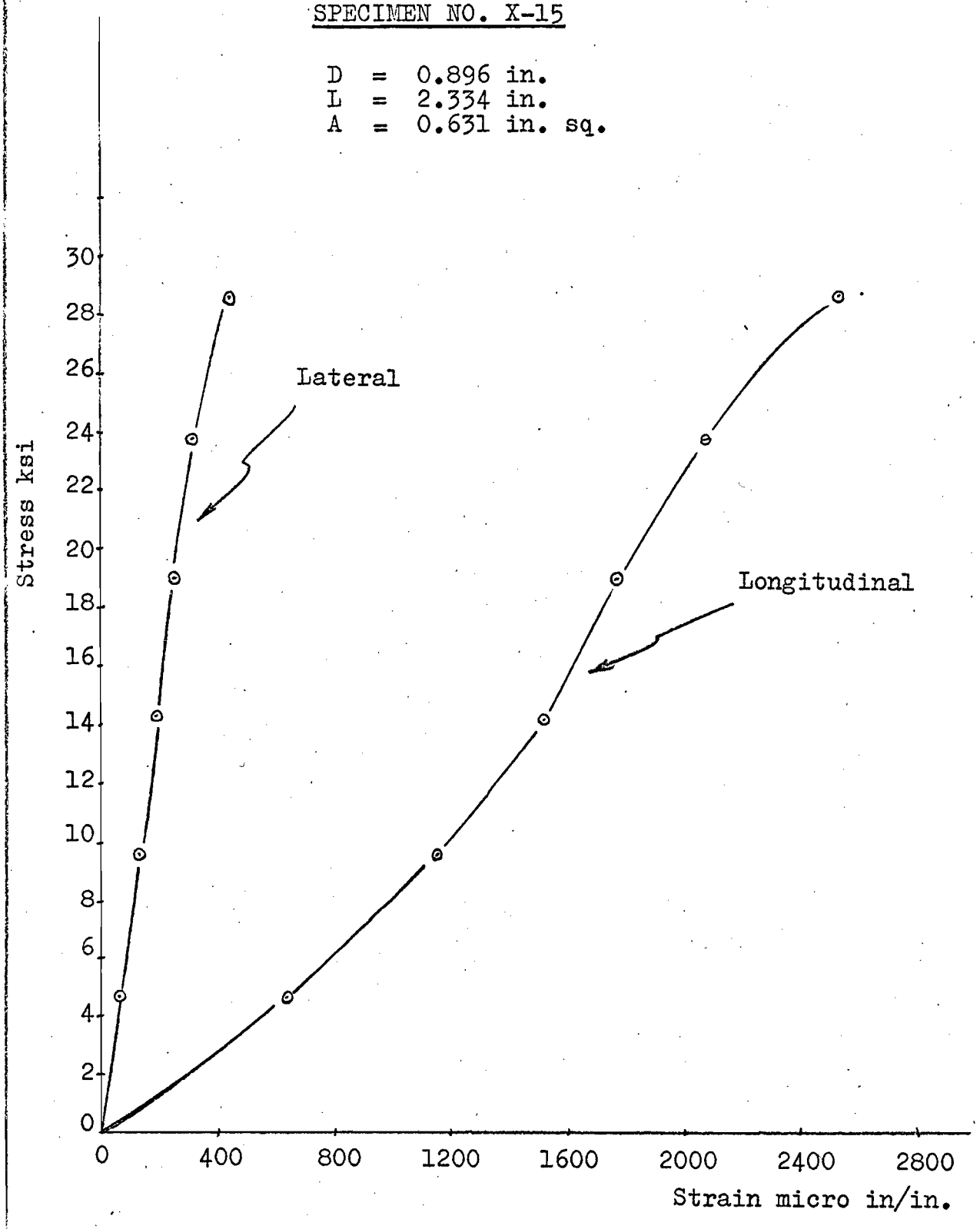

Figure 4-22: Stress-Strain Curve

Ref. Table 1B-4

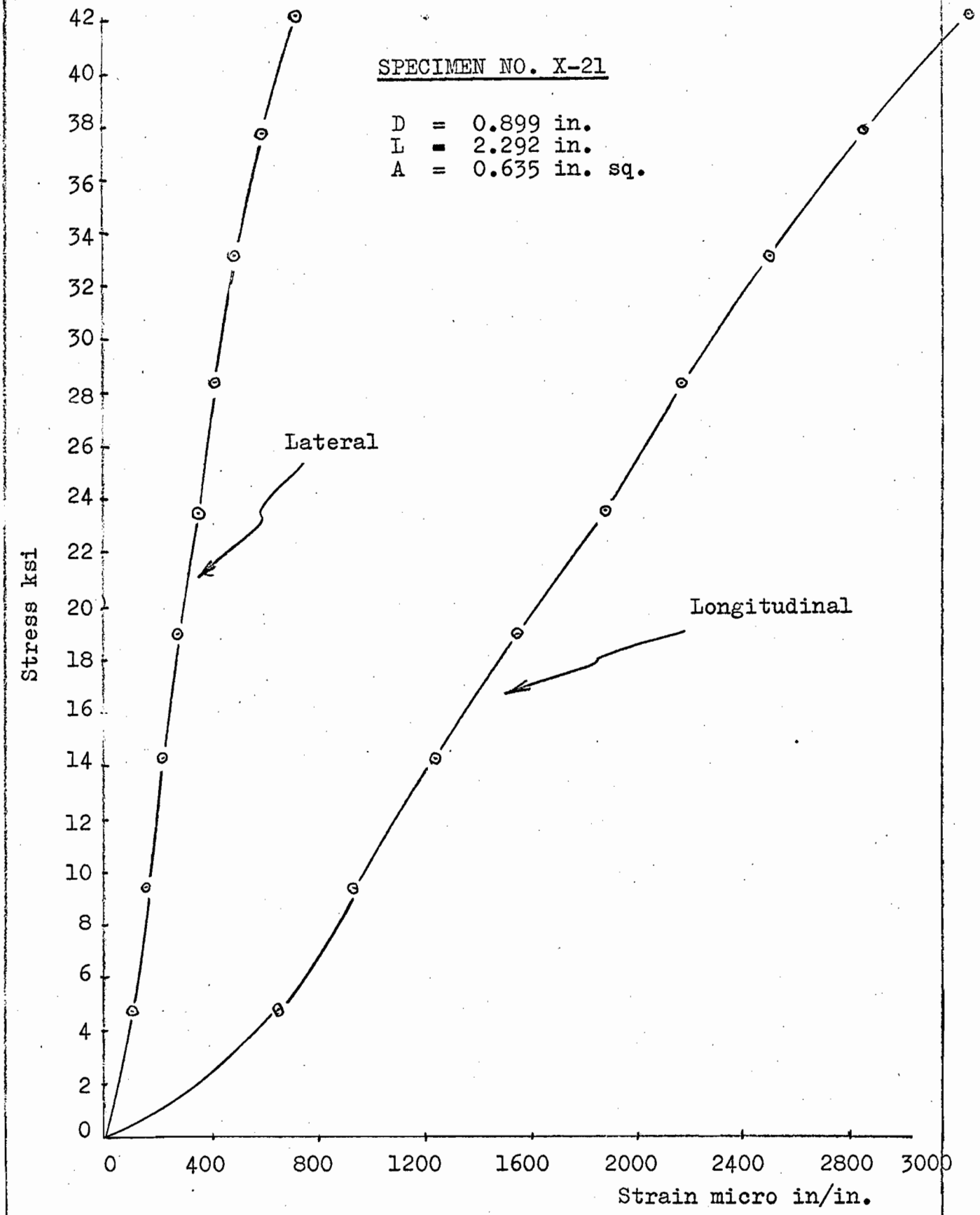

Figure 4-23: Stress-Strain Curve

Ref. Table 1B-5

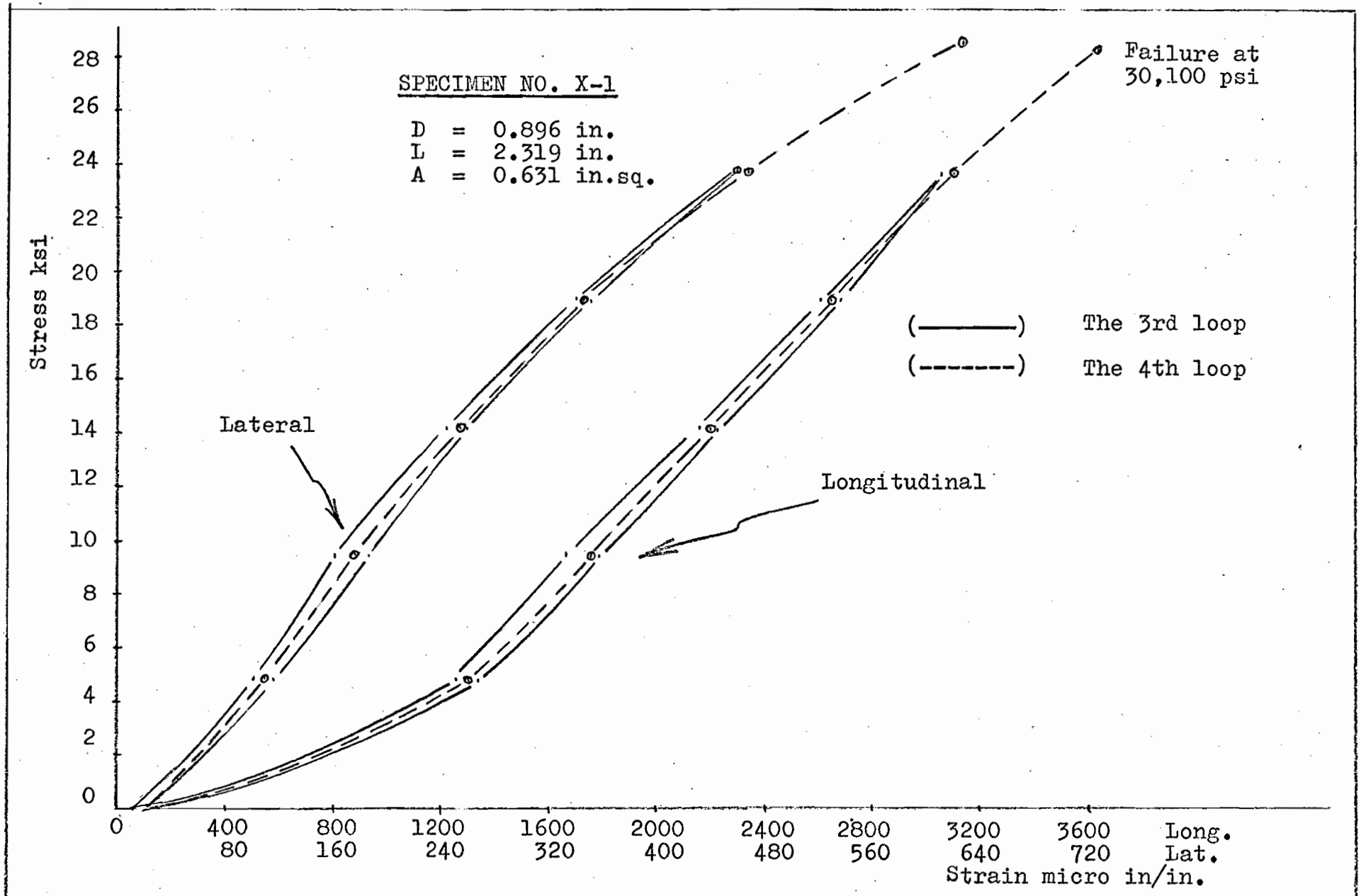

Figure 4-24: Hysteresis Loops on Stress-Strain Curve

Ref. Table 1B-6. The 3rd and 4th loops.

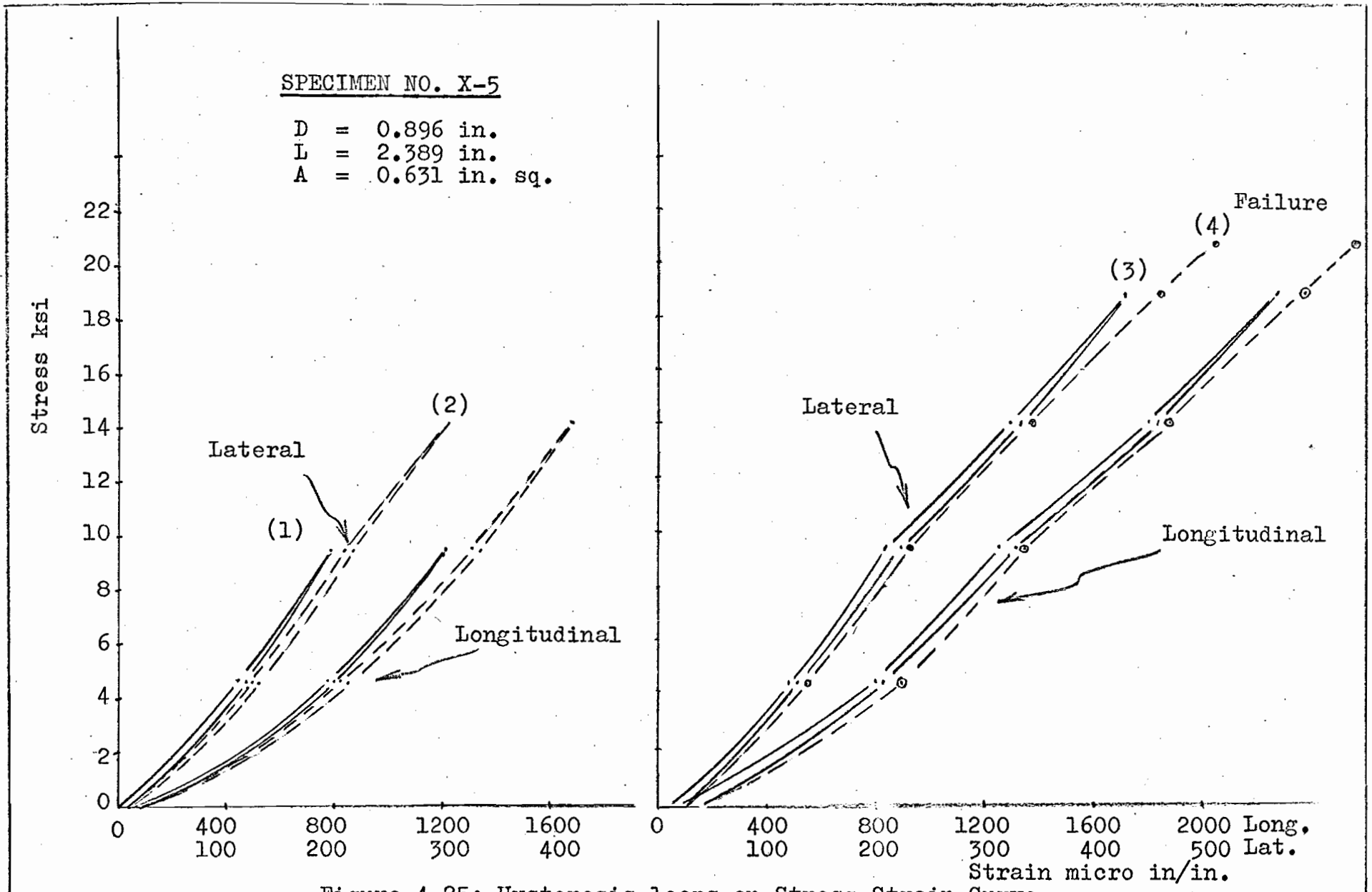

Figure 4-25: Hysteresis loops on Stress-Strain Curve

Ref. Table 1B-7

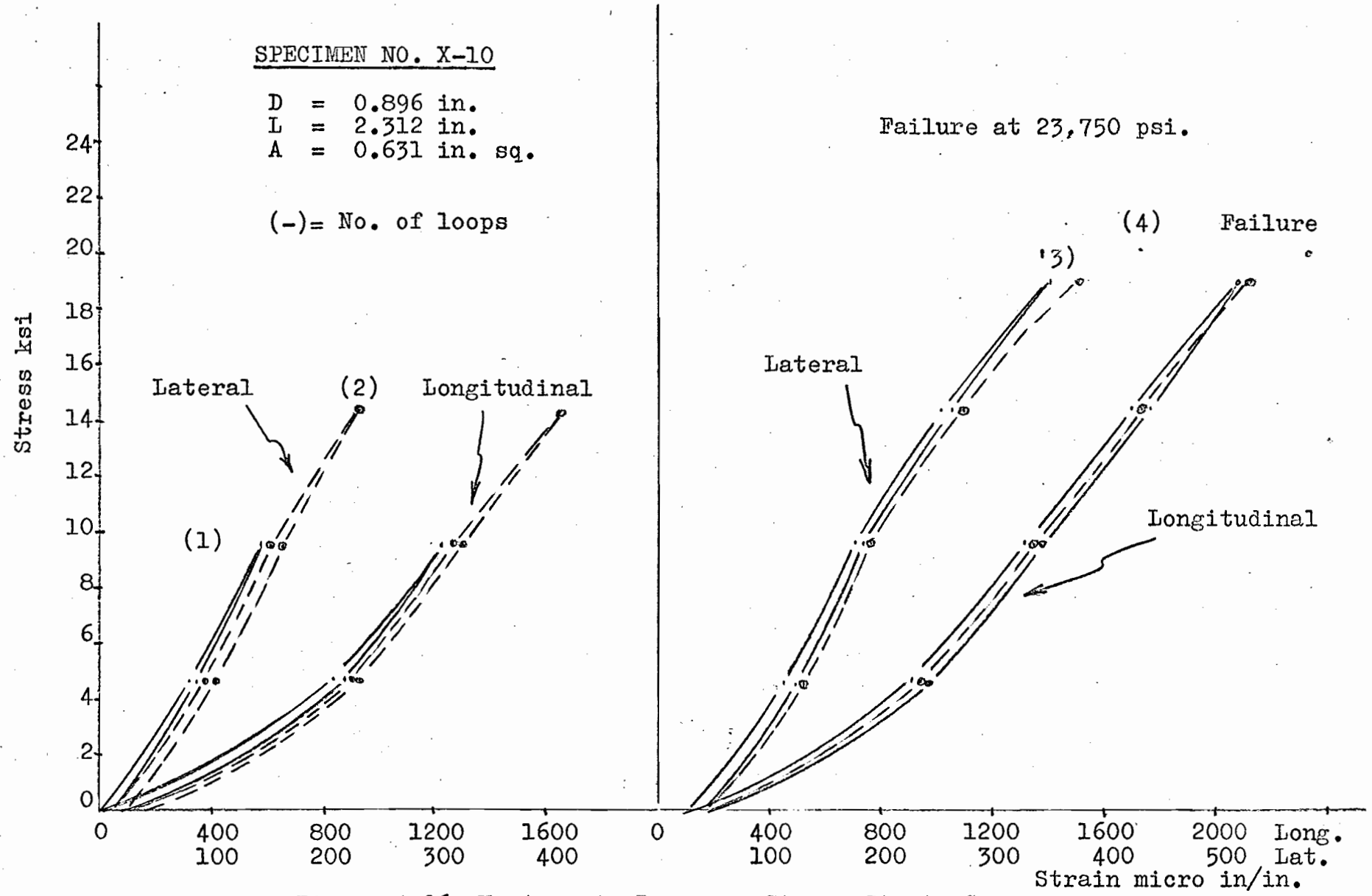

Figure 4-26: Hysteresis Loops on Stress-Strain Curve

Ref. Table 1B-8

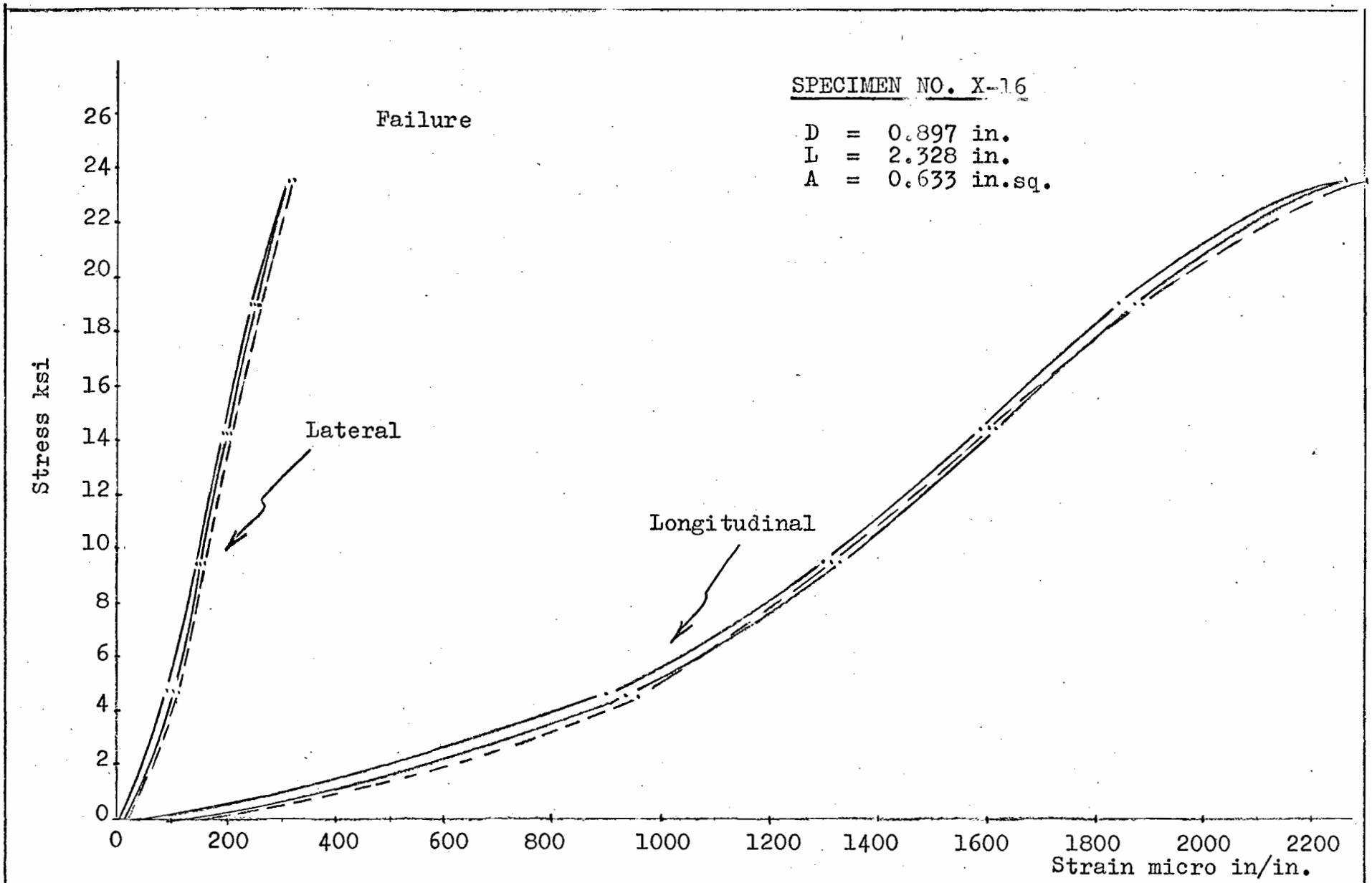

Figure 4-27: Hysteresis Loops on Stress-Strain Curve

Ref. Table 1B-10. Last two loops.

SPECIMEN NO. X-18

D = 0.896 in.
L = 2.420 in.
A = 0.631 in. sq.

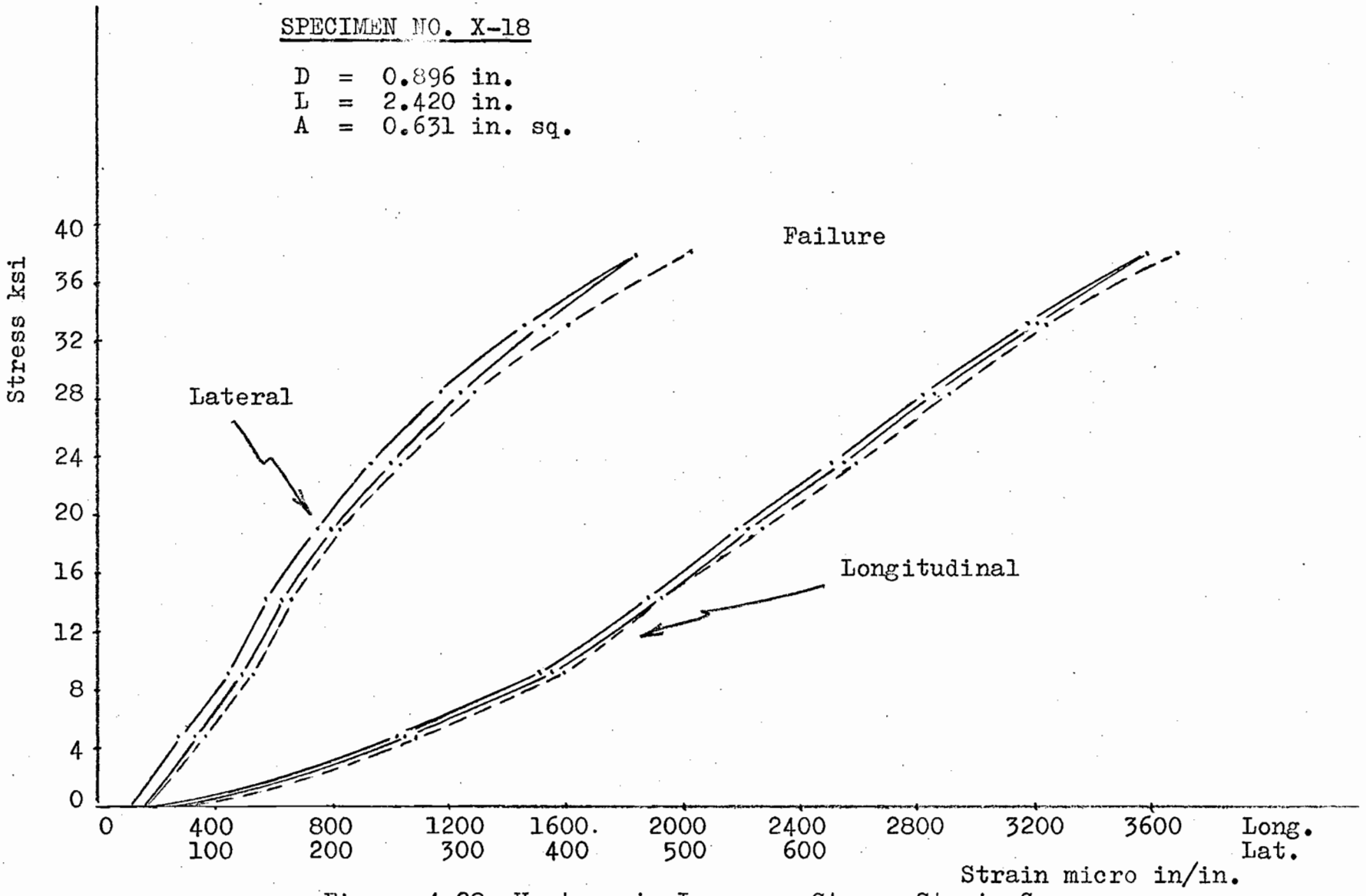

Figure 4-28: Hysteresis Loops on Stress-Strain Curve

Ref. Table 1B-11. Last two loops.

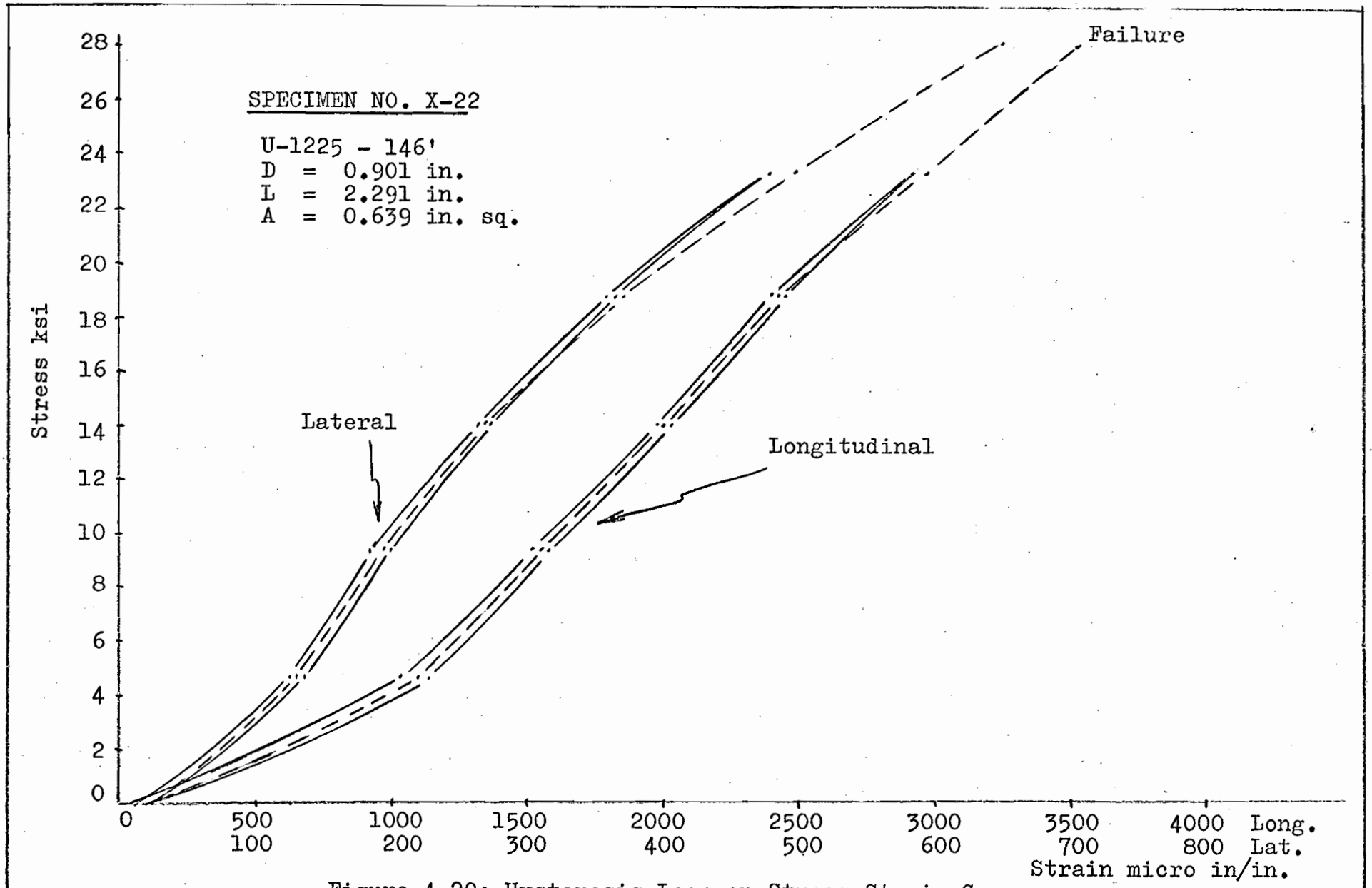

Figure 4-29: Hysteresis Loop on Stress-Strain Curve

Ref. Table 1B-12. The last two loops.

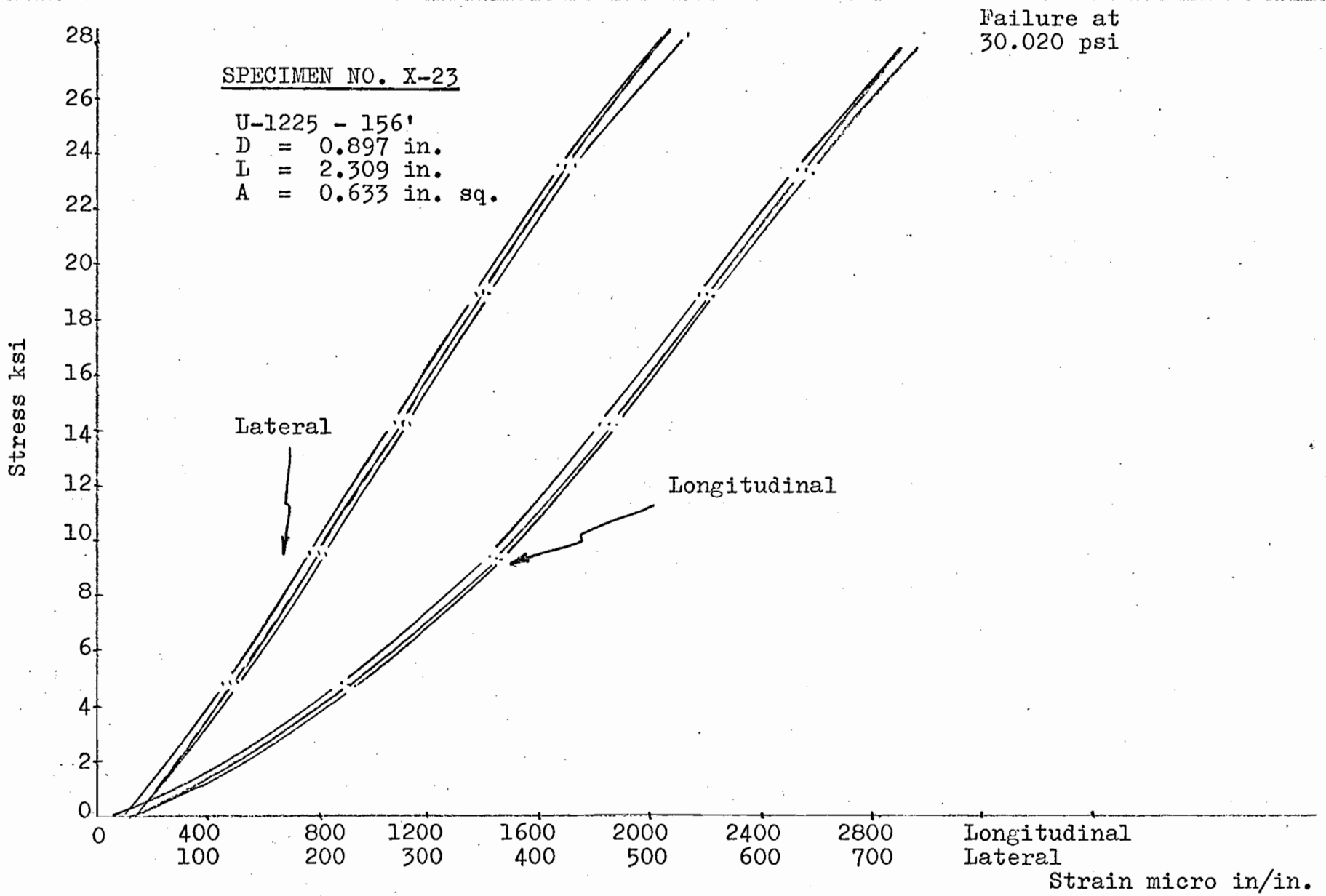

Figure 4-30: Hysteresis Loops on Stress-Strain Curve

Ref. Table 1B-13. Last two loops.

SPECIMEN NO. X-25

U-1225 - 169'
D = 0.896 in.
L = 2.329 in.
A = 0.627 in. sq.

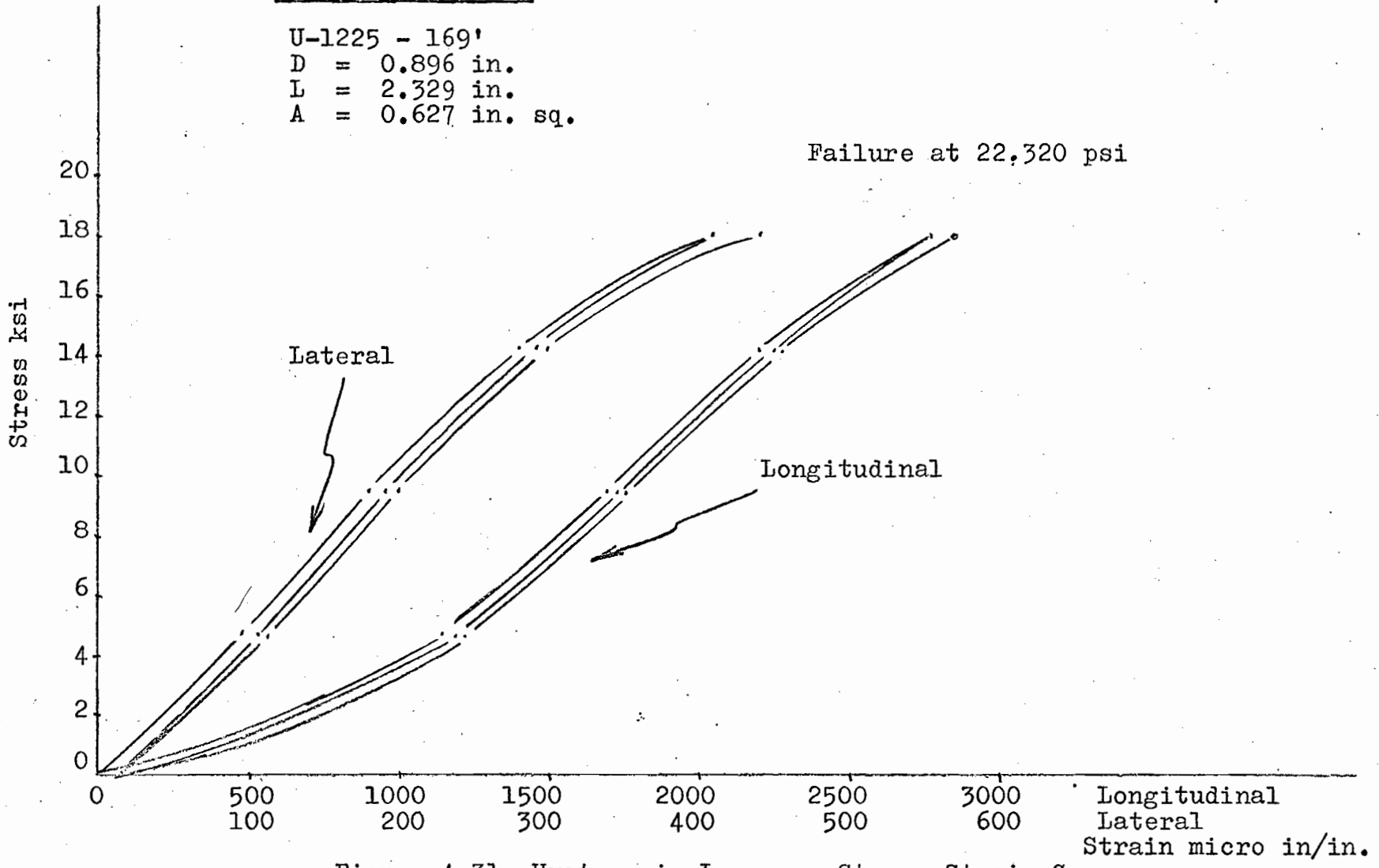

Figure 4-31: Hysteresis Loops on Stress-Strain Curve

Ref. Table 1B-14. Last two loops.

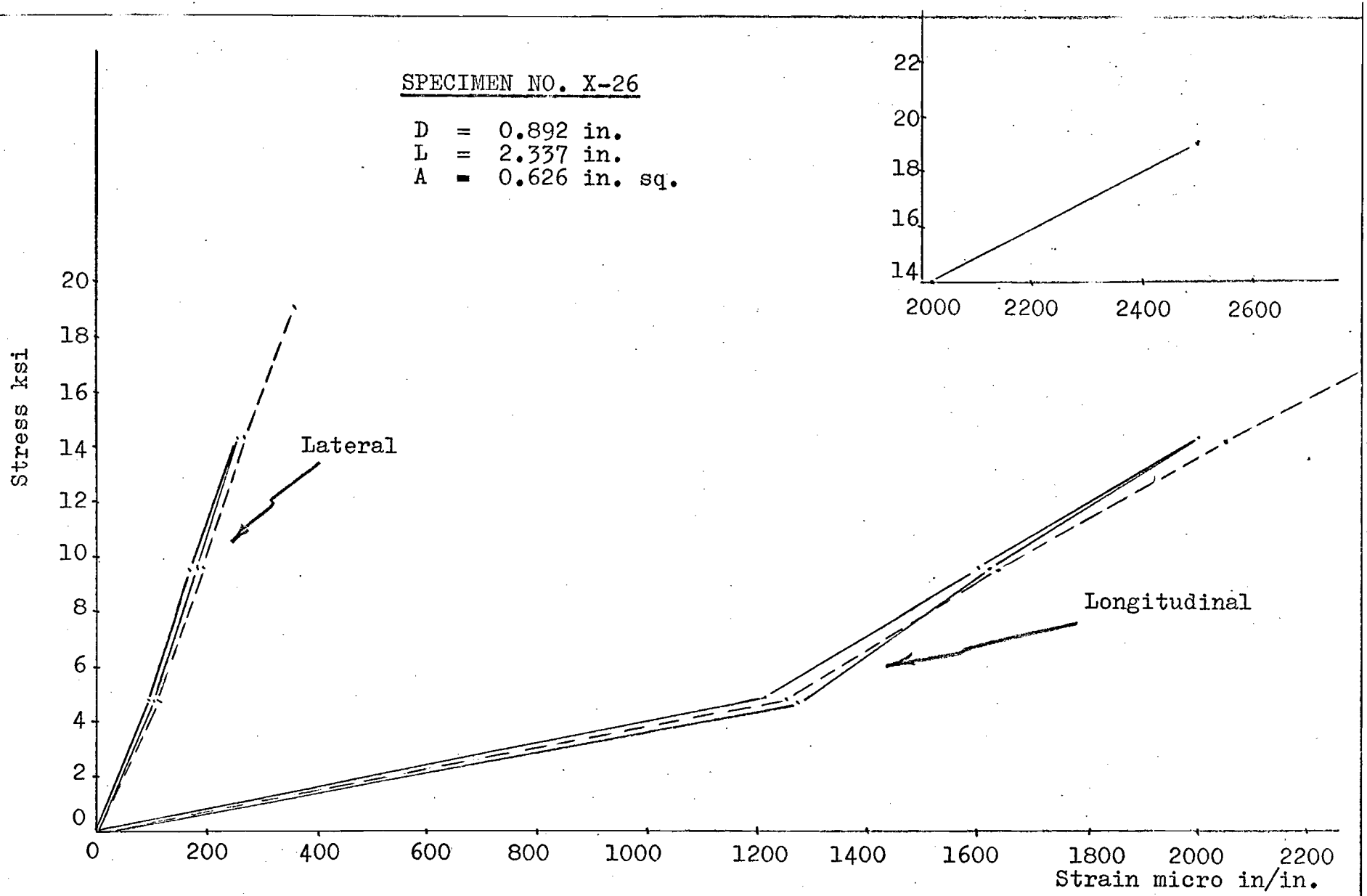

Figure 4-32: Hysteresis Loops on Stress-Strain Curve

Ref. Table 1B-15

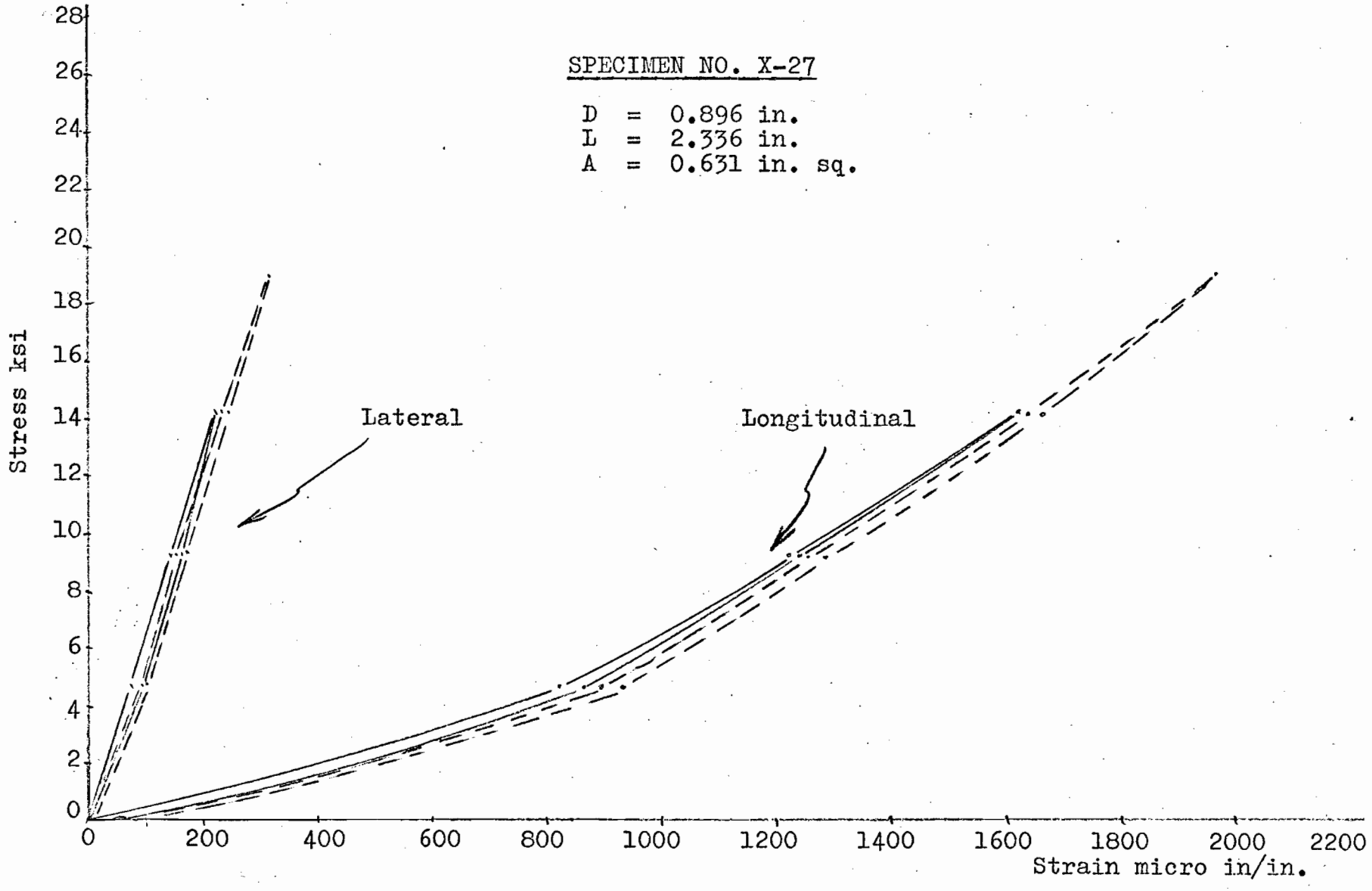

Figure 4-33 (a): Hysteresis Loops on Stress-Strain Diagram

Ref. Table 1B-16. The 1st and 2nd loops.

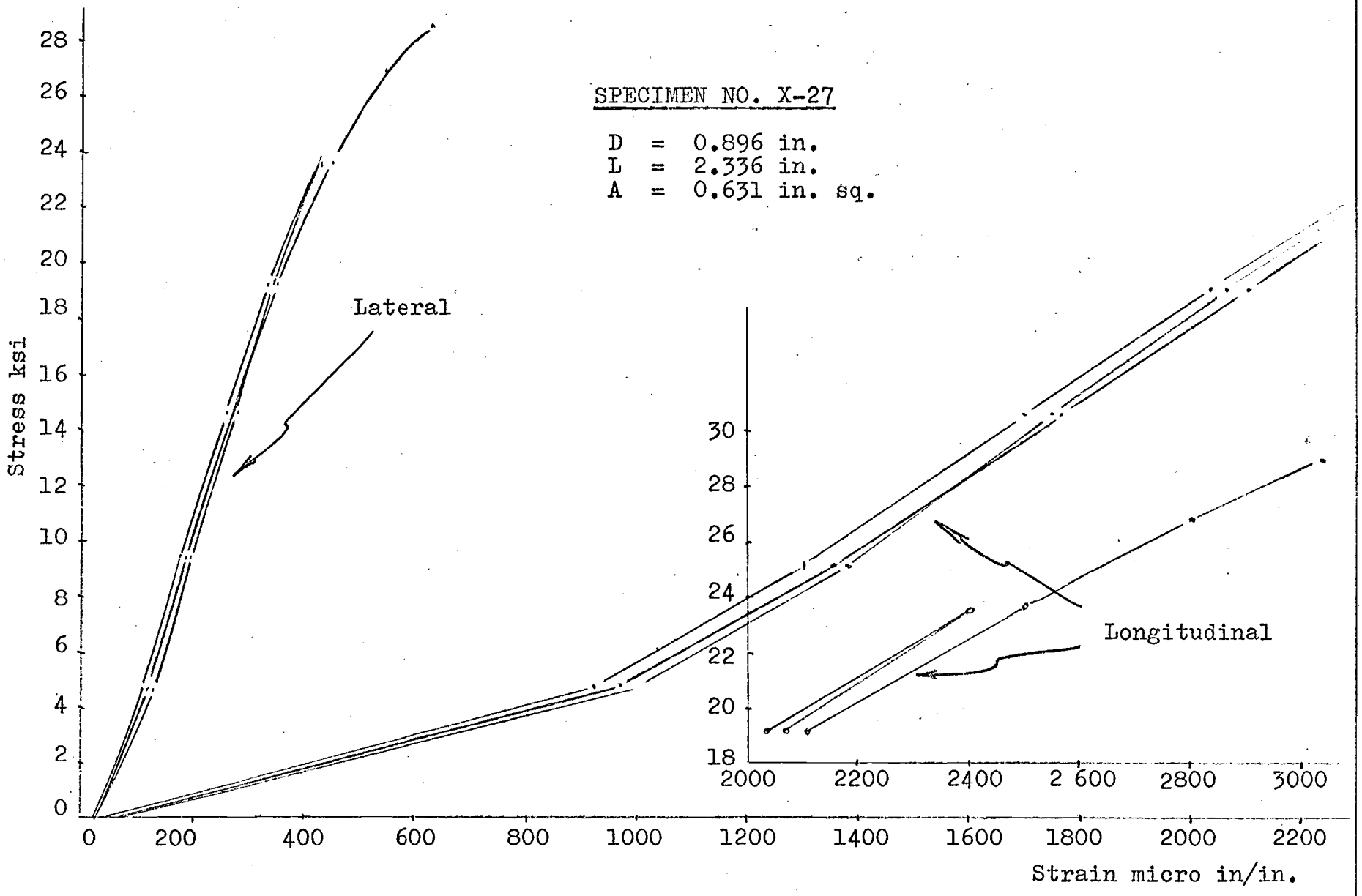

Figure 4-33 (b): Hysteresis Loops on Stress-Strain Curve

Ref. Table 1B-16. The 3rd and 4th loops.

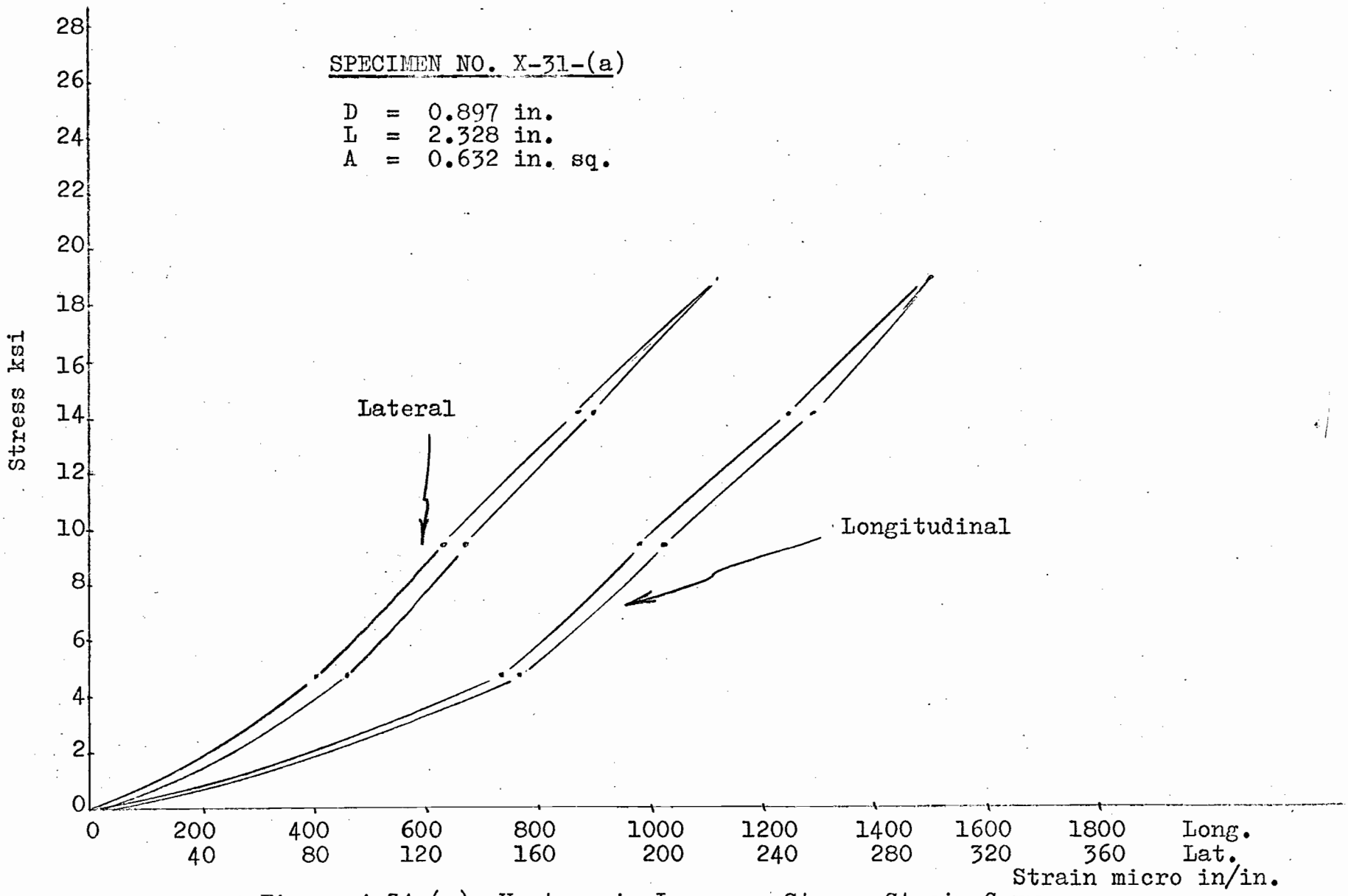

Figure 4-34 (a): Hysteresis Loops on Stress-Strain Curve

Ref. Table 1B-17. The first loop.

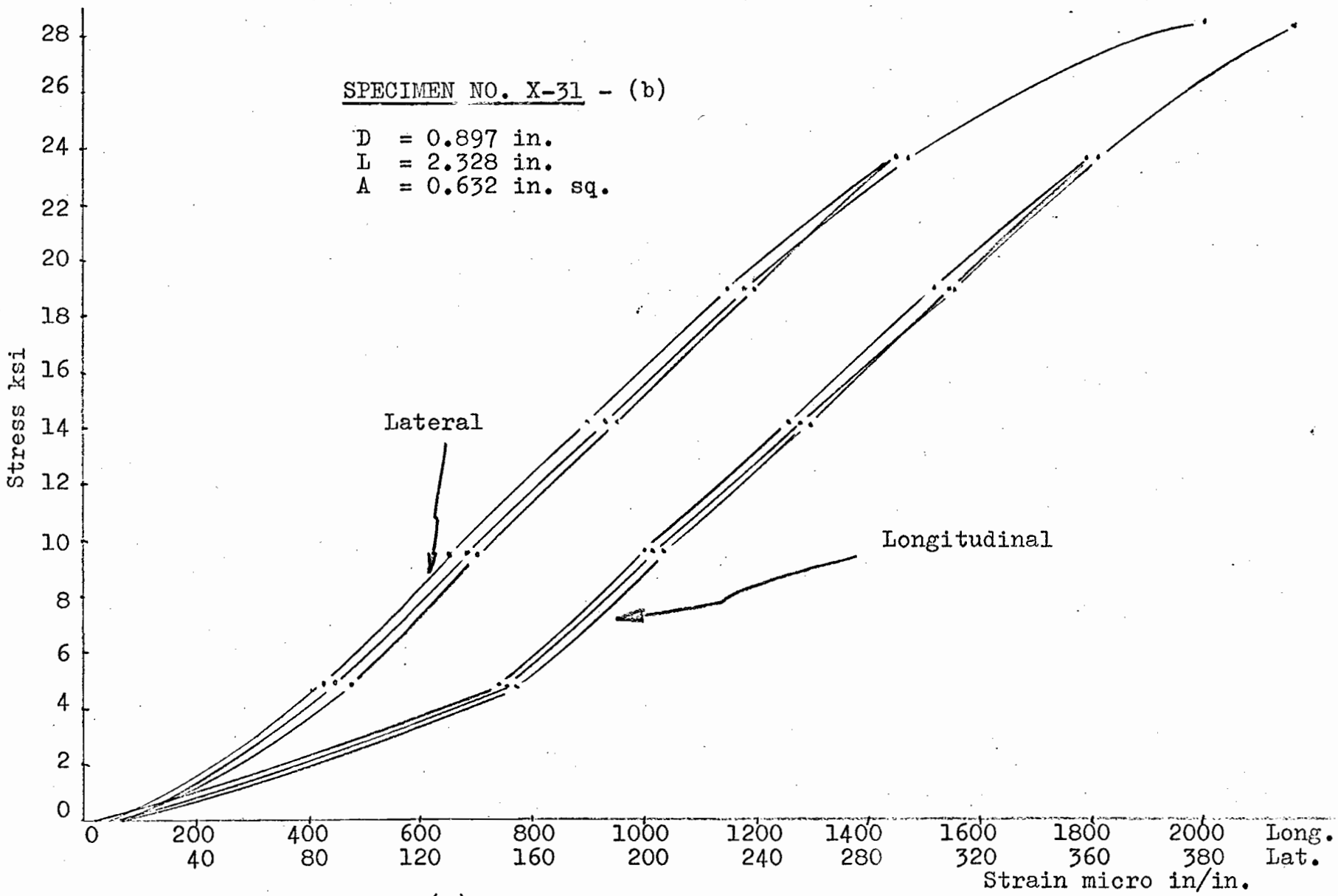

Figure 4-34 (b): Hysteresis Loops on Stress-Strain Curve

Ref. Table 1B-17. The 2nd and 3rd loop.

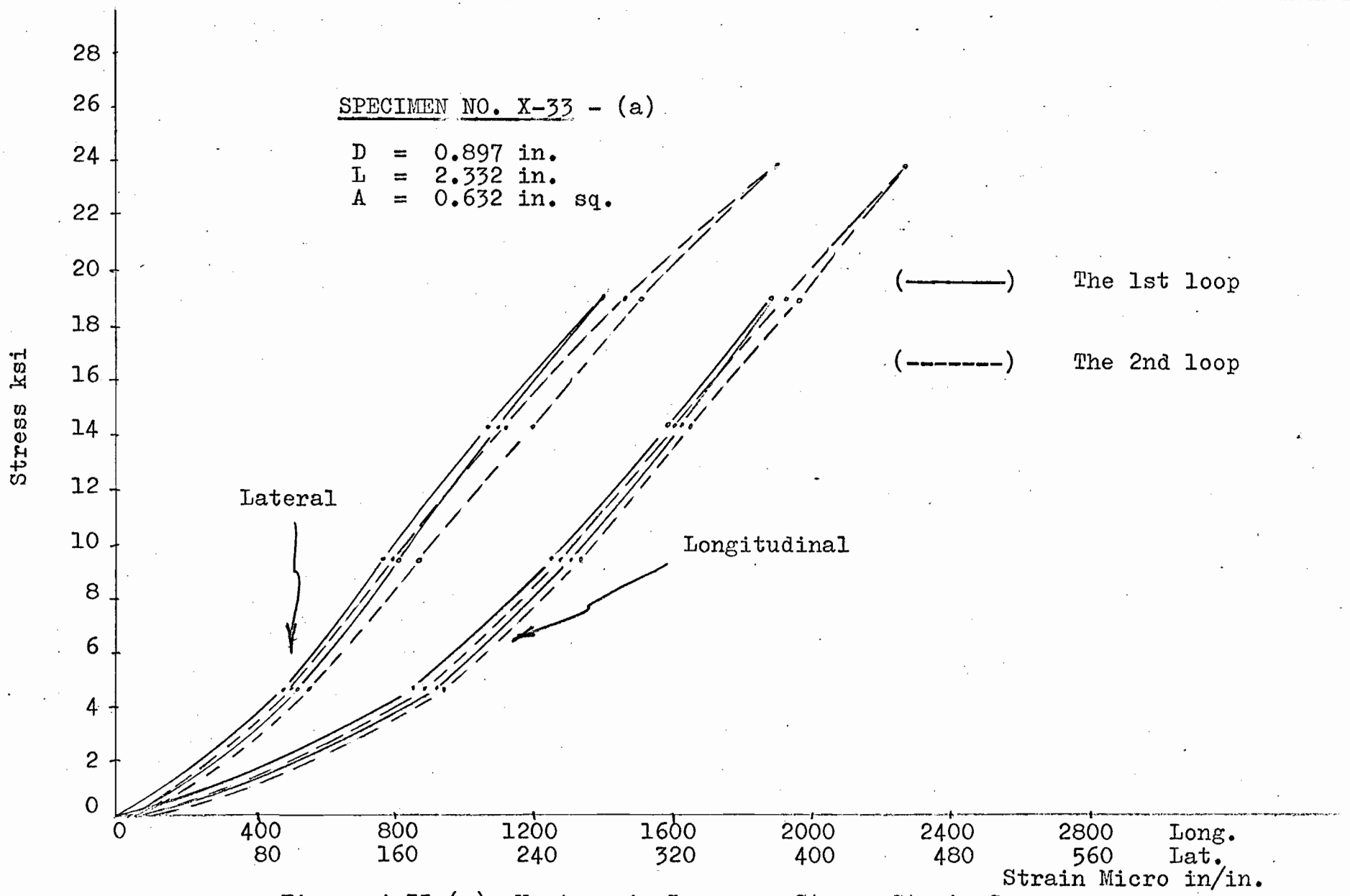

Figure 4-35 (a): Hysteresis Loops on Stress-Strain Curve

Ref. Table 1B-18. The 1st and 2nd loops.

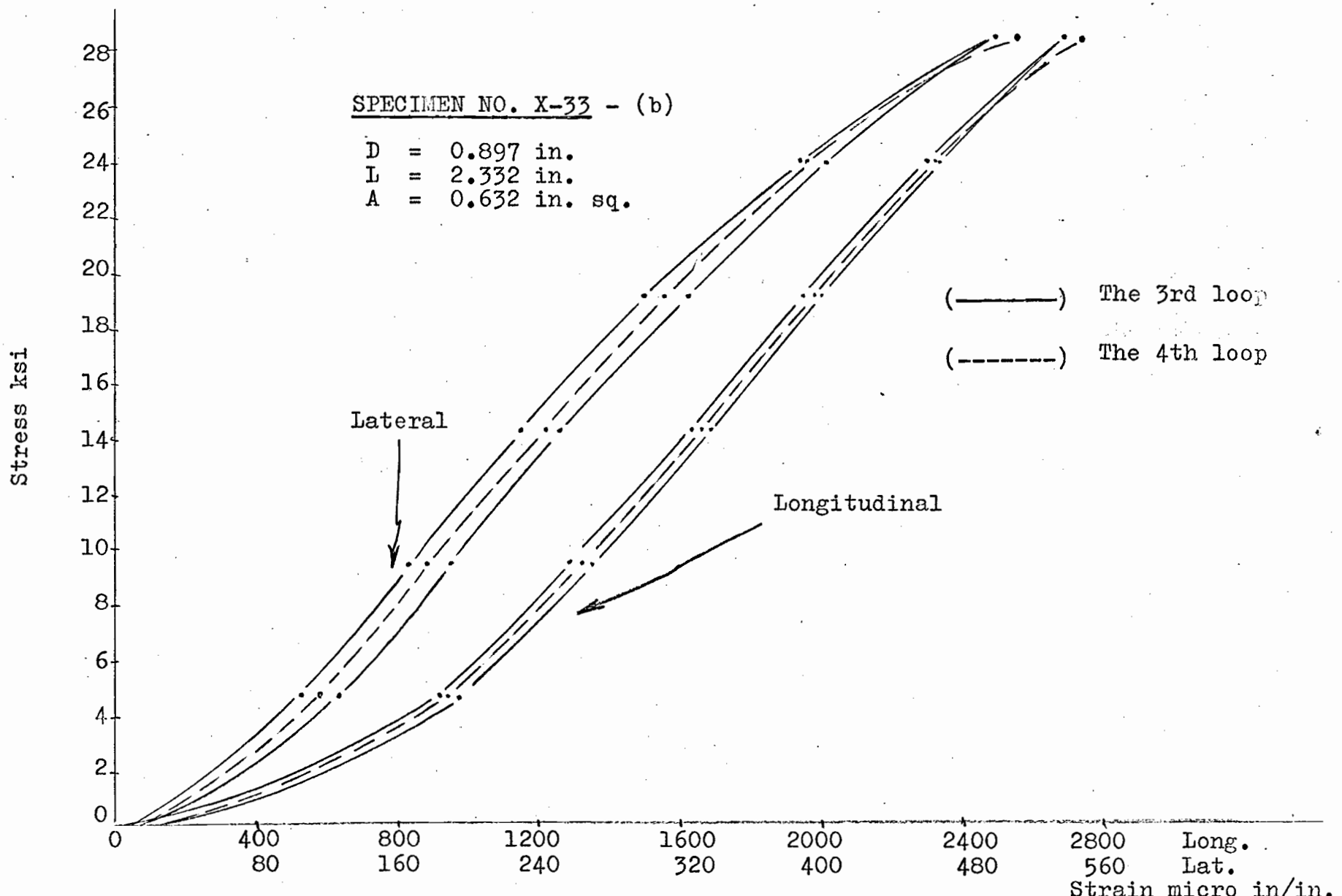

Figure 4-35 (b): Hysteresis Loops on Stress-Strain Curve

Ref. Table 1B-18. Last two loops.

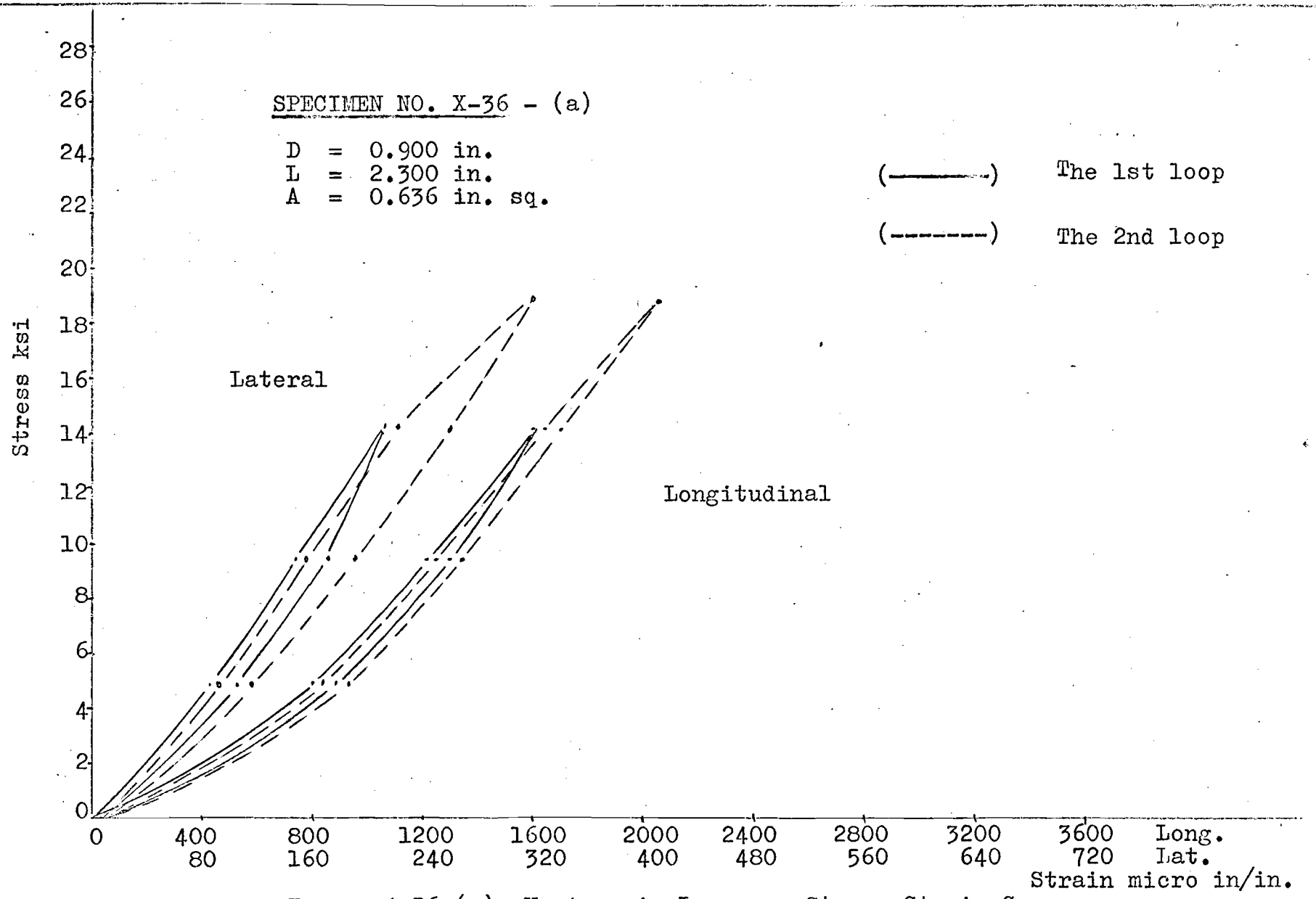

Figure 4-36 (a): Hysteresis Loops on Stress-Strain Curve

Ref. Table 1B-19. The 1st and 2nd loops.

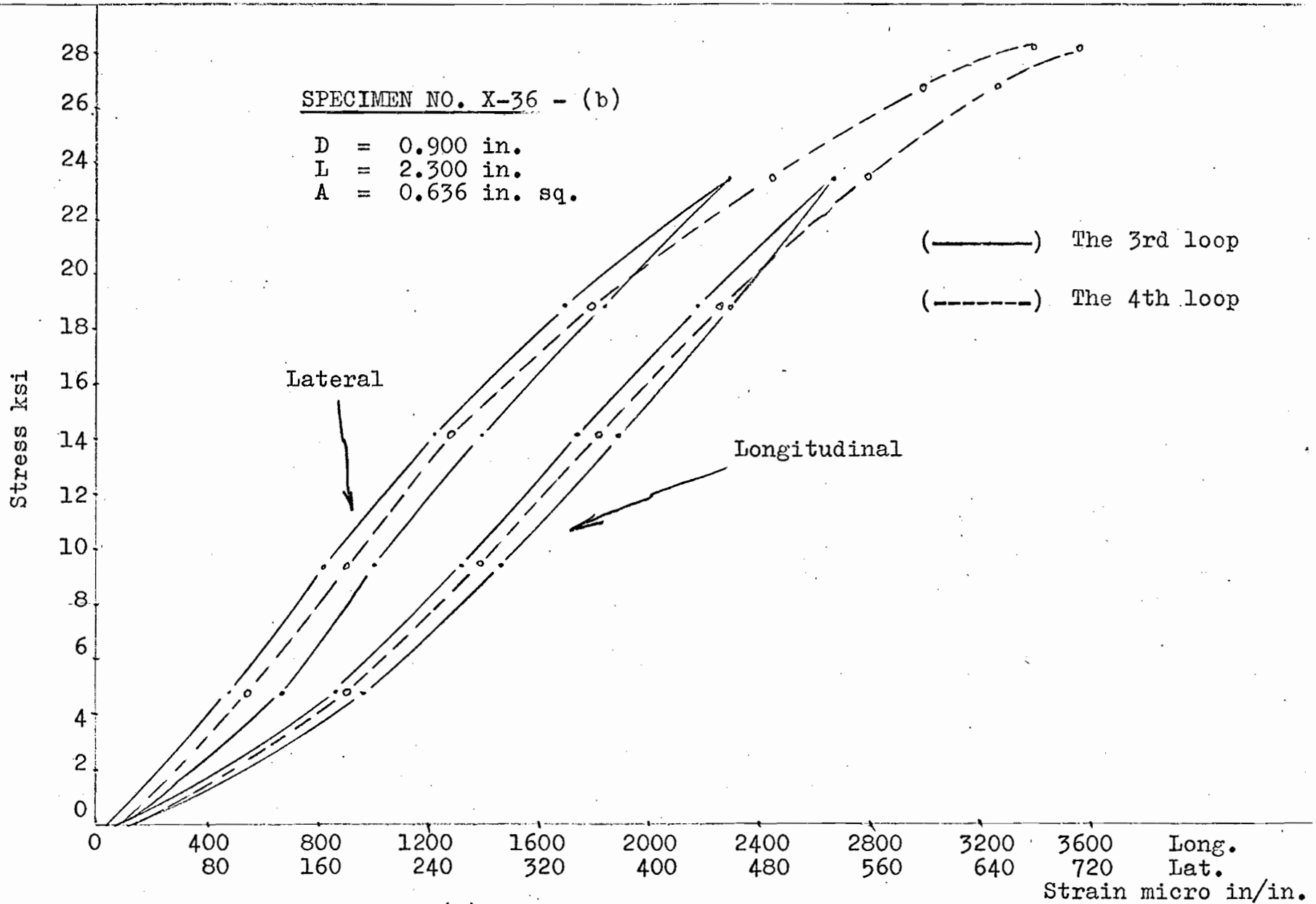

Figure 4-36 (b): Hysteresis Loops on Stress-Strain Curve

Ref. Table 1B-19. The 3rd and 4th loops.

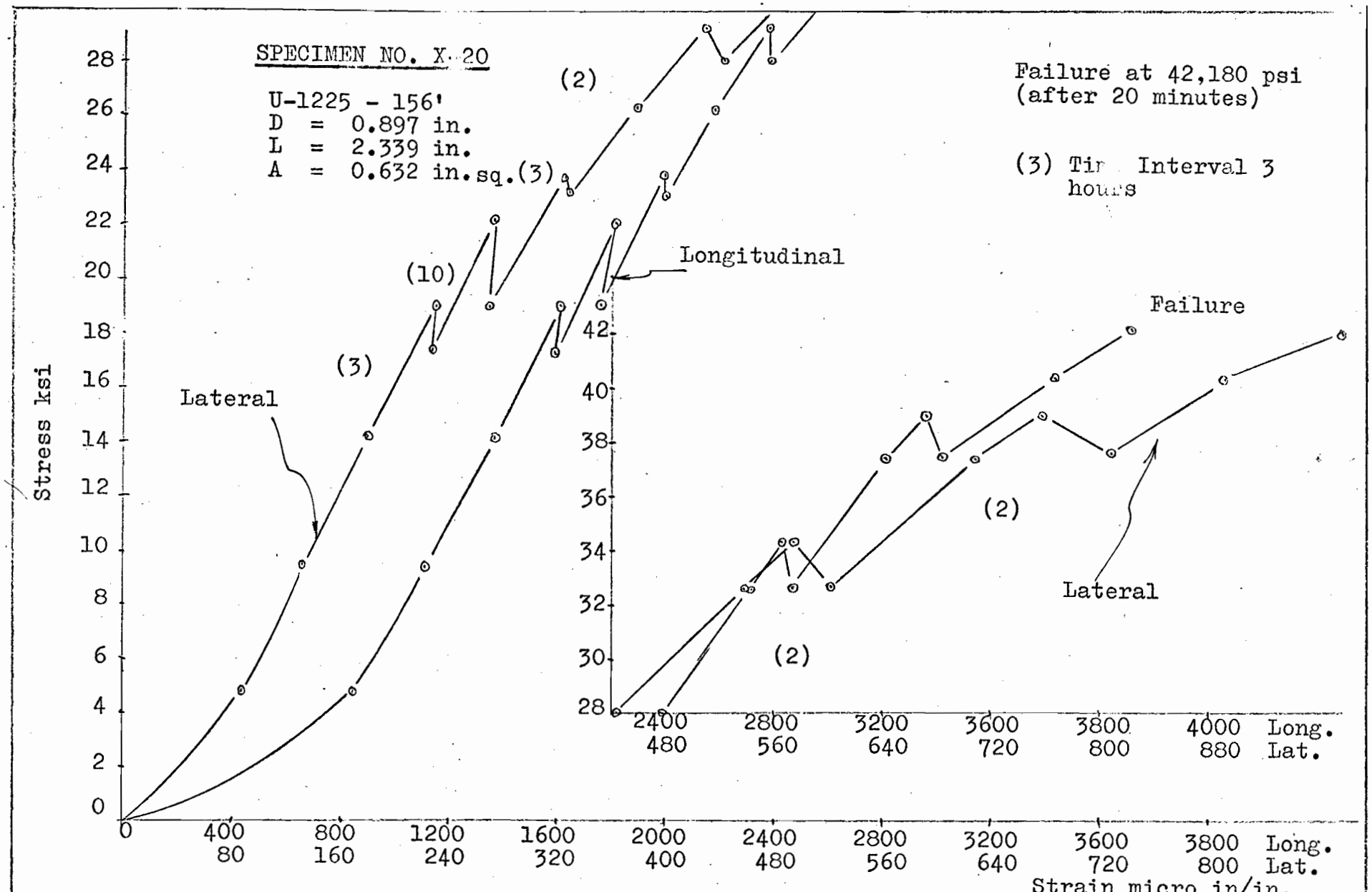

Figure 4-37: The Effect of Time on Stress-Strain Characteristic of Skarn

Ref. Table 1B-20

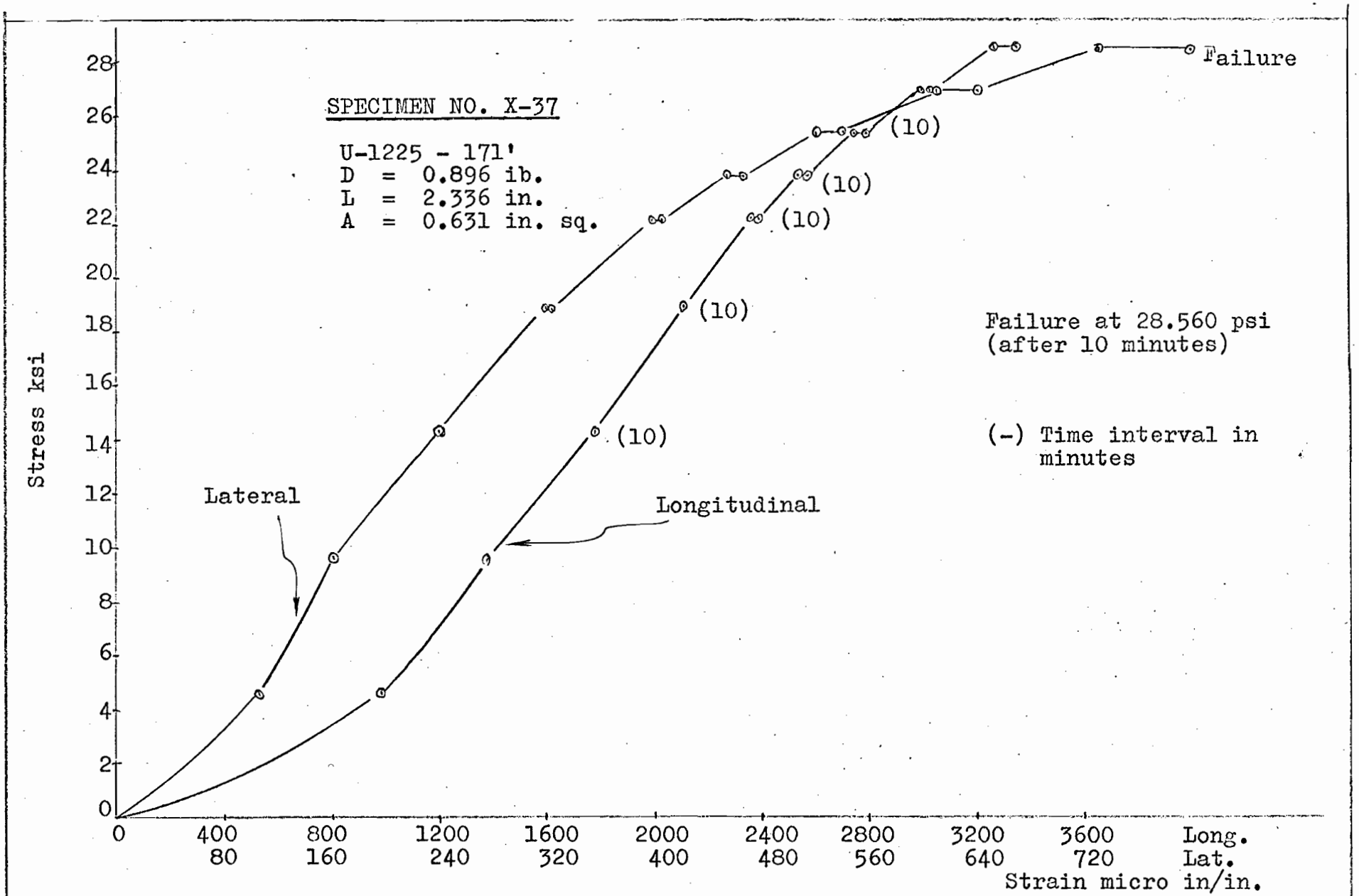

Figure 4-38: The Effect of Time on Stress-Strain Characteristic of Skarn

Ref. Table 1B-21

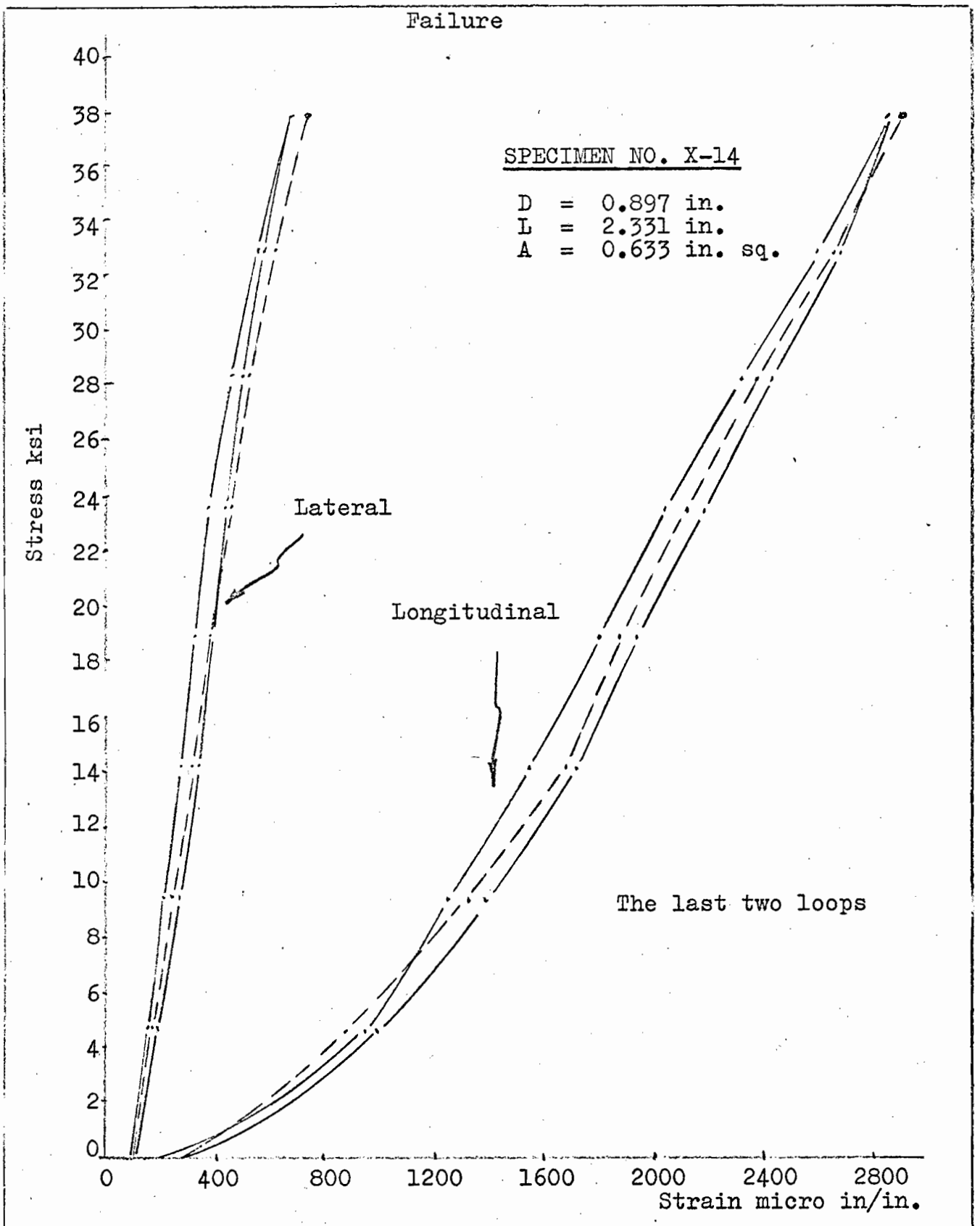

Figure 4-38 (b): Hysteresis Loops on Stress-Strain Curve

Ref. Table 1B-9

SPECIMEN NO. AB-1 - (a)

D = 2.112 in.
L = 5.686 in.
A = 3.50 in. sq.

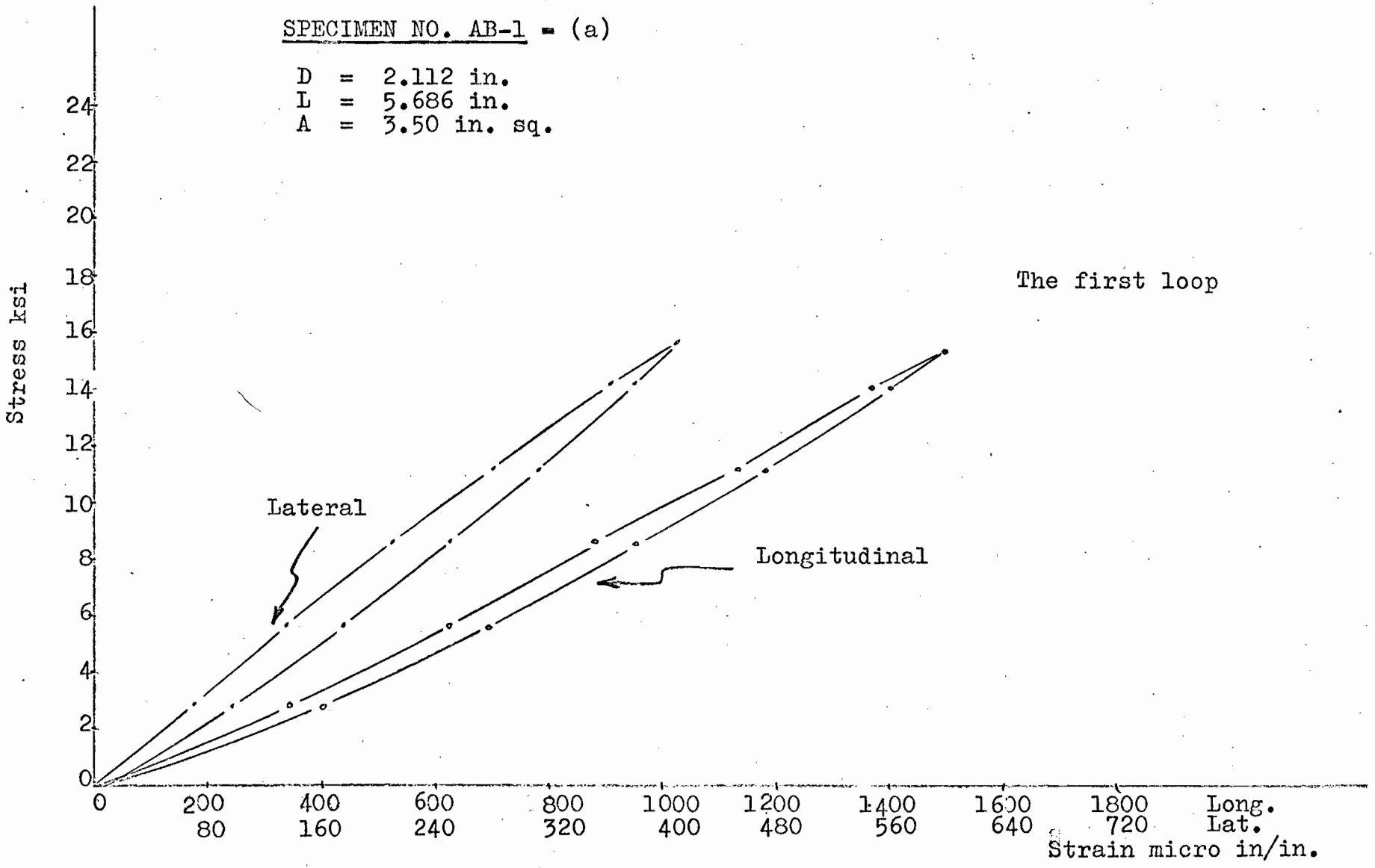

Figure 4-39 (a): Hysteresis Loop on Stress-Strain Curve

Ref. Table 1B-22. The 1st loop.

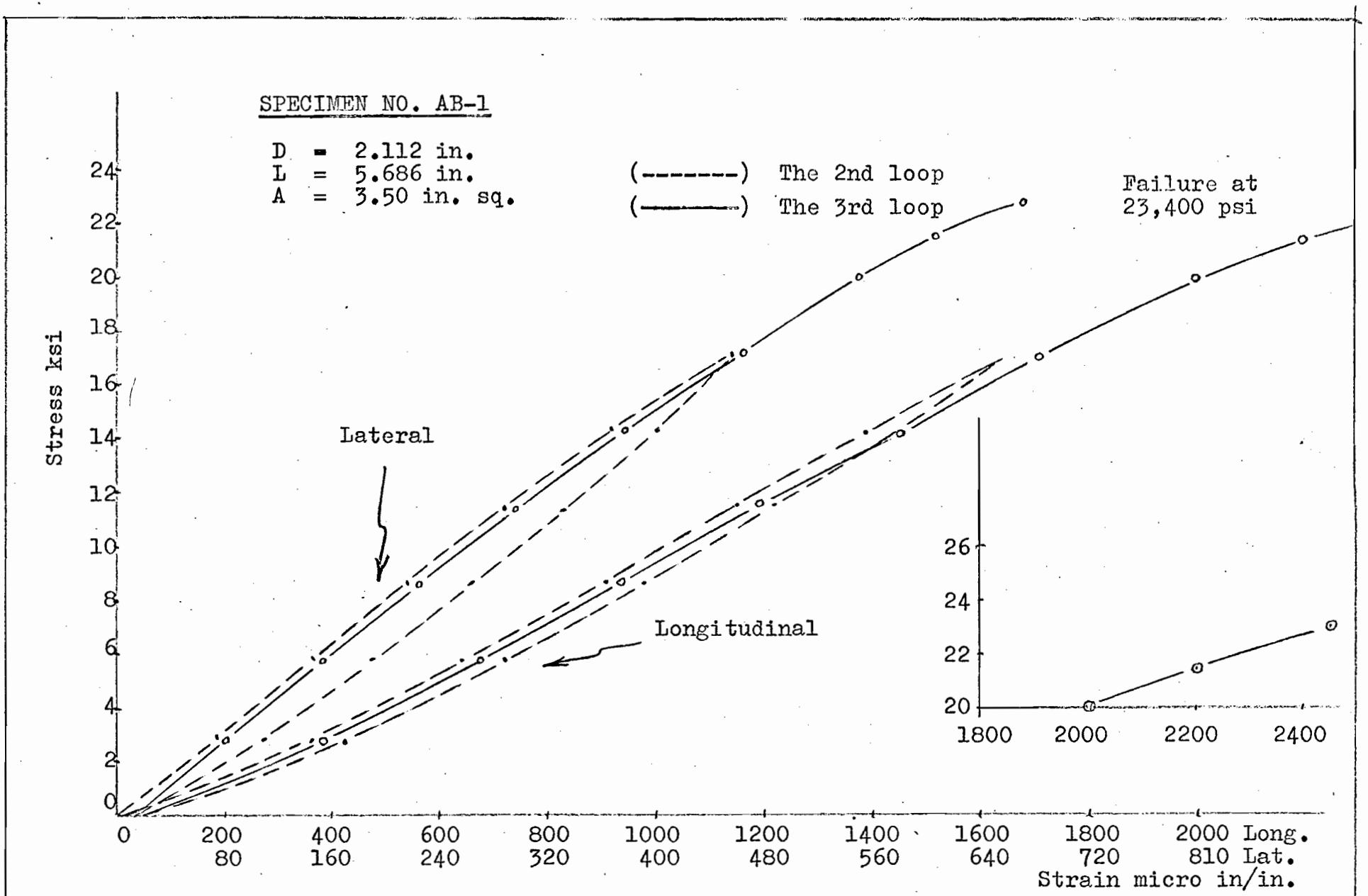

Figure 4-39 (b): Hysteresis Loops on Stress-Strain Curve

Ref. Table 1B-22 The 2nd and 3rd loops

(C) Lateral deformation tests

Two types of lateral deformation tests under uniaxial compression were carried out to examine the lateral strain distribution at different positions in the specimen. These are free end and lubricated end tests. The Louis Small Compression Tester and two strain gauge indicators, one for load reading and one for strain reading, (Figure 4-18), were employed for each type of test.

Specimens were prepared from NX-core (2-1/8 in. diameter) with an L/D ratio of approximately 2.5. Seven SR-4 strain gauges were placed on each specimen; five lateral strain gauges on one side and two longitudinal strain gauges at 90 degrees on either side, with respect to the lateral strain gauges, at the mid-height of the specimen.

Specimen No. AB-2 was tested with free ends. The load was applied to failure with a 5,000 pound loading interval. The strains were observed at each loading interval. The lateral strain distribution curve for various loads is shown in Figure 4-40 and the stress-strain curves for all gauges is shown in Figure 4-41. The detailed data for this specimen can be found in Table 1B-23 in the Appendix.

For lubricated ends, specimen No. AB-3 was tested. The load was applied to 60,000 lbs. with a 10,000 lb. loading interval returning the load to zero

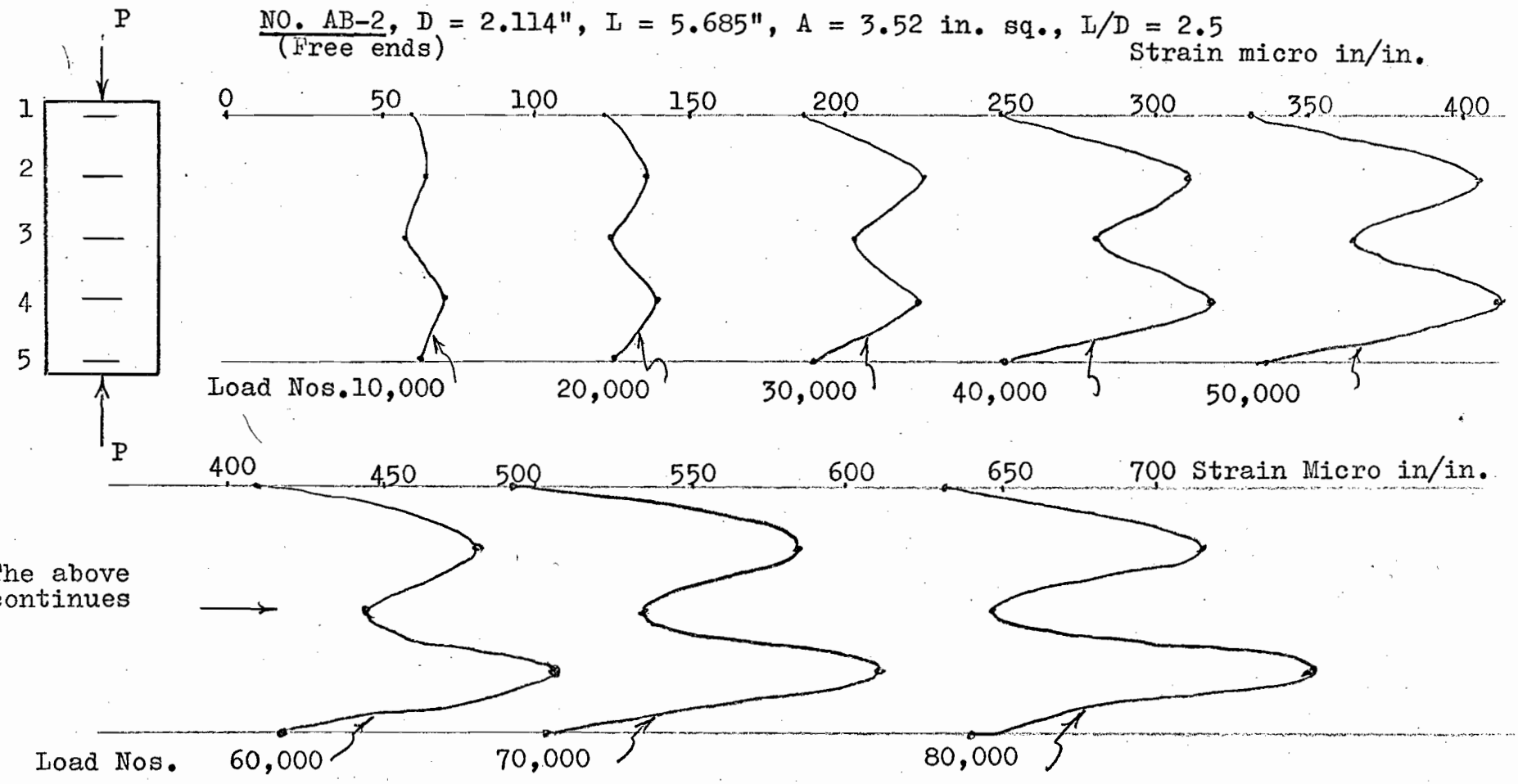

Figure 4-40: Lateral Deformation of Skarn with Free Ends under Uniaxial Compression

Ref. Table 1B-23

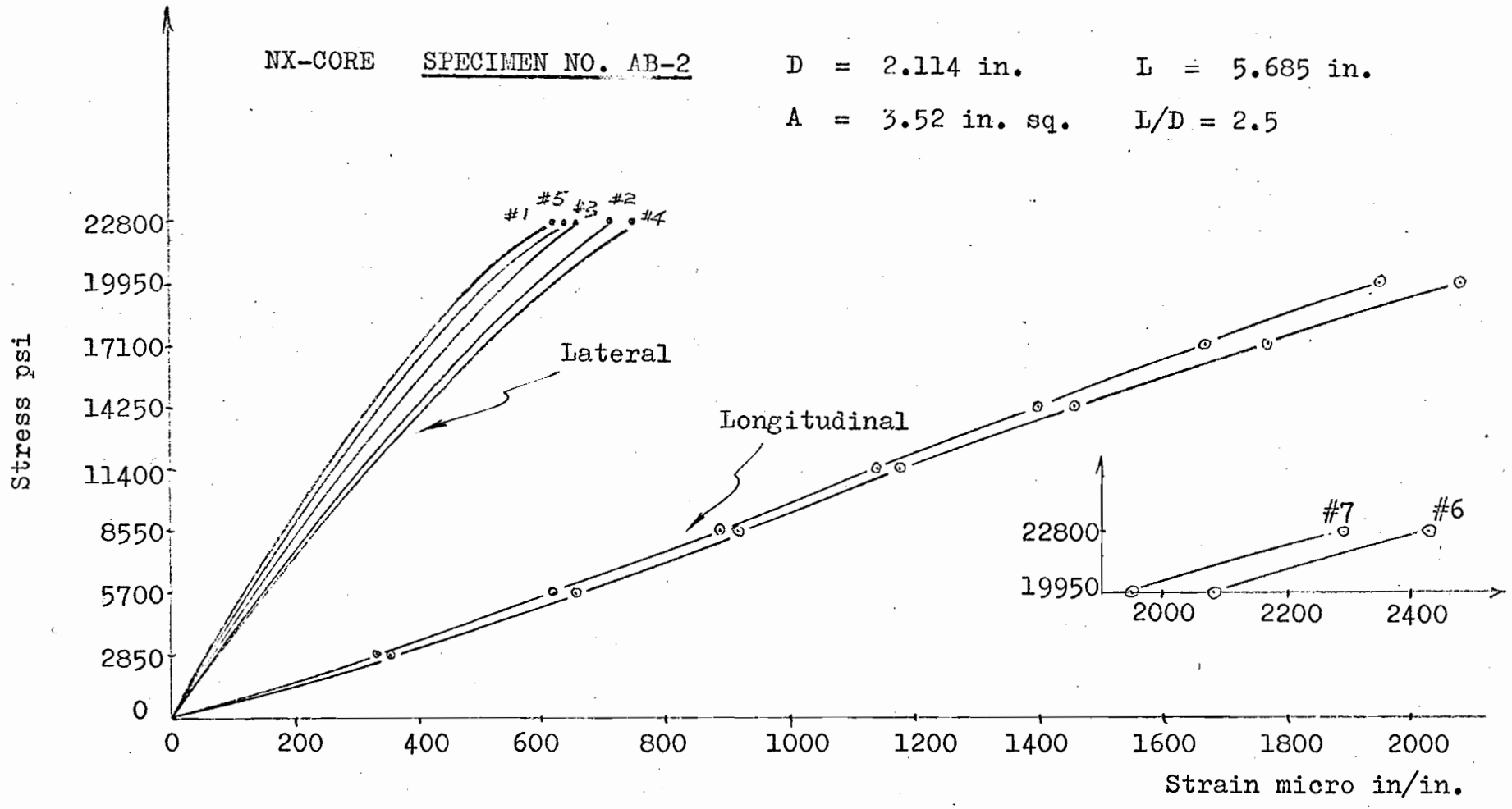

Figure 4-41: Stress-Strain Curve of Skarn with Free Ends Under Uniaxial Compression

Ref. Table 1B-23

through the same loading intervals. This gives the first loading and unloading cycle. The specimen was again loaded incrementally as in cycle No. 1 but continued to failure. Figure 4-42 shows the strain distribution for the lateral strain gauges during the second cycle. The stress-strain curves for all seven strain gauges on this specimen are shown in Figure 4-43. Table 1B-24, in the Appendix, gives the detailed data of this specimen.

This specimen, AB-3, with lubricated ends, failed at 22,800 psi with a tensile type of failure, as shown in Figure 4-12(a). Characteristic of this type of failure is the absence of any grinding effect in the failure plane which invariably is parallel to the major principal stress. The explanation for this type of failure rests with the condition of the specimen ends with respect to the platens and will be discussed later.

Specimen No. AB-5 was tested without lubrication over three loading and unloading cycles, the second of which is shown in Figure 4-44.

Following the above cycling, the specimen ends were dipped in liquid paraffin and cooled prior to further testing.

The specimen was then loaded incrementally at 10,000 lb. intervals to 40,000 lbs. and unloaded in similar intervals. The results for both free and lubricated ends for this specimen are shown in Figures 4-44 and 4-45. The detailed data for the tests

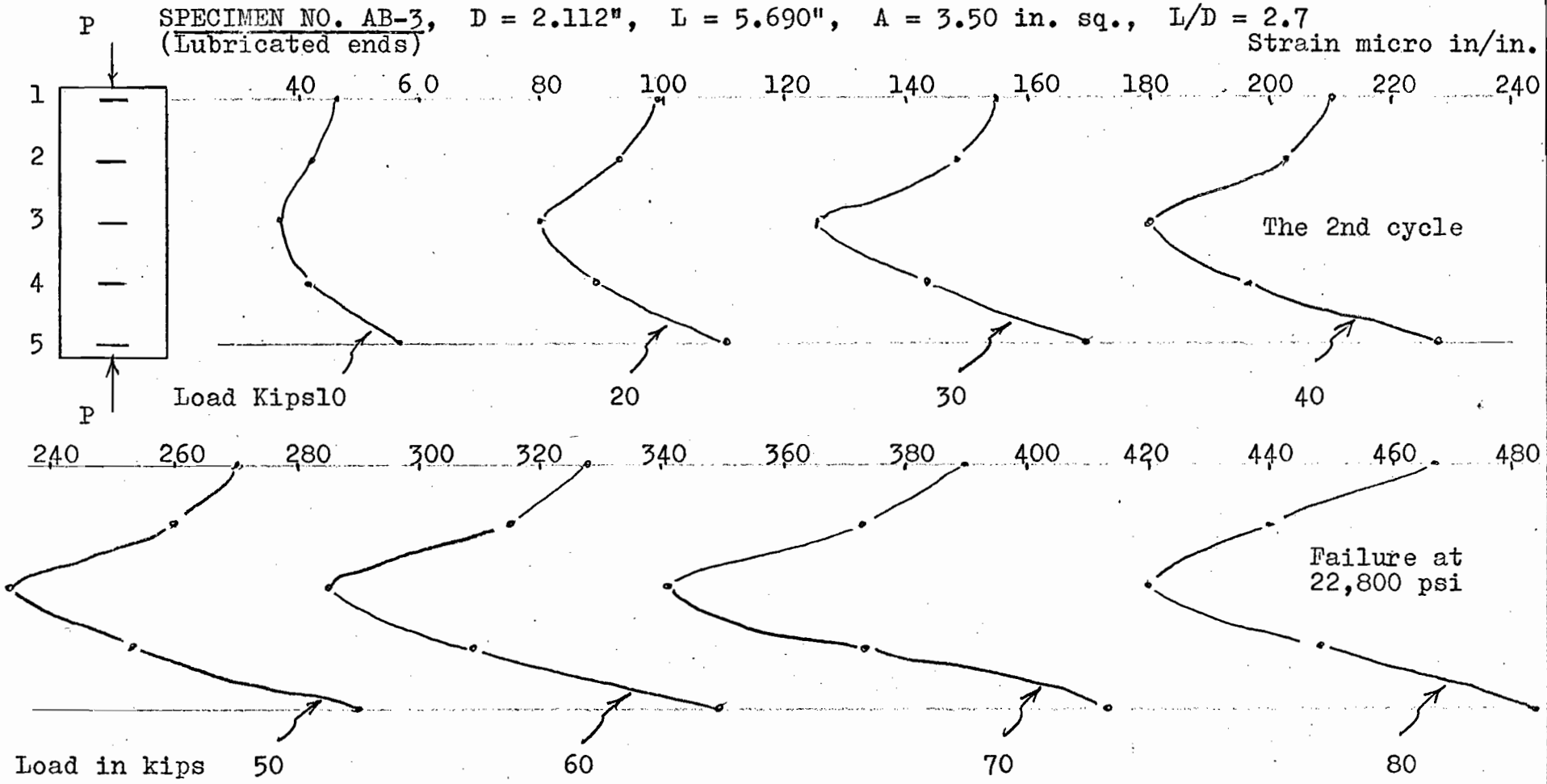

Figure 4-42: Lateral Deformation of Skarn with Lubricated Ends Under Uniaxial Compression

Ref. Table 1B-24

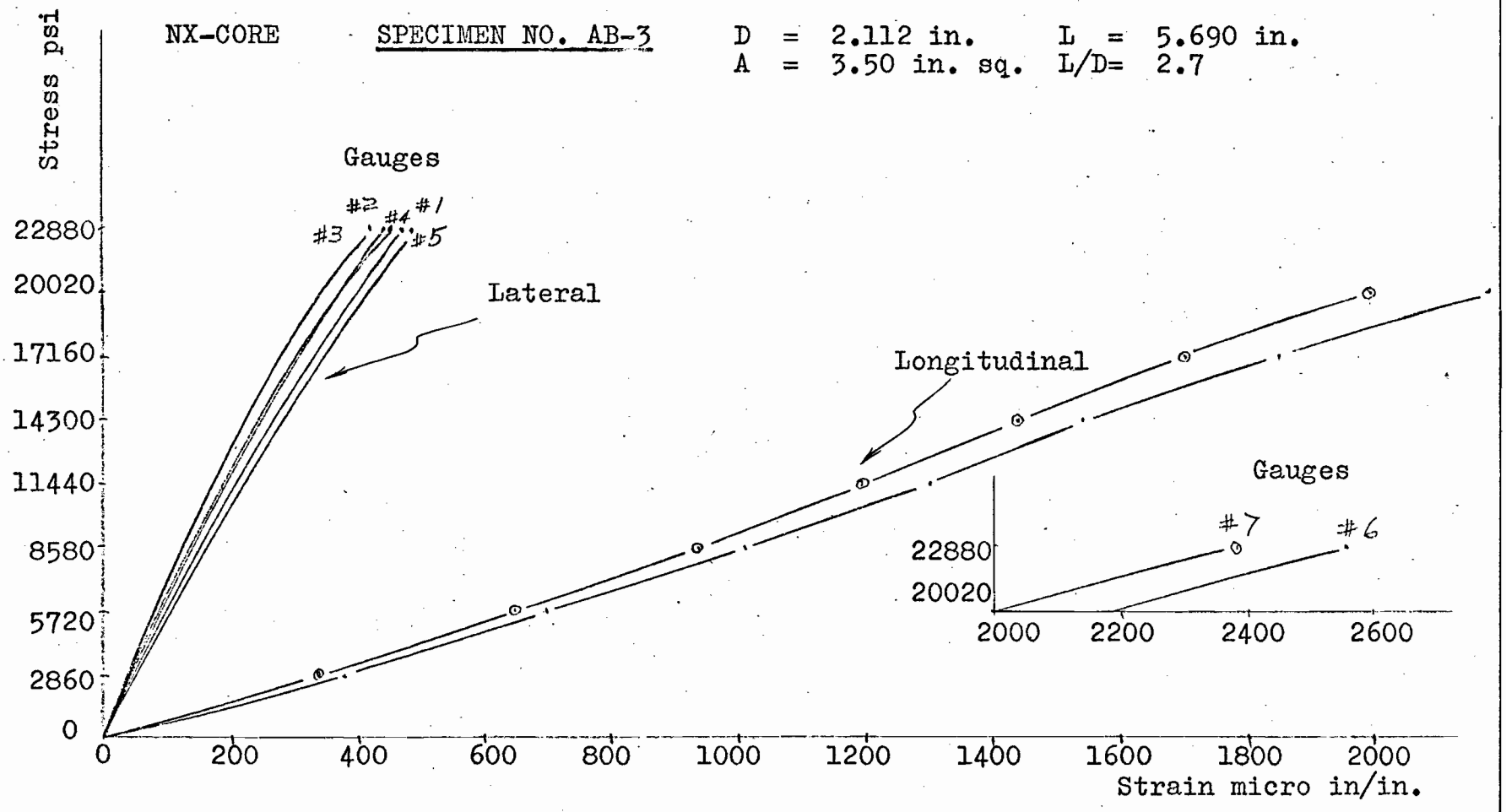

Figure 4-43: Stress-Strain Curve of Skarn with Lubricated Ends Under Uniaxial Compression

Ref. Table 1B-24

SPECIMEN NO. AB-5 NX-CORE D.D.H. U-1474

D = 2.109 in. L = 5.720 in. A = 3.50 in. sq. L/D = 2.7

Free ends

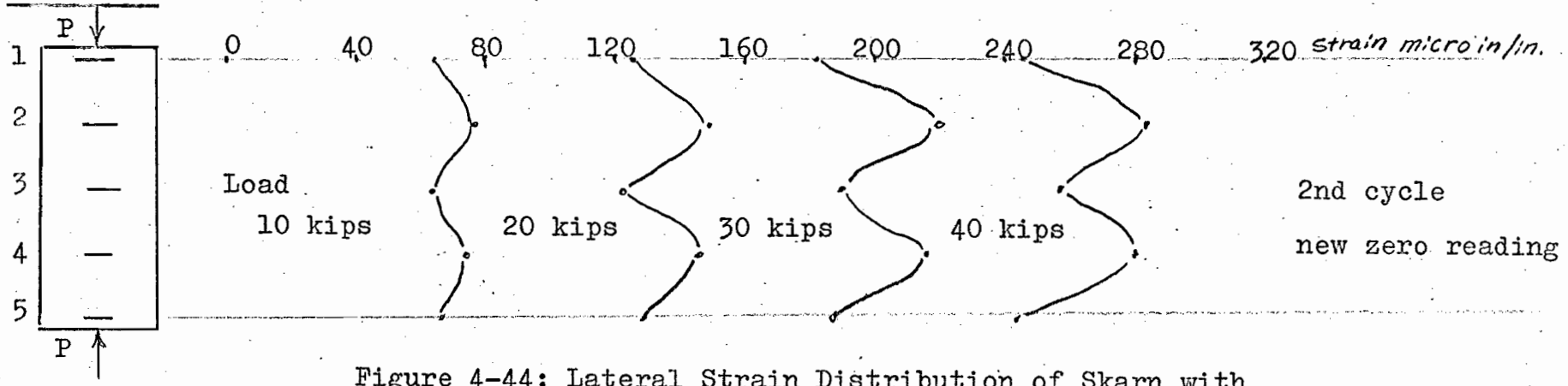

Figure 4-44: Lateral Strain Distribution of Skarn with Free Ends Under Uniaxial Compression

Lubricated ends

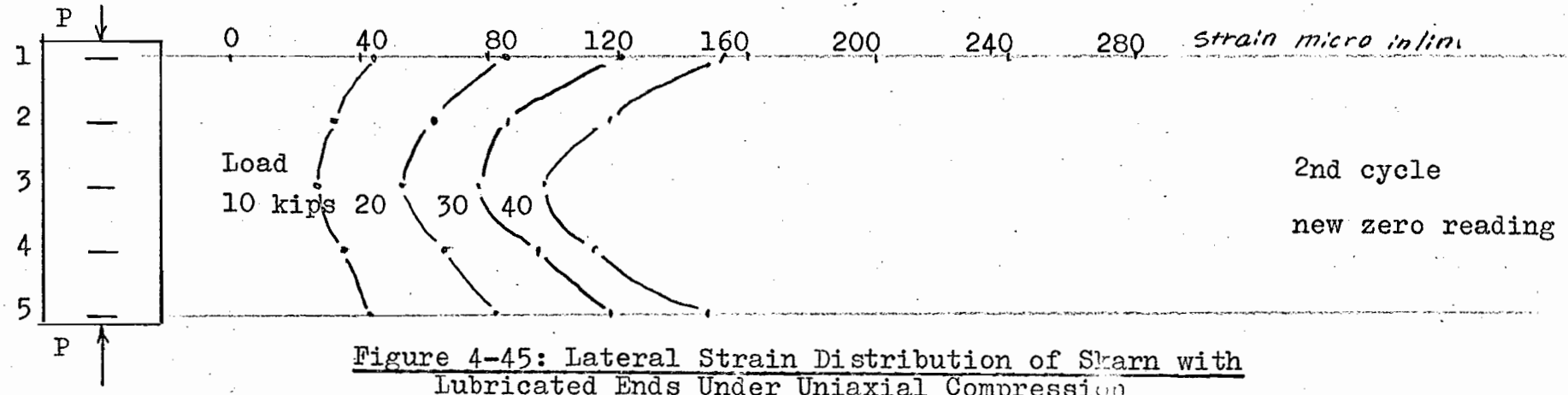

Figure 4-45: Lateral Strain Distribution of Skarn with Lubricated Ends Under Uniaxial Compression

Ref. Table 1B-26

is given in Table 1B-25 and Table 1B-26 in the Appendix.

Twelve SR-4 strain gauges were placed on NX-core specimen No. AB-6 (L/D = 2.1), two longitudinal strain gauges on the opposite sides and ten lateral strain gauges, five on each side (See Figure 4-46).

The specimen was tested first without lubrication over two loading and unloading cycles. The strains for all strain gauges were observed at each loading and unloading level and the average value of the lateral strain distribution of each corresponding two strain gauges for the two cycles were plotted in Figure 4-47. The detailed data is given in Table 1B-27 in the Appendix.

For lubricated end tests, this specimen, No. AB-6, was treated with the liquid paraffin, the same as specimen No. AB-5, and was then loaded to failure incrementally.

The specimen, with lubricated ends, failed at load of 42 kips (14,400 psi) with a tensile type failure plane parallel to the direction of the applied load.

The lateral strain distribution, with lubricated ends, averaged for each corresponding two strain gauges, is shown in Figure 4-48. The detailed data for this specimen can be found in Table 1B-28 in the Appendix.

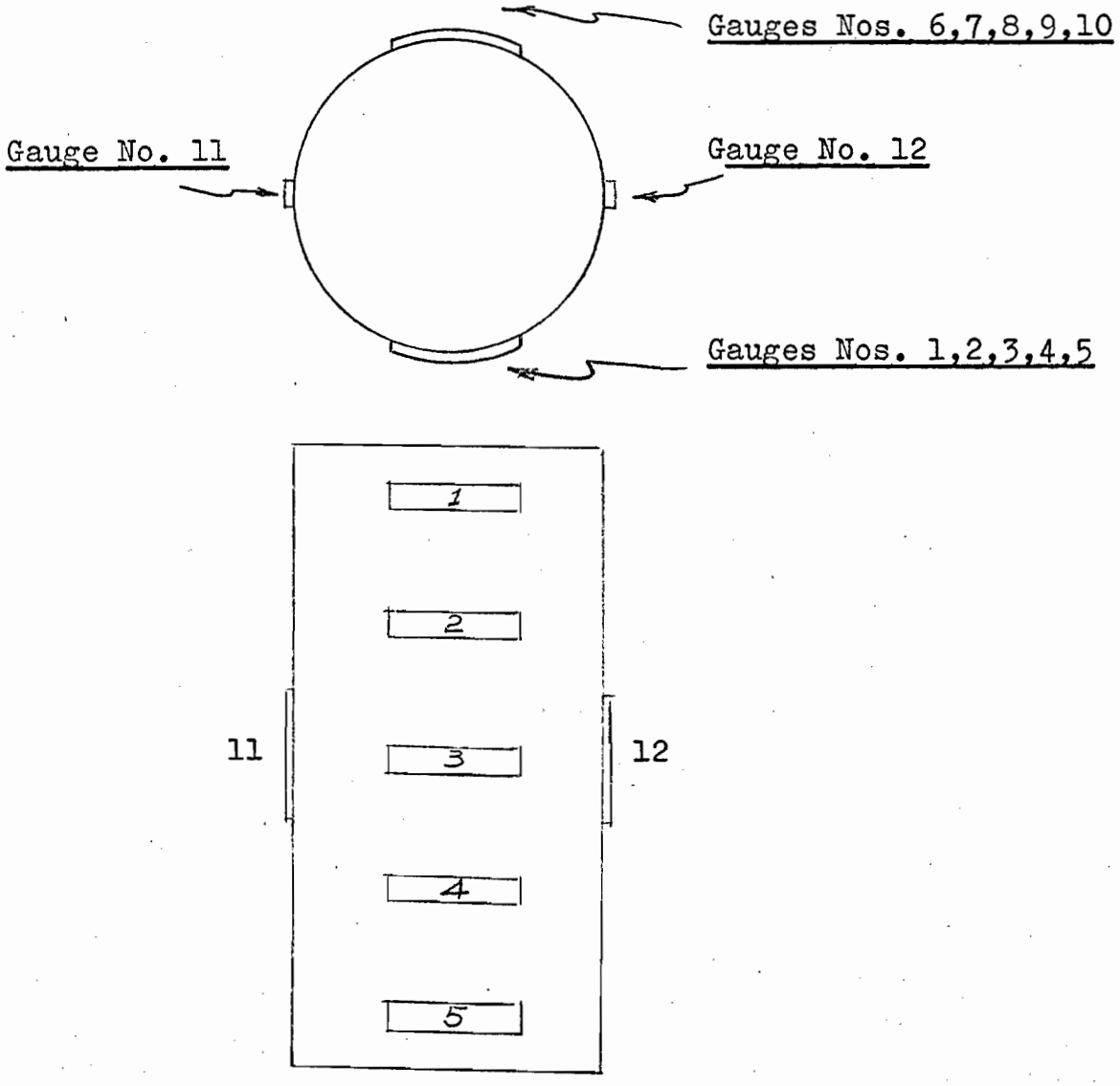

Figure 4-46: Location of Strain Gauges on Specimen

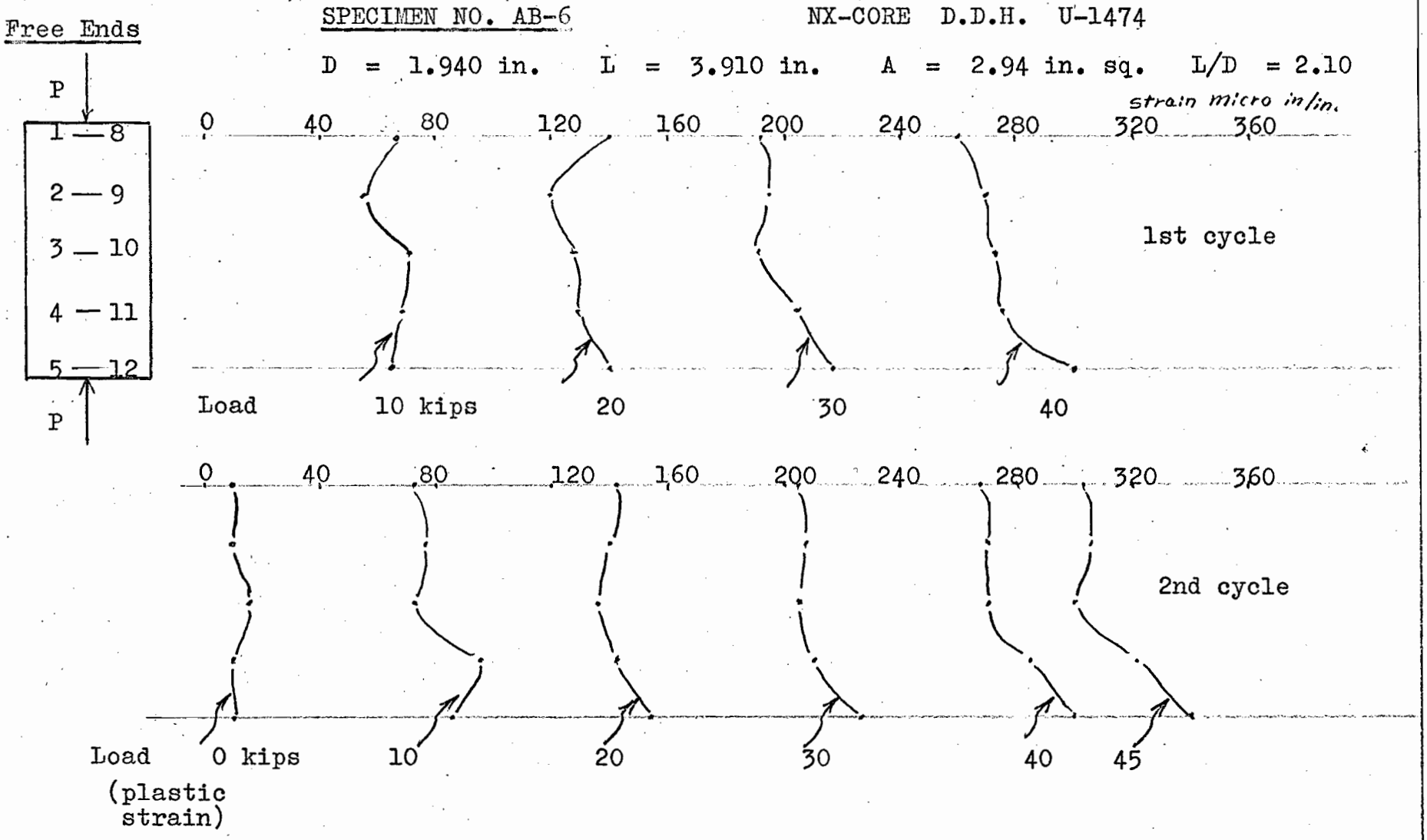

Figure 4-47: Lateral Strain Distribution of Skarn with Free Ends Under Uniaxial Compression

(Average Value of Two Corresponding Strain Gauges)

Ref. Table 1B-27

SPECIMEN NO. AB-6 NX-CORE D.D.H. U-1474

D = 1.940 in. L = 3.910 in. A = 2.94 in. sq. L/D = 2.10

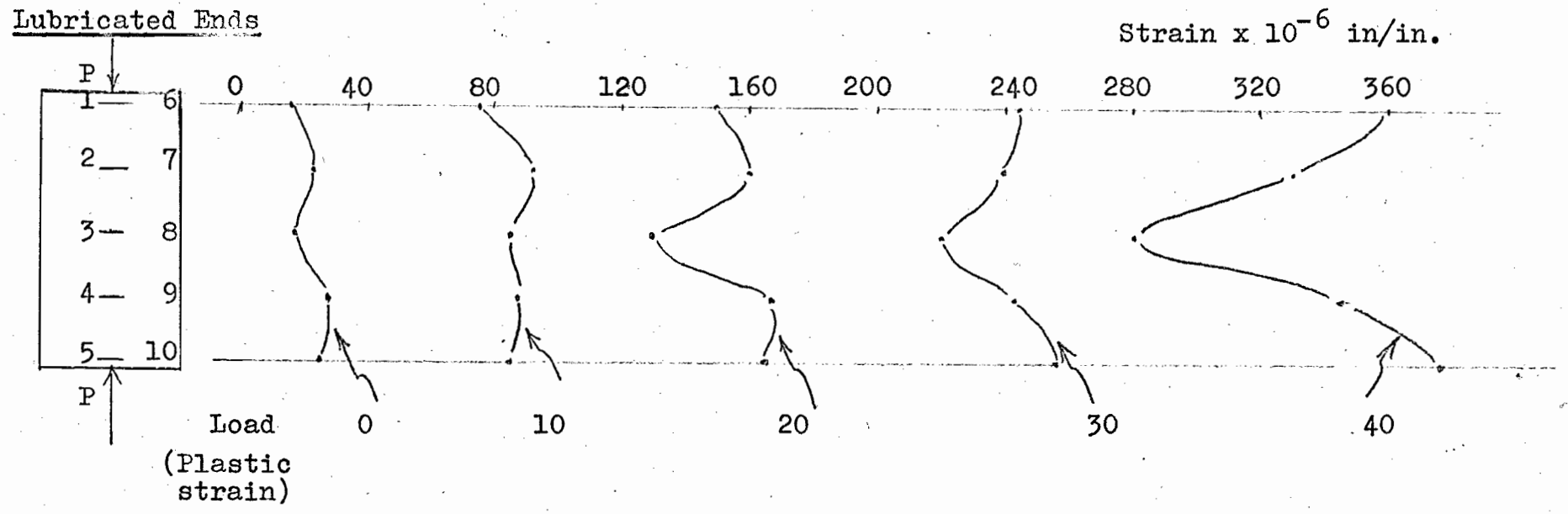

Failure at 42 kips (14,400 psi)

Figure 4-48: Lateral Strain Distribution of Skarn with Lubricated Ends Under Uniaxial Compression

(Average Value of Two Corresponding Strain Gauges)

Ref. Table 1B-28

Sigma Porphyry

Three specimens, SPN-2, SPN-5 and SPE-10 of the rock type of Sigma (C) porphyry, from Sigma Mines Ltd., (Quebec), were tested with and without lubricated ends for comparison with the above results and also to check Yu's results.[32]

The core sizes, the L/D ratios, the ends' conditions, the loading procedures and the testing results for each specimen are shown in Figures 4-49, 4-50, 4-51 and 4-52, respectively. The detailed data for free and lubricated ends for each specimen are given in Tables 1B-29, 1B-30, 1B-31, 1B-32 and Tables 1B-33, 1B-34, respectively. They vary from those reported by Yu[32] as regards the deformation for the lubricated ends.

A tensile type of fracture was obtained for all specimens when tested with lubricated ends. Figure 4-12(b) gives the typical tensile splitting fracture of specimen No. SPN-5.

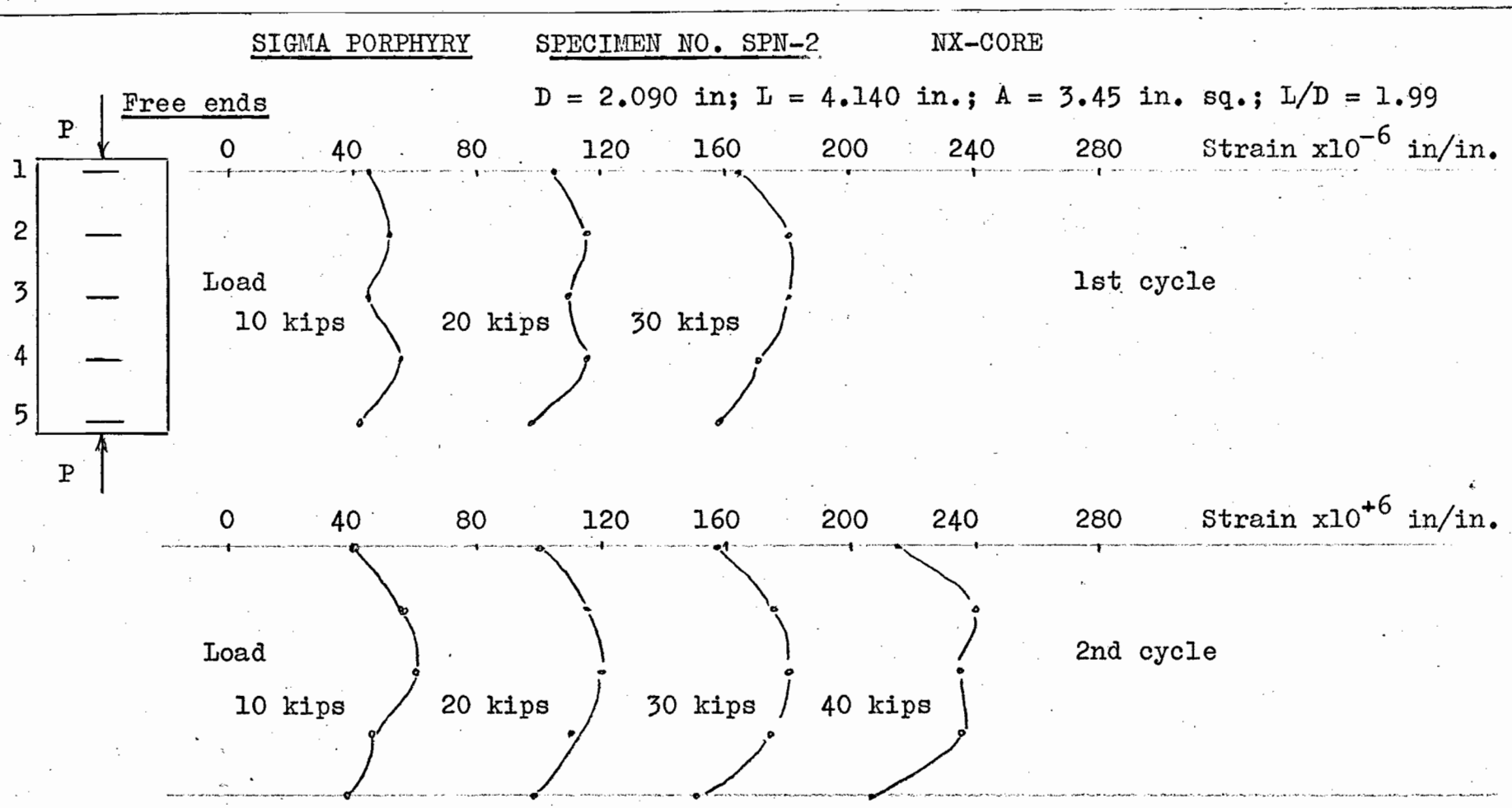

Figure 4-49: Lateral Strain Distribution of Sigma Porphyry with Free Ends Under Uniaxial Compression

Ref. Table 1B-29

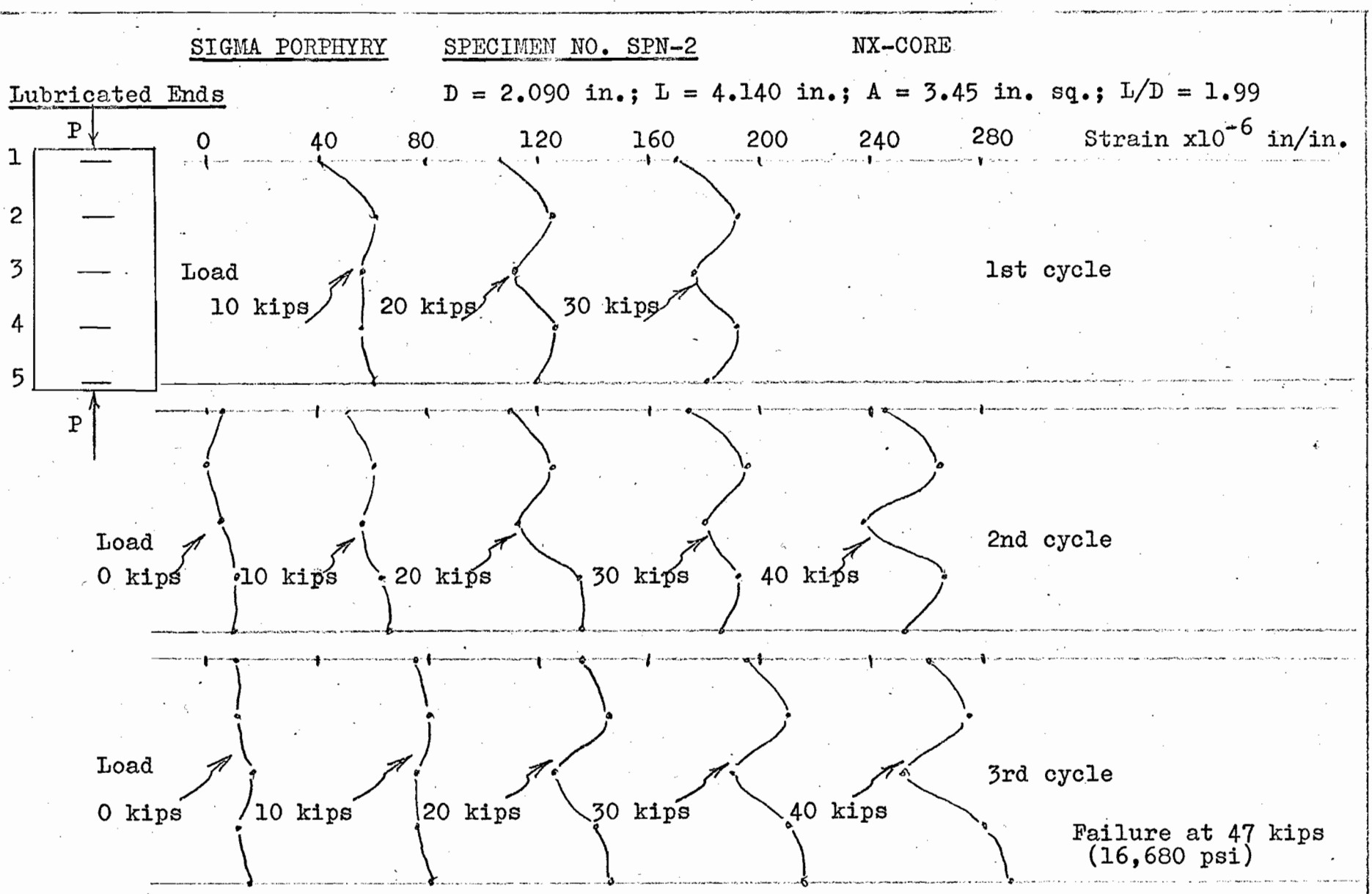

Figure 4-50: Lateral Strain Distribution of Sigma Porphyry with Lubricated Ends Under Uniaxial Compression

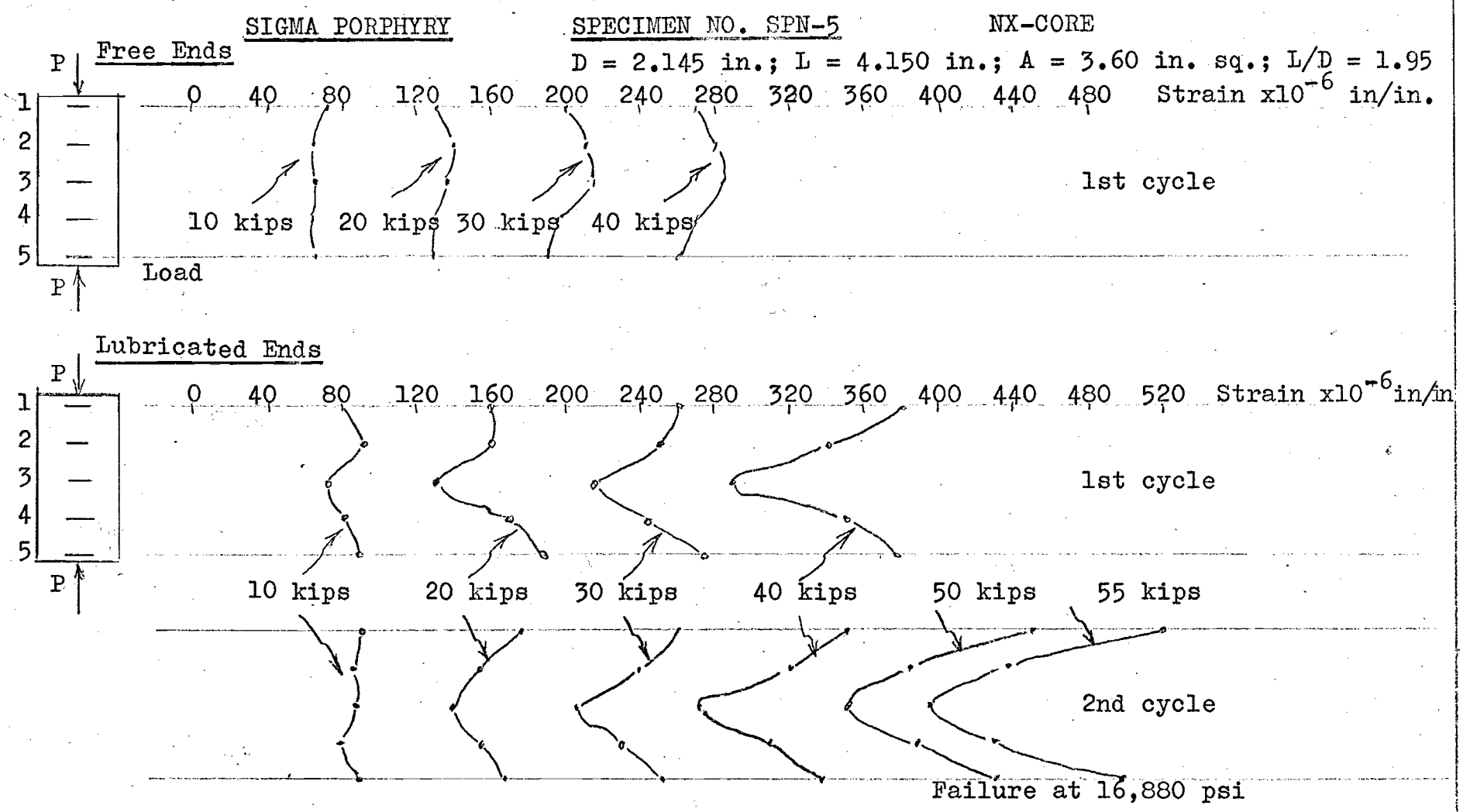

Figure 4-51: Lateral Strain Distribution of Sigma Porphyry With and Without Lubricated Ends Under Uniaxial Compression

Ref. Table 1B-31 and 1B-32

SIGMA PORPHYRY SPECIMEN NO. SPE-10 EX-CORE

Free Ends

D = 0.876 in. L = 2.71 in. A = 0.603 in. sq. L/D=3.1

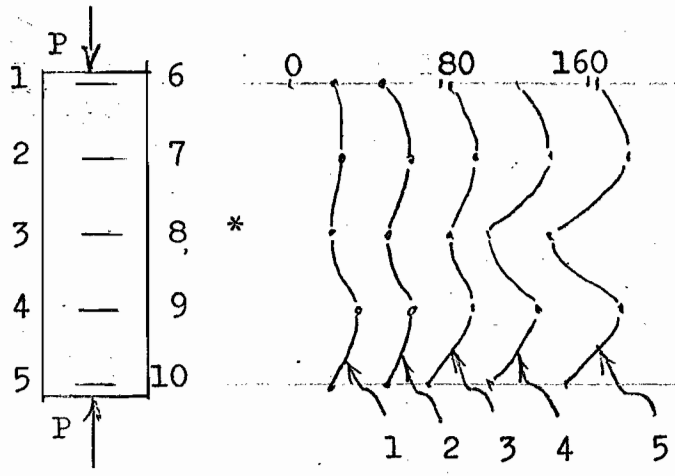

* Average value of two corresponding strain gauges

Lubricated Ends (New zero starting) (Failure at 11 kips, 17,930 psi)

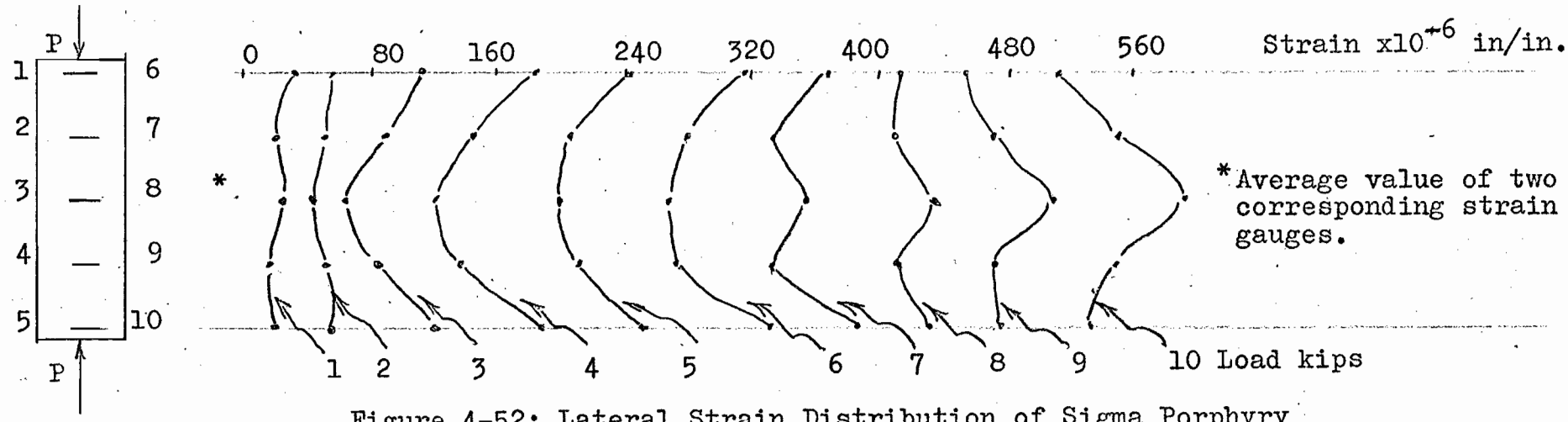

*Average value of two corresponding strain gauges.

Figure 4-52: Lateral Strain Distribution of Sigma Porphyry With and Without Lubricated Ends Under Uniaxial Compression

Ref. Tables 1B-33 and 1B-34

3-3 Triaxial tests

For triaxial compressive tests, a triaxial bomb, as illustrated in Figure 4-8(a), was used. The calibration curve for this is shown in Figure 4-53 and is determined, as follows:

$$P_1 = S_1(A_1 - A_2) = 11.14\ S_1,$$

$$P_2(P_3 - P_1) = (P_3 - 11.14\ S_1)$$

The compressive strength was calculated from the following formula:

$$S_2 = \frac{P_2}{A_2} = \frac{(P_3 - 11.14\ S_1)}{A_2}$$

where P_1 = Confining load, lbs.

S_1 = Confining pressure, psi.

A_1 = Area of piston, $in.^2$

A_2 = Area of specimen, $in.^2$

P_3 = Applied axial load reading in dial, lbs.

P_2 = Effective axial load, lbs.

S_2 = Effective axial pressure, psi.

$(A_1 - A_2) = 11.14$

Table 4-3 summarizes the results of triaxial compressive tests, which are plotted in Figure 4-54. A definite relationship between the confining pressure and the compressive strength is established. The maximum and minimum values plotted here are an indication of the range of values.

Specimens used in triaxial tests often failed

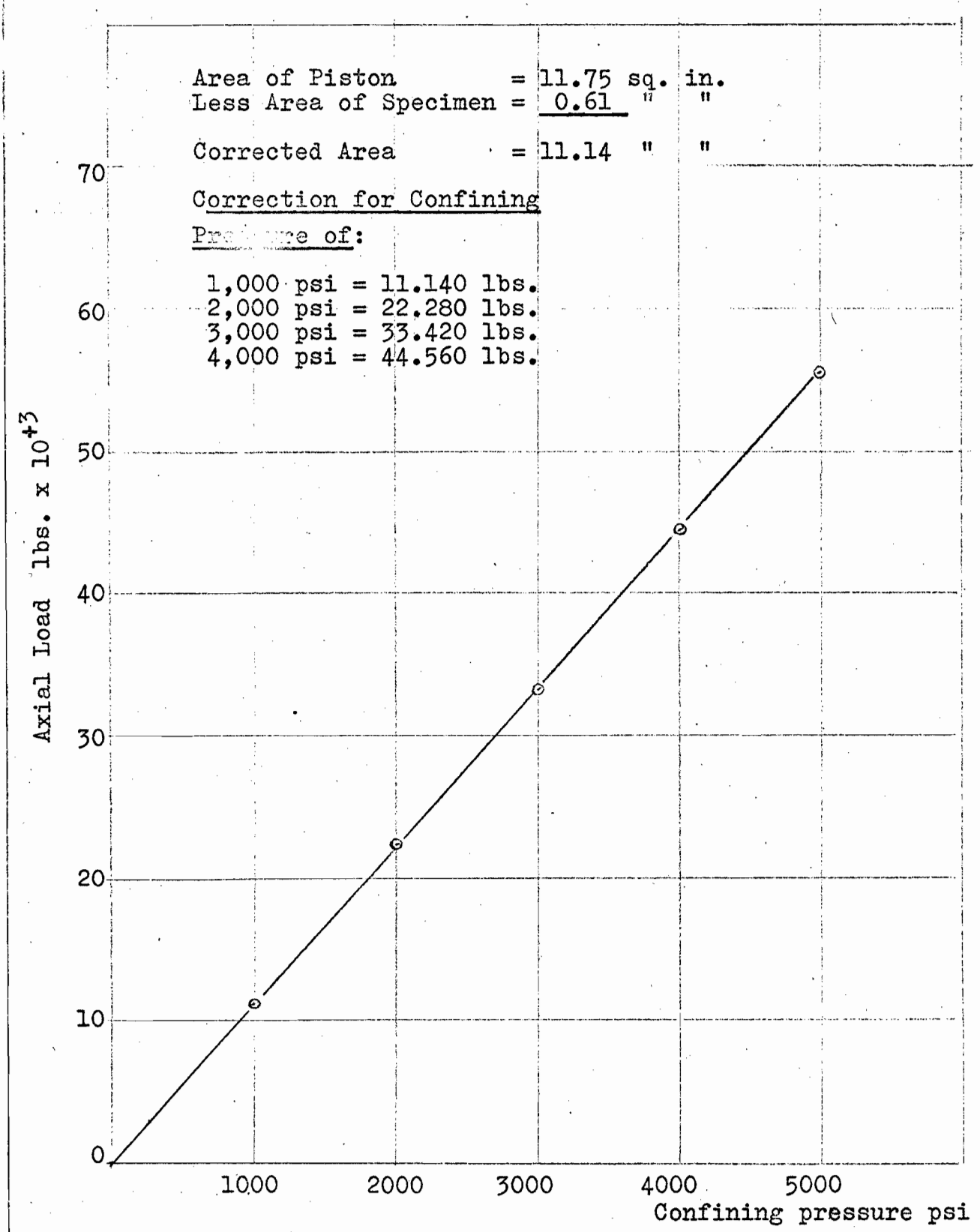

Figure 4-53: Calibration Curve for the Triaxial Bomb

TABLE 4-3

Summary of Triaxial Compressive Results - L/D = 2.0

No. of Specimen	Confined Pressure psi	Compressive Strength			Standard Deviation psi	Coeff. of Variation %	Fracture Angle	
		Max.Value psi	Mean psi	Min.Value psi			Measured degree	Expected
* 20	0	44.000	31.400	17.400	6560	20.9		15.7
** 10	1000	62.000	42.400	25.700	9150	21.6	21.7	20.6
** 10	2000	75.000	51.930	35.300	10120	19.6	22.9	21.3
** 10	3000	82.700	61.050	46.700	11550	19.0	24.2	21.5

*Ex-Core U-1225, Uniaxial Value for L/D = 2.0

**Ex-Core U-1526

Mean = $31.900 + 9.8\ P_c$

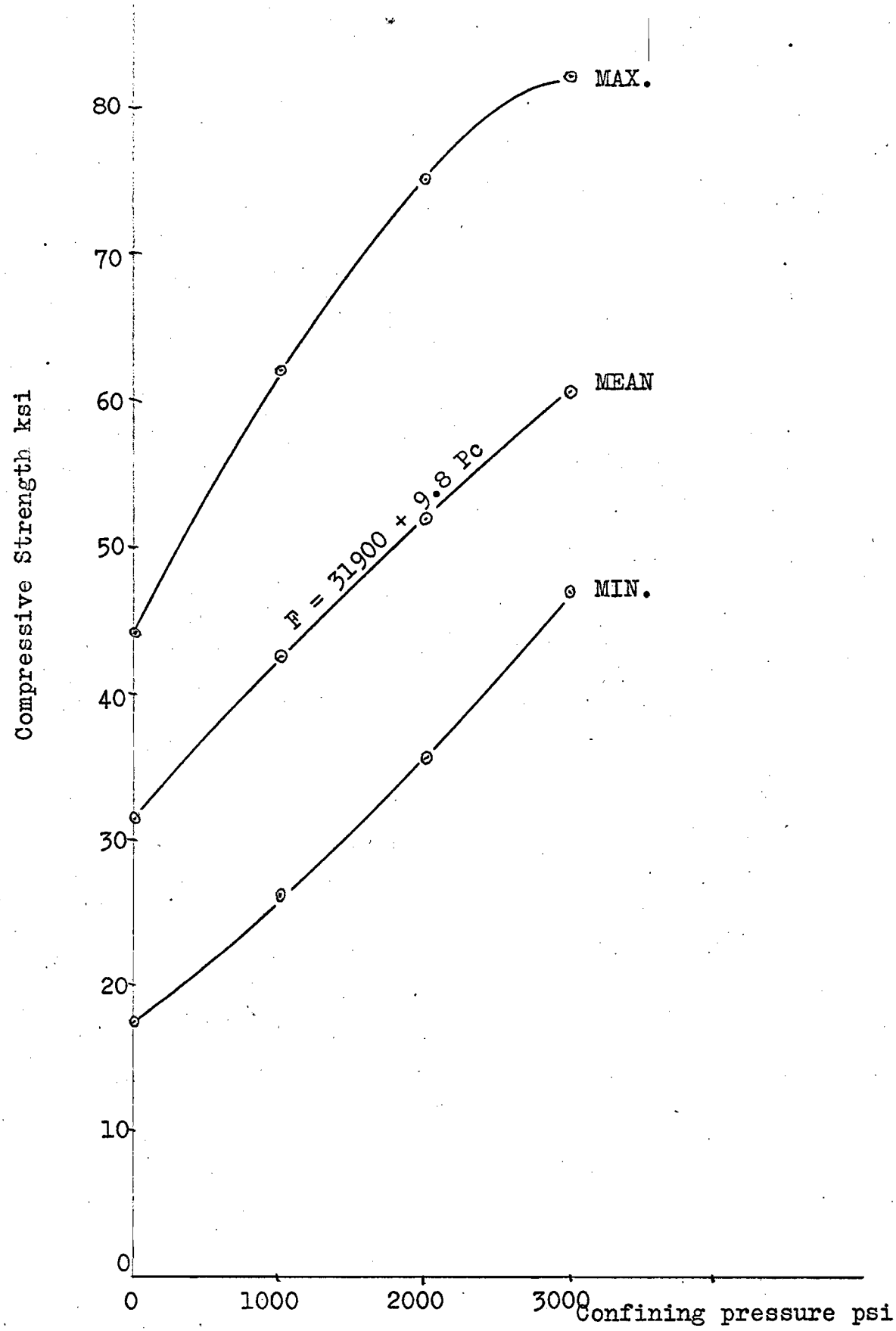

Figure 4-54: Relationship Between Confining Pressure and Compressive Strength

Ref. Table 4-3

in shearing on a diagonal curved failure plane. These planes invariably passed through one end, Figure 4-13(a) or both ends, Figure 4-13(b), at their intersection with the edge of the specimen. The grinding effects, as shown in Figure 4-13(c) due to shearing, is conspicuous on the surfaces of such failure planes.

V. TENSILE TESTS

(1) Selection and Preparation of Specimens

Unless otherwise stated, the selection of specimens is the same as for the uniaxial compressive tests.

For the pull test, the specimens were cut to an L/D ratio of approximately 2.5 and the diameters were measured to an accuracy of 0.001 inch. A mold for casting plastic grips on the ends of specimens is shown in Figure 5-1. A glass plate, coated with vaseline, is used to seal off any leakage of the resin prior to hardening. Waldor W 502 Resin and WH 951 Hardener were mixed together in a beaker in the ratio of 10:1 by volume. The mixture was thoroughly stirred with a glass rod and was then poured into the mold to cover the specimen (Figure 5-2), part of which was protected from the resin by a plasticine wrapper. The resin was hardened in the mold, at room temperature, for 48 hours and was then shaped for most effective testing.

For Brazilian tests, specimens from NX-core, 2-1/8 in diameter (U-1474 diamond drill hole) were cut approximately to the following ratios of $\frac{\text{thickness (t)}}{\text{Diameter (D)}}$: 0.15, 0.27, 0.36, 0.54 and 1.08. To insure uniform thickness grinding both ends was also required for most specimens.

For bending tests, specimens were cut to lengths of approximately 2.5, 3.5 and 5.5 inches for fitting the

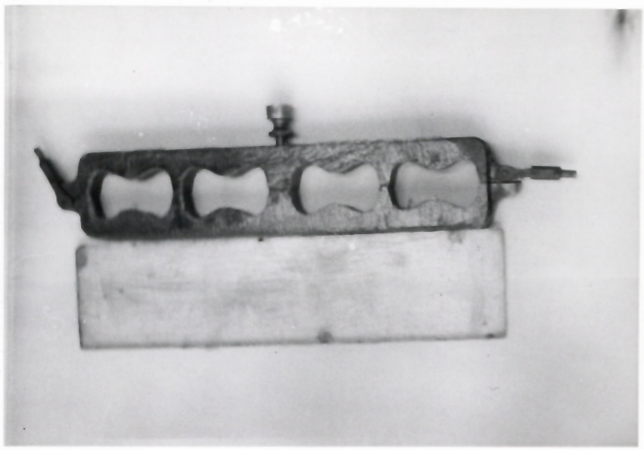

Figure 5-1:

Mold and glass plate.

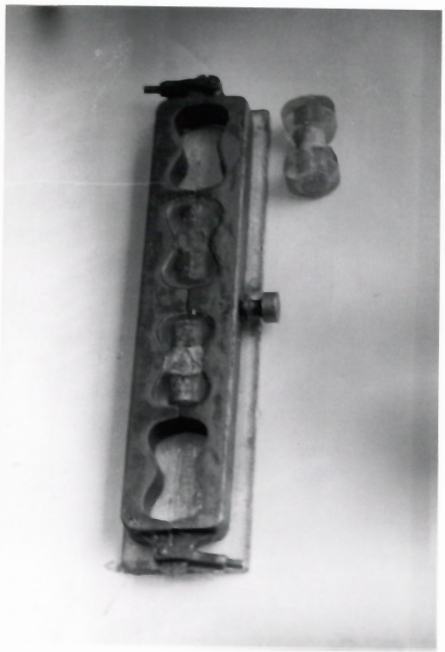

Figure 5-2:

Preparation of specimens for pull test.

Figure 5-3:

Tinius Olsen Testing Machine.

testing jigs with spans of 2.0, 3.0 and 5.0 inches, respectively.

(2) Testing Apparatus and Loading Procedures

The Tinius Olsen Testing Machine, shown in Figure 5-3 was used for both the pull and bending tests. This machine has three loading ranges; they are 5,000 lbs., 25,000 lbs. and 50,000 lbs. The lowest range of 5,000 lbs. maximum was employed for both pull and bending tests.

For pull test, the loading procedures are, as follows:

The specimen was fixed in the pull jack (Figure 5-4) and a small initial load was applied to adjust the specimen, as close to the vertical loading axis as possible. The load was then increased to failure, at a loading rate of 0.05 inches per minute. By using this slow loading rate, dynamic effects can be ignored.

For bending tests, the loading jig was fixed on the testing machine and the specimen was placed and centered on the loading jig (Figure 5-5). Load was then applied to failure at a rate of 0.05 inches per minute and the load was observed when specimen failed.

The Louis Small Compression Tester was used for the Brazilian test. The specimen was placed and centered between the loading platens and load was then applied to failure (Figure 5-7). A strain gauge indicator was used to obtain load readings.

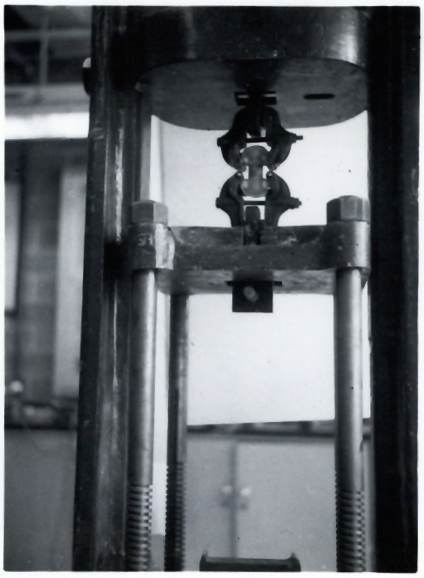

Figure 5-4:

Set up for pull test.

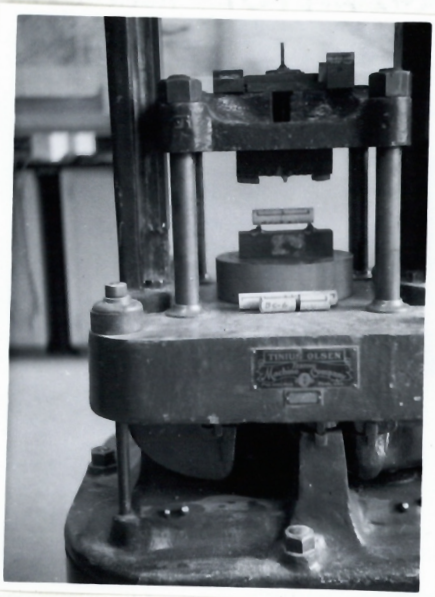

Figure 5-5:

Set up for bending test.

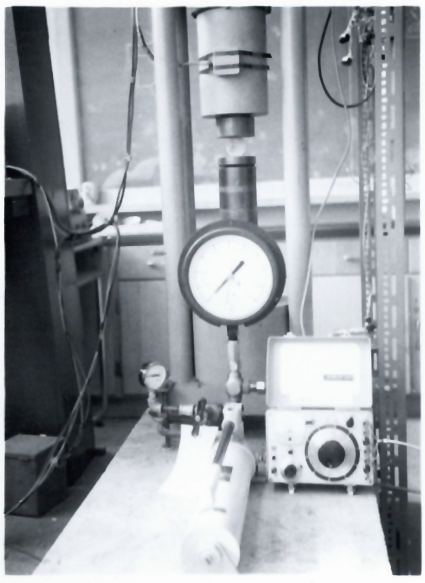

Figure 5-6:

Set up for Brazilian test.

(3) Testing Results

(3-1) Tensile strength

The tensile strength of the rock in the pull test can be expressed by the following equation:

$$T = \frac{P}{A} ,$$

where T = Tensile strength, psi.

P = Applied load at failure, lbs.

A = Initial cross-section are of specimen in^2.

For this test, the tensile stress is assumed to be constant and uniformly distributed for all cross-section. Actually, the load is directly applied to the grips which are sufficiently irregular to transmit some abnormal stress to the specimen. This may result in failure within the grips due to composite stresses.

Specimens which fail outside the grips are considered clean breaks (Figure 5-7), and the specimens which fail within the grips are doubtful breaks (Figure 5-8). For 39 specimens, only 16 specimens failed in clean break and 23 specimens failed in doubtful break.

The tensile strengths and the breaking angles for all specimens, divided as to clean and doubtful breaks, are summarized in Table 5-1. This table shows, with rather high coefficients of variation, that the mean strengths for the clean and doubtful breaks are, respectively, 1,110 psi and 1,200 psi compared with the

Figure 5-7: Clean breaks by pull test.
Specimen PA-15 and PA-33.

Figure 5-8: Doubtful breaks by pull test.
Specimen PB-8 and PB-22.

TABLE 5-1

Summary of Tensile Strength* Pull Tests

Tensile Failure	No. of Specimen	Tensile Strength			Breaking Angle		
		Mean Value psi	Standard Deviation psi	Coeff. of Variation %	Mean Value deg.	Standard Deviation deg.	Coeff. of Variation %
o Clean	16	1110	301	27.1	81.1	11.2	13.7
** Doubtful	23	1200	380	31.7	75.7	10.2	13.5
Total	39	1165	345	29.6	78.0	9.6	12.5

* Ex-Core U-1526

o Clean = Clean Break Between Grips

** Doubtful = Break Influenced by Grips

EX - U-1526 GASPE SKARN

No. of Specimens	= 39
Mean Value	= 1160 psi
Max. Value	= 2110 psi
Min. Value	= 600 psi
Standard Deviation	= 346 psi
Coefficient of Variation	= 29.6%

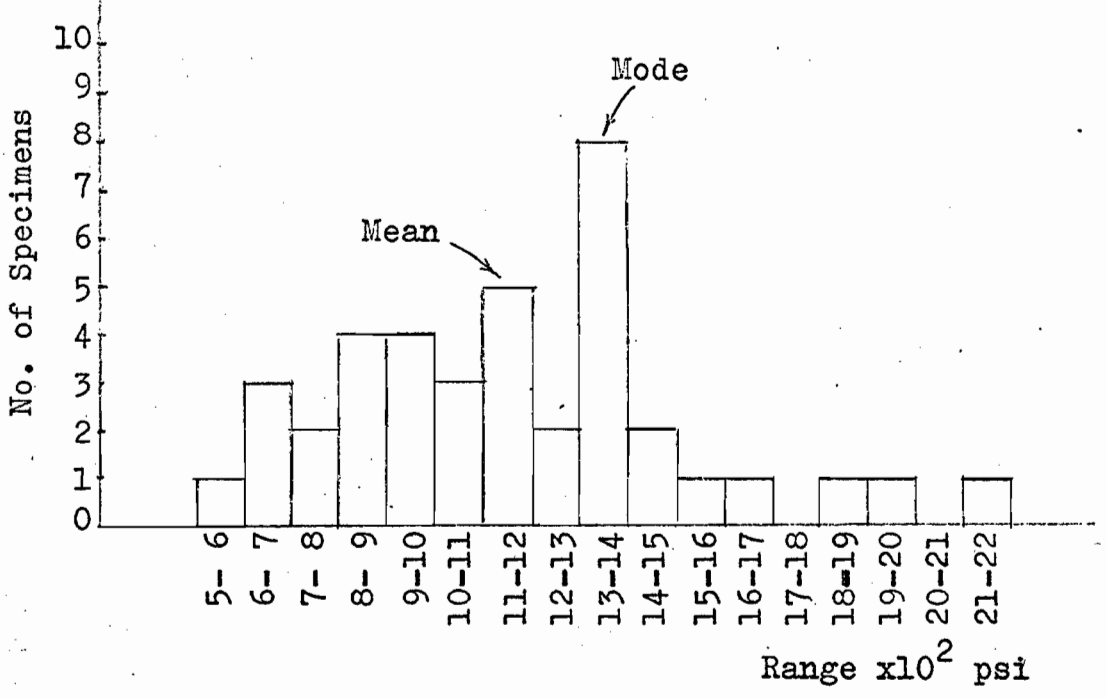

Figure 5-9: Distribution Diagram for Tensile Strength (Pull Test)

Ref. Table 2A-3

average of 1,165 psi. The detailed data for each specimen can be found in Table 2A-1 to Table 2A-3 in the Appendix.

The distribution diagram for the tensile strengths of all specimens (39) is shown in Figure 5-9. This diagram indicates a wide spread in tensile strength.

The breaking angle for the clean breaks was 81.1 degrees compared with 75.7 degrees for the doubtful breaks.

(3-2) Splitting strength

The Brazilian test also is now used to establish a comparative tensile strength for brittle materials. This method has been applied by investigators to determine the tensile strengths of concrete[11], coal[12], [13] and rocks.[14]

For this test, a circular disk is subjected to directly opposed uniform line compressive loads at the extremities of a diameter. A uniform tensile stress is set up across most of the length of the loaded diameter (Figure 5-10). The magnitude of this tensile stress can be determined from the following equation:[13], [14]

$$S_c = \frac{2P}{\pi D t} \quad \text{.....(A)}$$

where S_c = Tensile stress, psi

P = Applied load, lbs.

D = Diameter of specimen, in.

t = Thickness of specimen, in.

As a result of the applied load, a compressive stress is also developed parallel to the loaded diameter

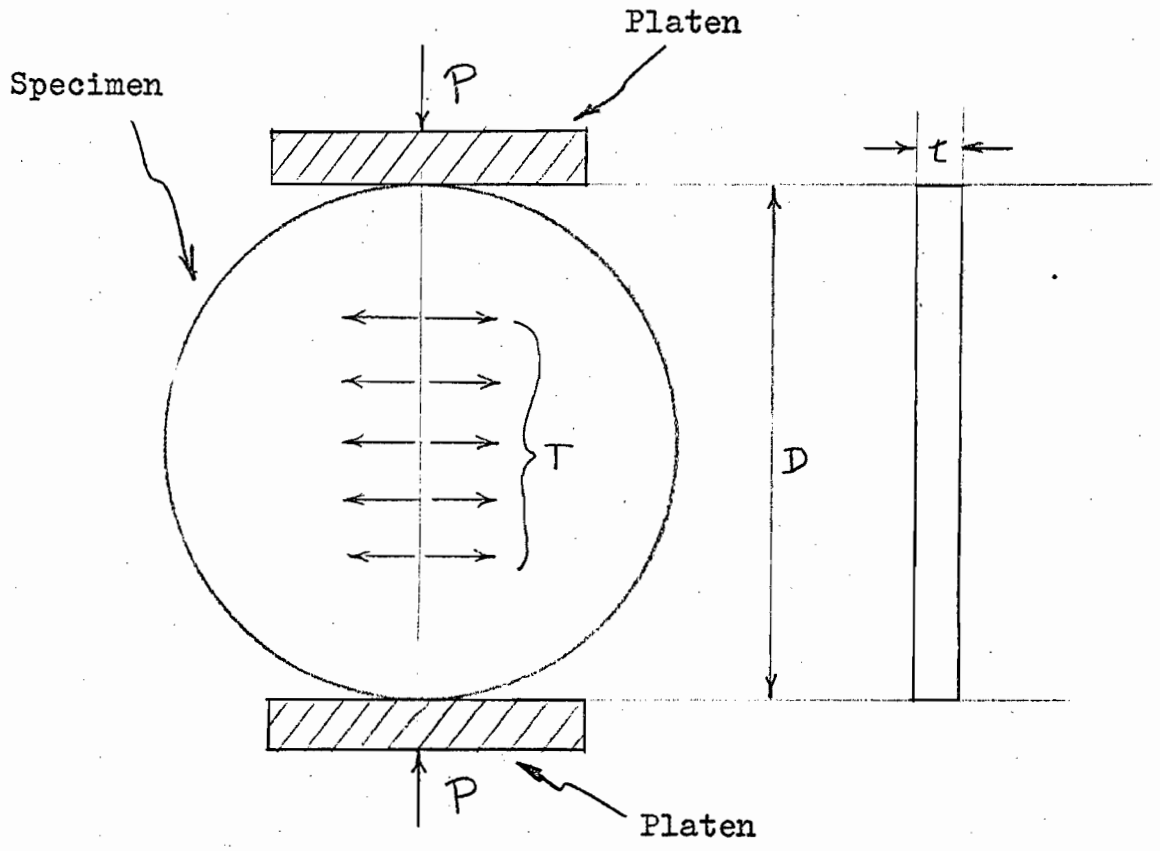

Figure 5-10: Tensile Stress (T) Set up Due to a Compressive Load (P).

of the disk. This compressive stress can be determined by the following equation:[13], (14)

$$S_o = \frac{2P}{\pi t}\left(\frac{2}{D-2r} + \frac{2}{D+2r} - \frac{1}{D}\right) \quad \text{.....(B)}$$

where S_o = Compressive stress, psi

r = The distance from center measured along the load diameter, in.

This equation shows that the compressive stress varies in magnitude from point to point with a minimum value of $\frac{6P}{\pi Dt}$ at the center (r=0), to an infinite value at the points of loading.

A summary of testing results with t/D ratios, varying from 0.15 to 1.08 is given in Table 5-2. The supporting data for each specimen is listed in Table 2B-1 to Table 2B-5 in the Appendix.

The splitting strengths from Table 5-2 for various t/D ratios were plotted in Figure 5-11. This figure shows that increasing the t/D ratio results in decreased strength. The maximum and minimum values are plotted as an indication of the spread of value.

The distribution diagram for the splitting strength of 117 specimens was plotted in Figure 5-12, and approaches a Gaussian's distribution.

All specimens failed by tension with a failure plane from the top to the bottom loading points. At the vicinity of loading points, the evidence of shear failure developed by equation (B) is apparent (Figure 5-13).

TABLE 5-2

Summary of Splitting Strength*

Brazilian Tests

No. of Specimen	t/D Ratio	Splitting Strength			Standard Deviation psi	Coeff. of Variation %
		Max. Value psi	Mean psi	Min. Value psf		
30	0.155	4080	2410	1390	710	29.5
28	0.273	3560	2310	1260	630	27.3
21	0.358	3180	2090	1290	417	22.5
21	0.545	3090	1920	1220	512	26.7
17	1.083	2790	1970	1120	472	23.9
117	(Total)	4080	2180	1120	612	27.8

*NX-Core U-1474
Mean = y = 2230 - 196 t/D

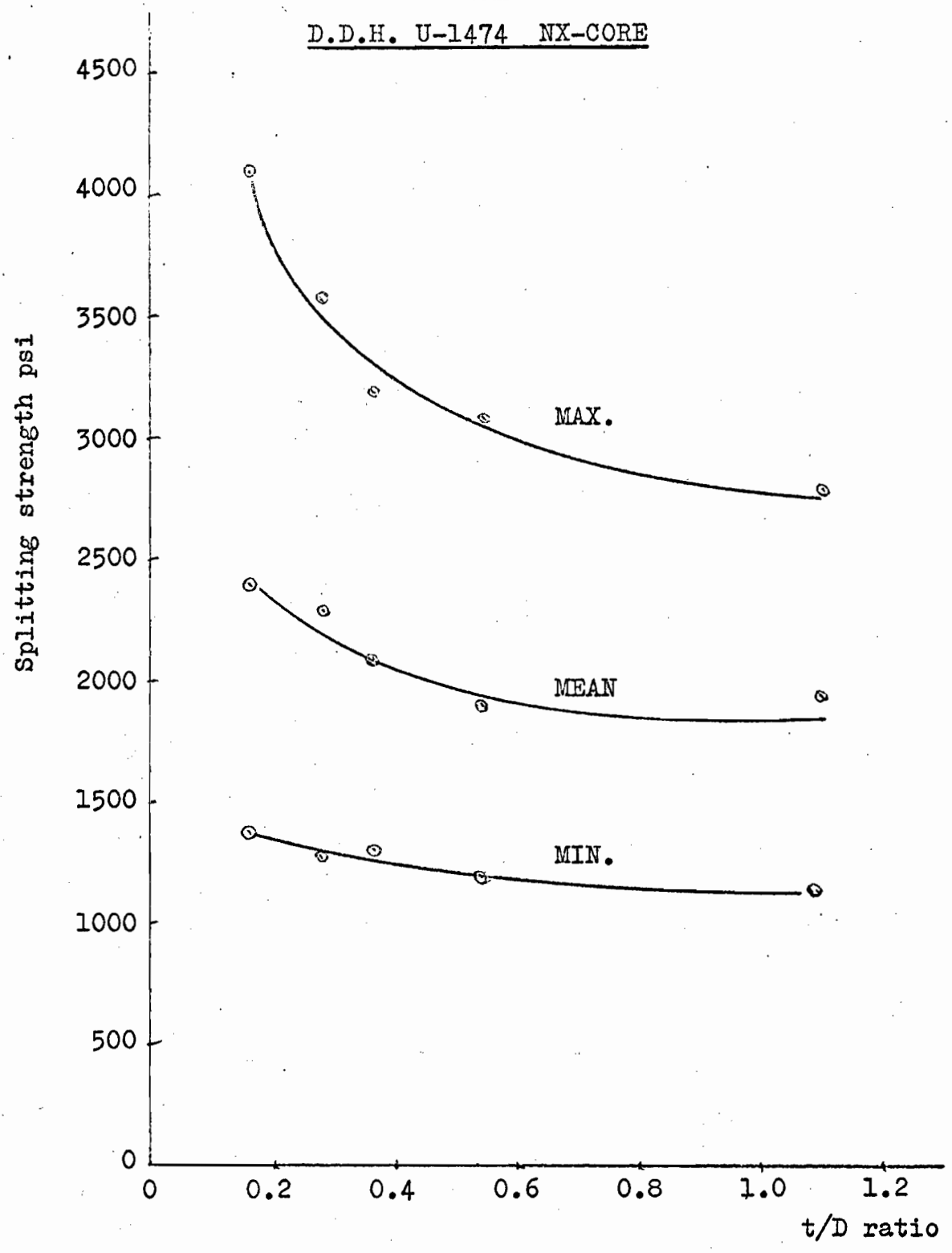

Figure 5-11: Relationship Between t/D Ratio and Splitting Strength

Ref. Table 5-2

97

NX - U-1474 GASPE SKARN

No. of Specimens = 117
Mean Value = 2180 psi
Max. Value = 4080 psi
Min. Value = 1120 psi
Standard Deviation = 612 psi
Coeff. of Variation = 28%

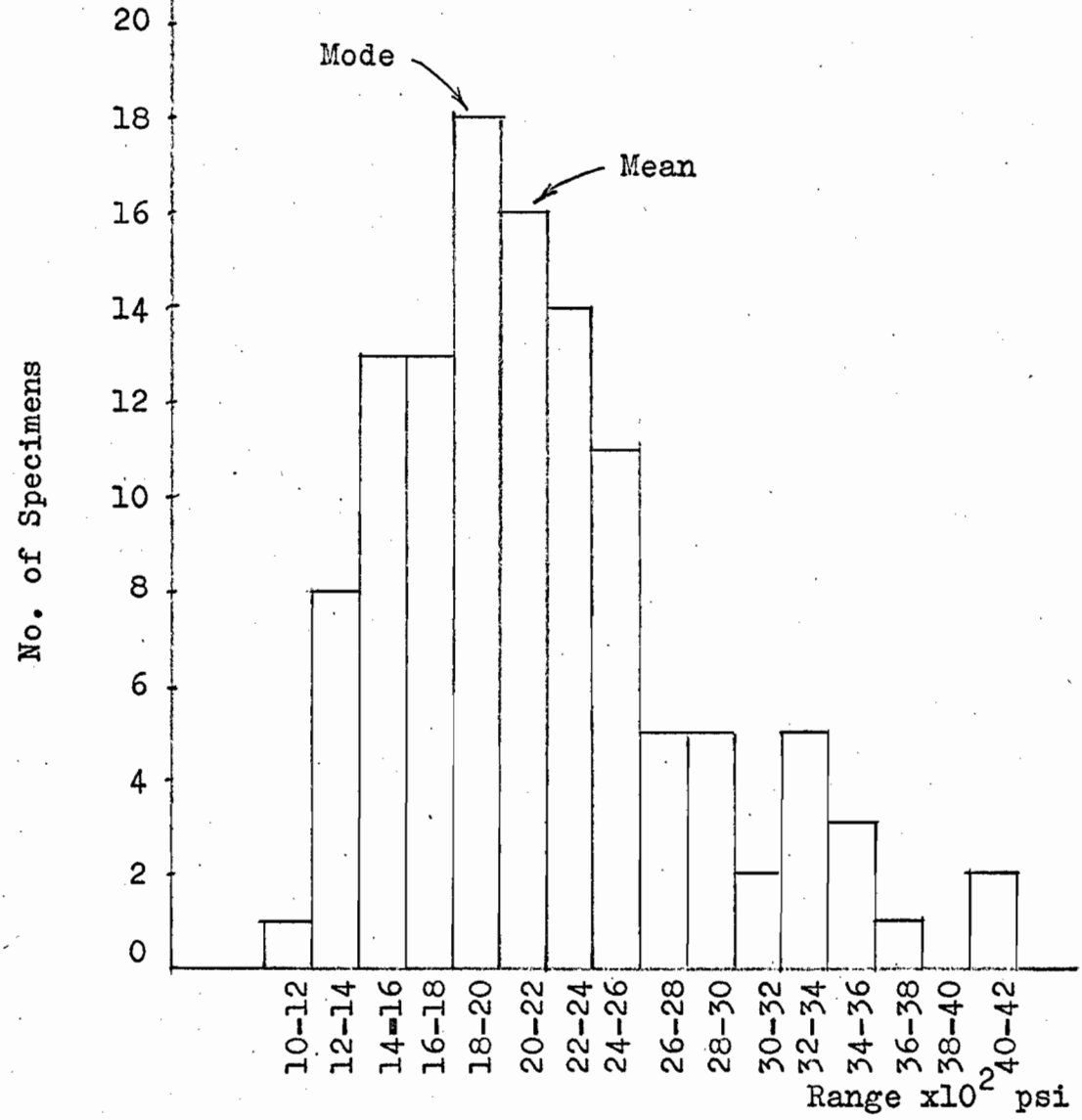

Figure 5-12: Distribution Diagram for Splitting Strength by Brazilian Test

Ref. Tables 2B-1 to 2B-5

(3-3) Flexural strength

The modulus of rupture is a measure of tensile strength of the outer fibers of the cylindrical specimen which is subjected to bending.

For cylindrical specimen, the flexural strength is determined from the following equation:

$$R = \frac{8PL}{\pi D^3},$$

where R = Flexural strength, psi.

P = Applied load, lbs.

L = Length of span between supporting points, in.

D = Diameter of specimen, in.

For this test, the rock specimen is assumed to be elastic and homogeneous in all cross-sections with the same stress—strain behaviour in the outer and inner fibers under tensile and compressive stresses, respectively.

The experimental results of the bending tests with spans varying from 2.0 in. to 5.0 in. are summarized in Table 5-3, detailed data are given in Table 2C-1 to Table 2C-3 in the Appendix.

The flexural strength for varying lengths of span were plotted as shown in Figure 5-14. This figure shows that the flexural strength is a function of the span. The maximum and minimum values are an indication of the coefficient of variation.

The distribution diagram for flexural strength of

Figure 5-13: Tensile failure, Brazilian test.
Specimens TA-4, TB-20, TE-17.

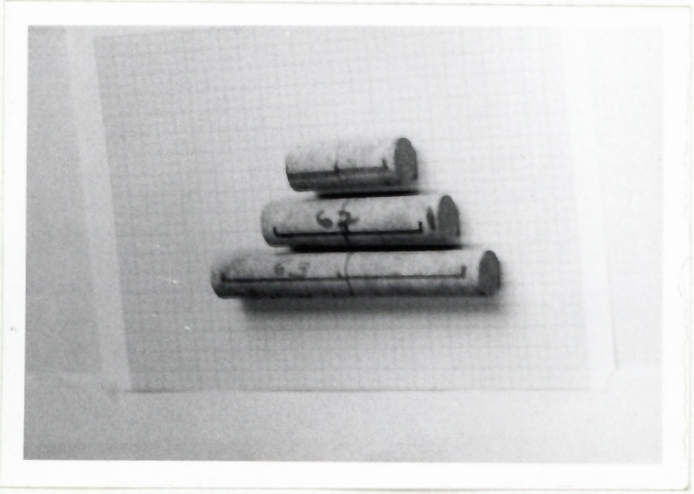

Figure 5-16: Tensile failure, bending test.
Specimen BB-15, BC-3*, BD-4*

* = Marks on specimens are footage of core.

TABLE 5-3

Summary of Modulus of Rupture* Bending Tests

Length of Span in.	No. of Specimen	Modulus of Rupture Max.Value psi	Mean psi	Min.Value psi	Standard Deviation psi	Coeff. of Variation %
2	42	5800	3510	1710	982	28.0
3	30	5300	3190	1510	984	30.9
5	21	4710	3070	1165	1116	36.4
Total	93	5800	3300	1165	1035	31.4

* - Ex-Core U-1526

Mean = 3804 - 144S

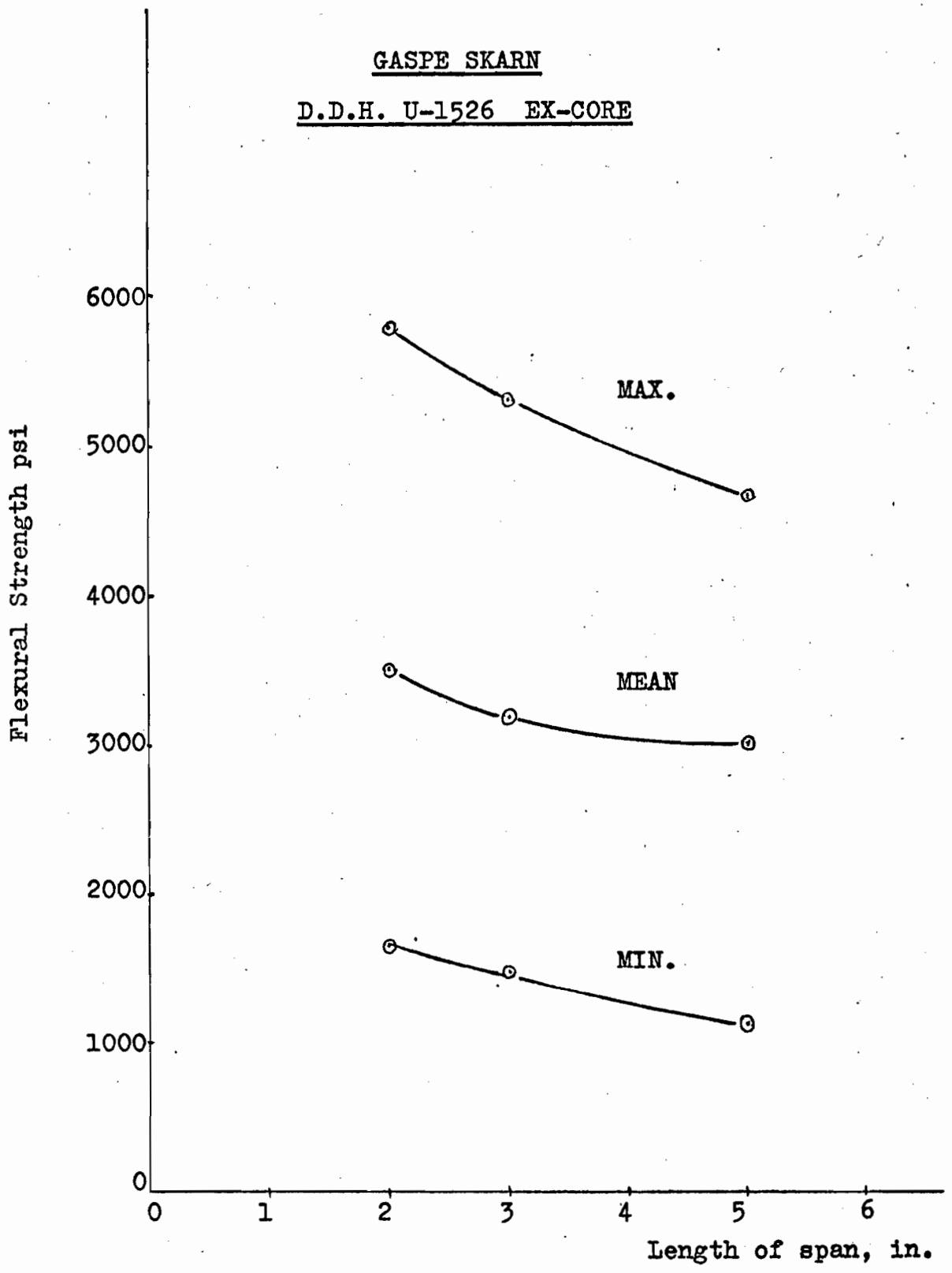

Figure 5-14: Relationship Between Length of Span and Flexural Strength

Ref. Table 5-3

EX - U-1526 GASPE SKARN

No. of Specimens = 93
Mean Value = 3300 psi
Max. Value = 5800 psi
Min. Value = 1165 psi
Standard Deviation = 1035 psi
Coeff. of Variation = 31.4%

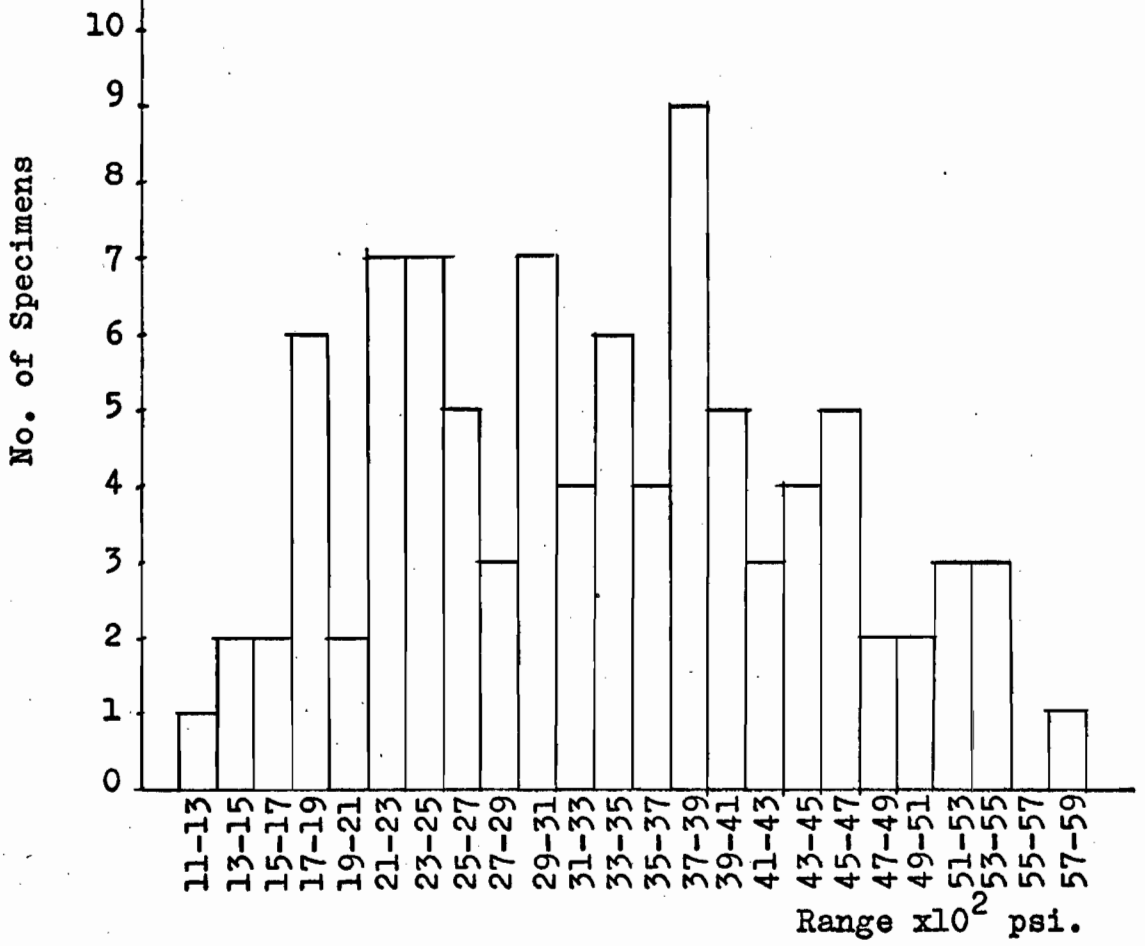

Figure 5-15: Distribution Diagram for Modulus of Rupture

Ref. Tables 2C-1 to 2C-3

93 specimens is shown in Figure 5-15.

Tensile fracture at the middle loading point with a failure plane perpendicular to the tensile stress was obtained in all specimens (Figure 5-16).

VI. SHEARING TESTS

(1) Selection and Preparation of Specimens

Core from EX-diamond drill hole U-1526 was used for shearing tests. Specimens were cut to a length of approximately 2.5 inches and the diameter of each specimen was reduced by careful grinding to fit, with close tolerance, into the shear block. In order to insure that the ends of the specimen are parallel, for applying the uniform axial load, grinding of the ends was also required for biaxial shearing tests.

(2) Testing Apparatus and Loading Procedures

The basic apparatus for direct double shearing tests is the shear block as shown in Figure 6-1. This apparatus consists of a frame and a central movable blade, the loading of which will be apparent from the illustration. For biaxial shearing tests, a small Blackhawk hydraulic ram and a loading frame are also required, (Figure 6-2). The calibration certificate of this Blackhawk hydraulic ram is shown in Figure 6-3.

For direct double shearing tests, the specimen was fitted in the shear block which was placed on the platen of a compressive machine and the load was then applied directly to failure on the central movable blade by a Tinius Olsen Testing machine with a loading rate of 0.05 inches per minute.

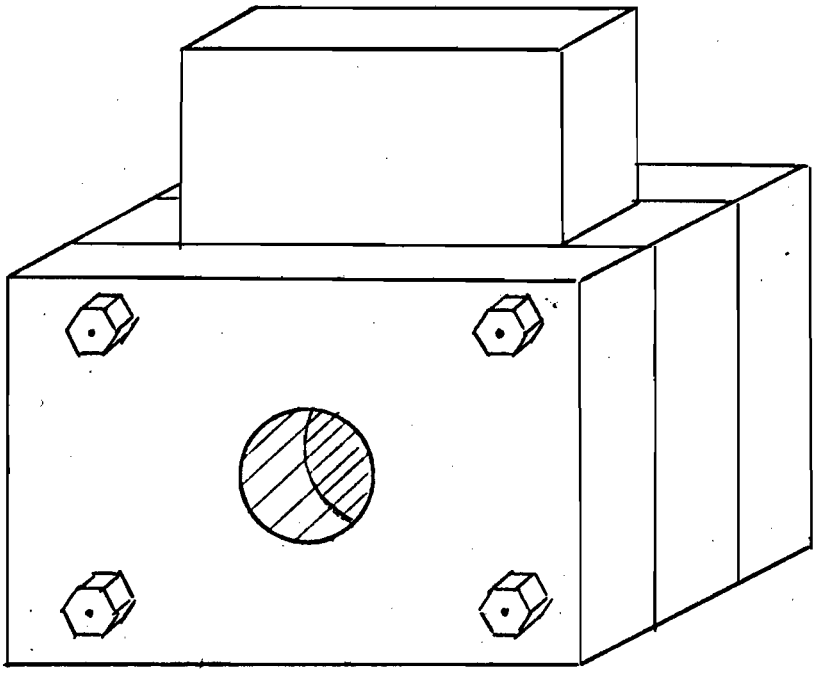

Figure 6-1: The Shearing Block Used for the Double Shear Test

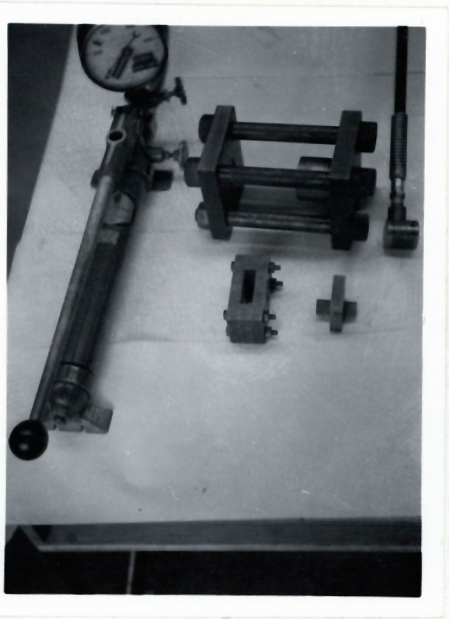

Figure 6-2: Biaxial shear testing apparatus

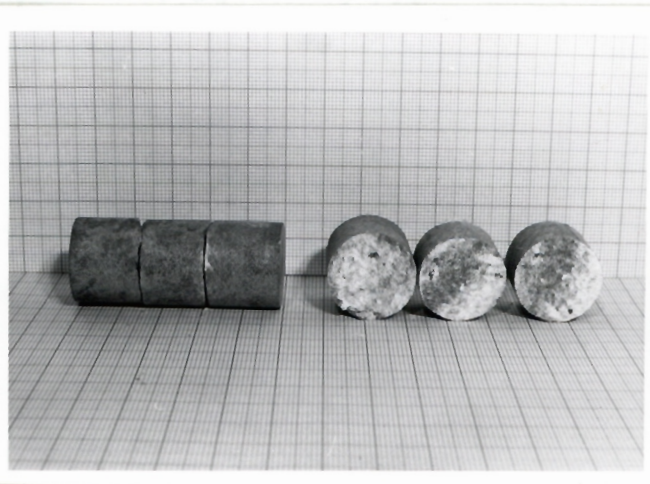

Figure 6-6: Shear failure with two planes,
Biaxial shear test
Specimen SA-28 and SA-37
Axial pressure = 2534 psi.

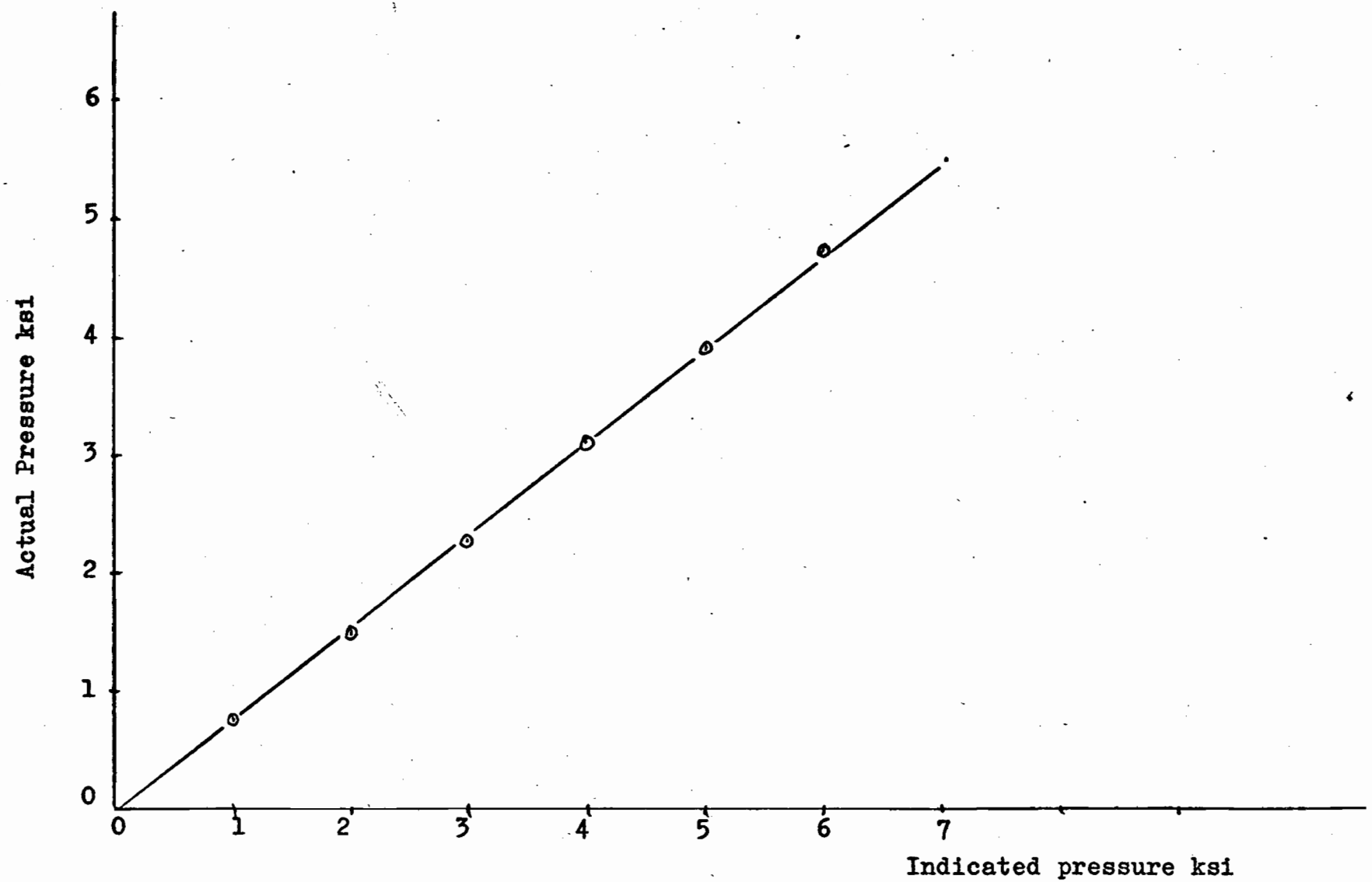

Figure 6-3: Calibration Certificate of Blackhawk Hydraulic Ram

For the biaxial shearing tests, after the specimen was fitted in the shear block, an axial pressure to the specimen ends was applied to a required level and was kept constant. The shear block was centered in the compressive machine and loaded to failure with the same loading rate as the direct double shearing tests.

(3) Testing Results

The shearing strength of a material is a measure of the resistance to shearing stress. For rocks, the resistance is a combination of the cohesion and internal friction and can be represented by Coulomb's equation:

$$J = c + N\tan\phi$$

where J = Shearing strength, psi

c = Apparent cohesion, psi

N = Normal stress, psi

ϕ = Angle of internal friction, deg.

Direct shear testing results with axial pressure varying from 0 psi to 2,534 psi are summarized in Table 6-1. The detailed data for each specimen are given in Table 3A to Table 3C in the Appendix.

The shearing strengths from Table 6-1 for various axial pressures were plotted as shown in Figure 6-4. This figure indicates that the shearing strength is a function of the axial pressure.

The distribution diagrams for the shearing strength for various axial pressures were plotted in Figure 6-5

TABLE 6-1

Summary of Shearing Strength

Ex-Core D.D.H.-1526

No. of Specimen	Axial Pressure psi	Shearing Strength			Standard Deviation psi	Coeff. of Variation %
		Max.Value psi	Mean psi	Min.Value psi		
13	0	4180	3040	1840	591	19.5
12	1267	12700	9850	7100	1480	15.0
14	2534	17600	13160	9640	2180	16.6

110

GASPE SKARN

D.D.H. - U-1526 EX-CORE

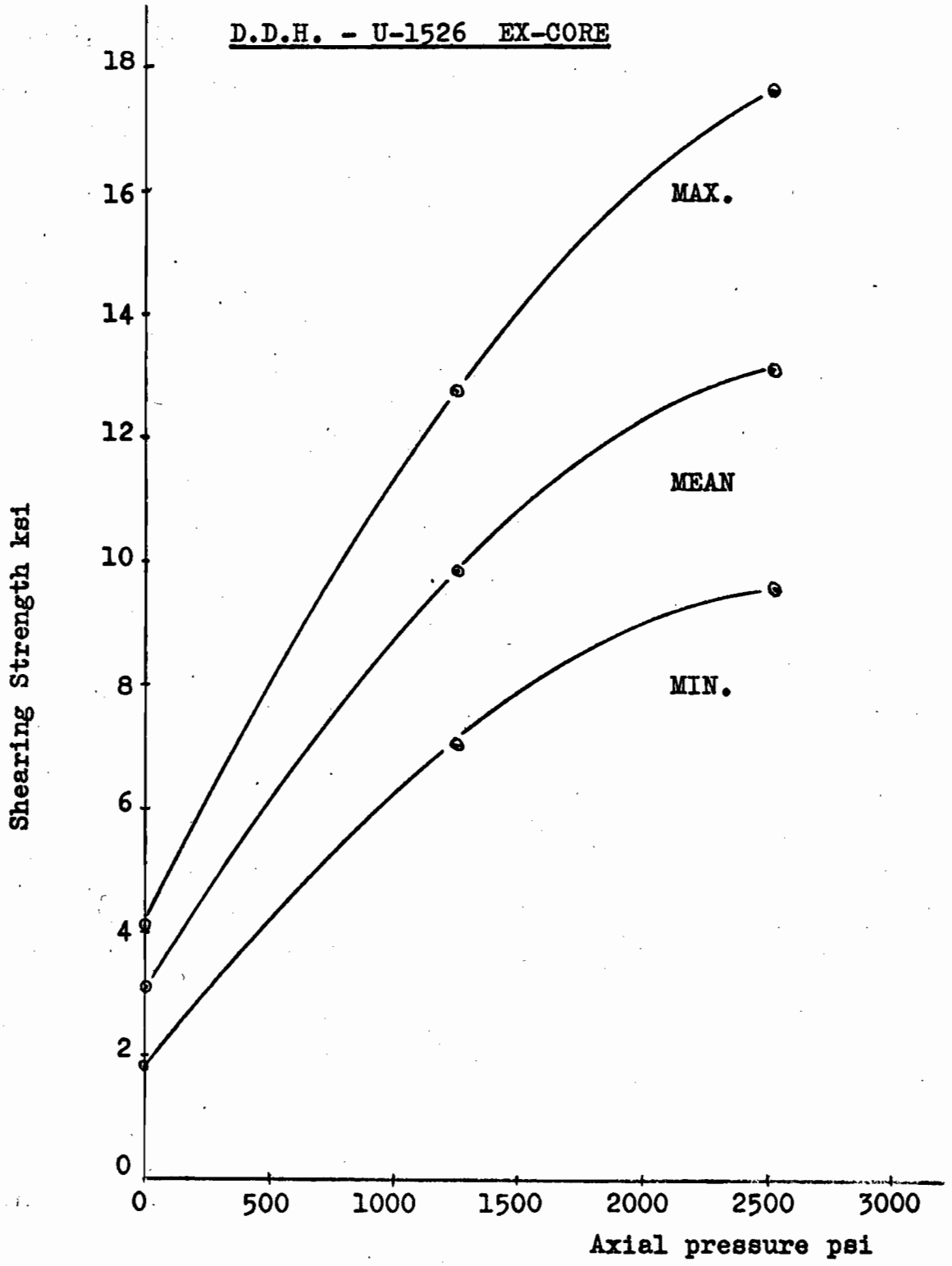

Figure 6-4: Relationship Between Axial Pressure and Shearing Strength

Ref. Table 6-1

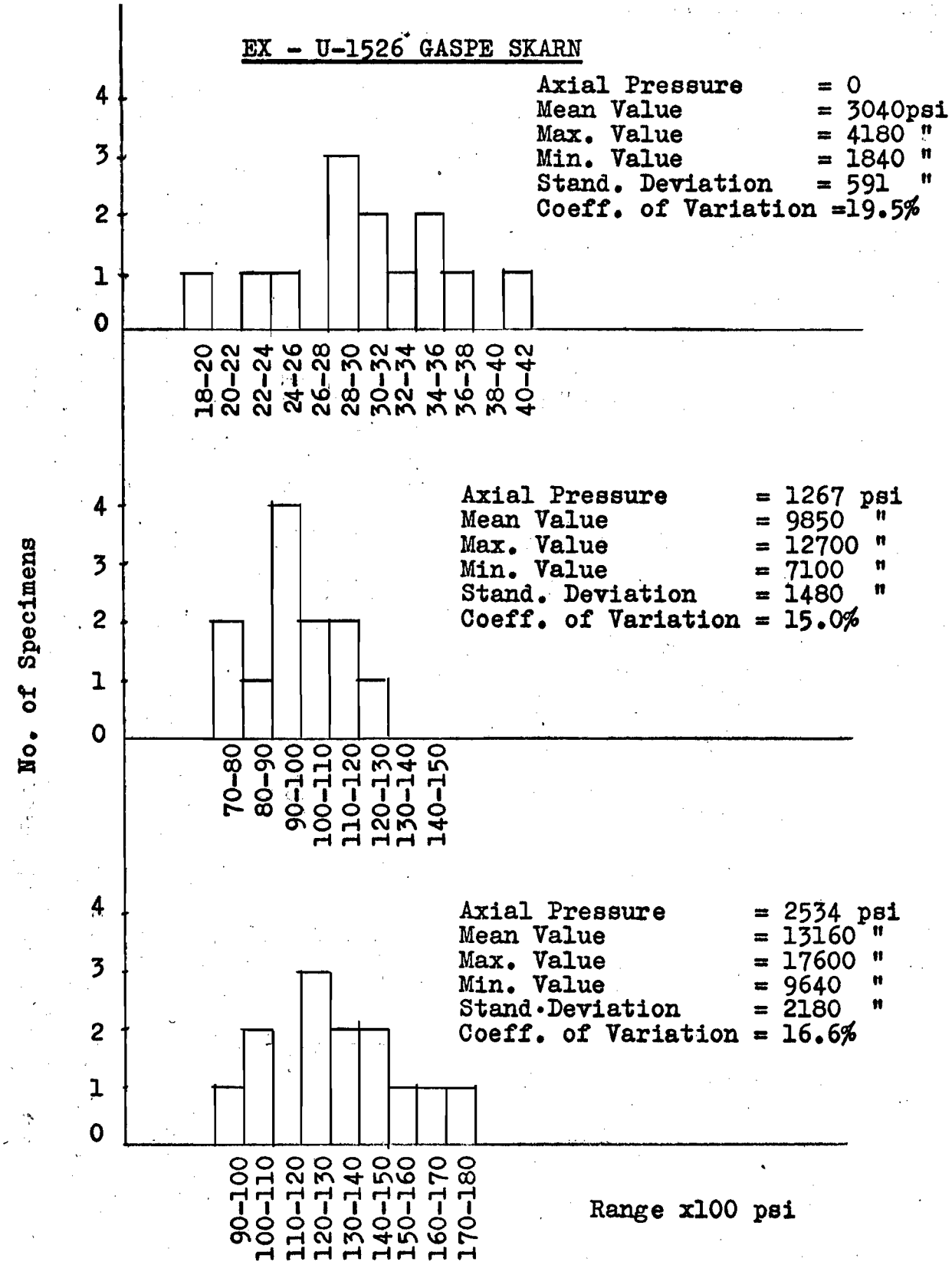

Figure 6-5: Distribution Diagram for Shearing Strength

individually.

For biaxial shearing tests, shearing fracture planes parallel to the direction of shearing stress were obtained in all specimens. These planes show fine powders resulting from the grinding effect associated with shear (Figure 6-6). This effect was most pronounced with biaxial loading. A few specimens failed on more than the two planes of double shear. This may indicate an initial bending failure prior to shear failure.

VII. DISCUSSION OF TESTING RESULTS

(1) Compressive Tests

(1-1) Effect of L/D ratio on compressive strength

Since the rocks are not perfectly isotropic, elastic and homogeneous, variations in test value are to be expected. Size effects and experimental techniques add to this variation.

Early work[15] has shown that the uniaxial compressive strength increases with increasing L/D ratio. Others[16],[17],[18] have established a decrease in compressive strength with increasing L/D ratio for rocks and concrete and this is confirmed for Gaspe skarn. Figure 4-9 shows the relationship between uniaxial compressive strength and L/D ratio.

According to Griffith's theory, infinitesmal cracks with a random distribution exist in all solid materials. If a solid specimen is subjected to a sufficient load, some of these cracks will become self-propagating and spread throughout the specimen, resulting in failure at loads which will be below the forces of molecular bonding.

It is assumed that a specimen (A), (L/D=1) contains N number of cracks of random distribution as to size and direction. If the diameter of the specimen is

kept constant and the length is doubled (i.e. 2L), then the number of cracks will be increased. The possibility of larger cracks occurring in directions favourable to shear will be increased also. Thus, increasing the volume of the specimen should result in a decreasing unit strength in tension or compression.

Skinner[17] has introduced the "Weakest Link Concept" to explain the size effect. Consistent with Griffith, he suggested that strength is determined by the weakest link and the larger specimen will contain more and perhaps larger defects.

(1-2) Effect of cross-section on uniaxial compressive strength

Two types of cores (EX-core, 7/8 in. diameter; NX-core, 2-1/8 in. diameter) were tested in compression to determine the compressive strength. Specimens with an L/D ratio of 2.5 were taken for comparison between EX-core and NX-core. Table 7-1 and Figure 7-1 show that increasing the cross-section of specimens results in a decrease in uniaxial compressive strength. This relationship agrees with Skinner's work[17] on anhydrite and Tucker's work[18] on concrete, but some[15],[19],[20] do not confirm this.

Applying Griffith's theory to this relationship, Skinner's explanation is that the decrease in strength with increase of the area of cross-section is the result of increasing the probability that a randomly oriented

Table 7-1: Comparison of Compressive Strength on EX-and NX - Core

No. of Specimen	Core Size	Specimen Diameter in.	Specimen Area in.sq.	Compressive Strength psi	Standard Deviation psi	Coeff. of Variation %
21	EX	0.896	0.631	28.900	6.850	23.7
2	NX	2.112	3.510	23.800	400	1.20

* —— Table 1A-6

** —— Table 1B-22, 1B-23.

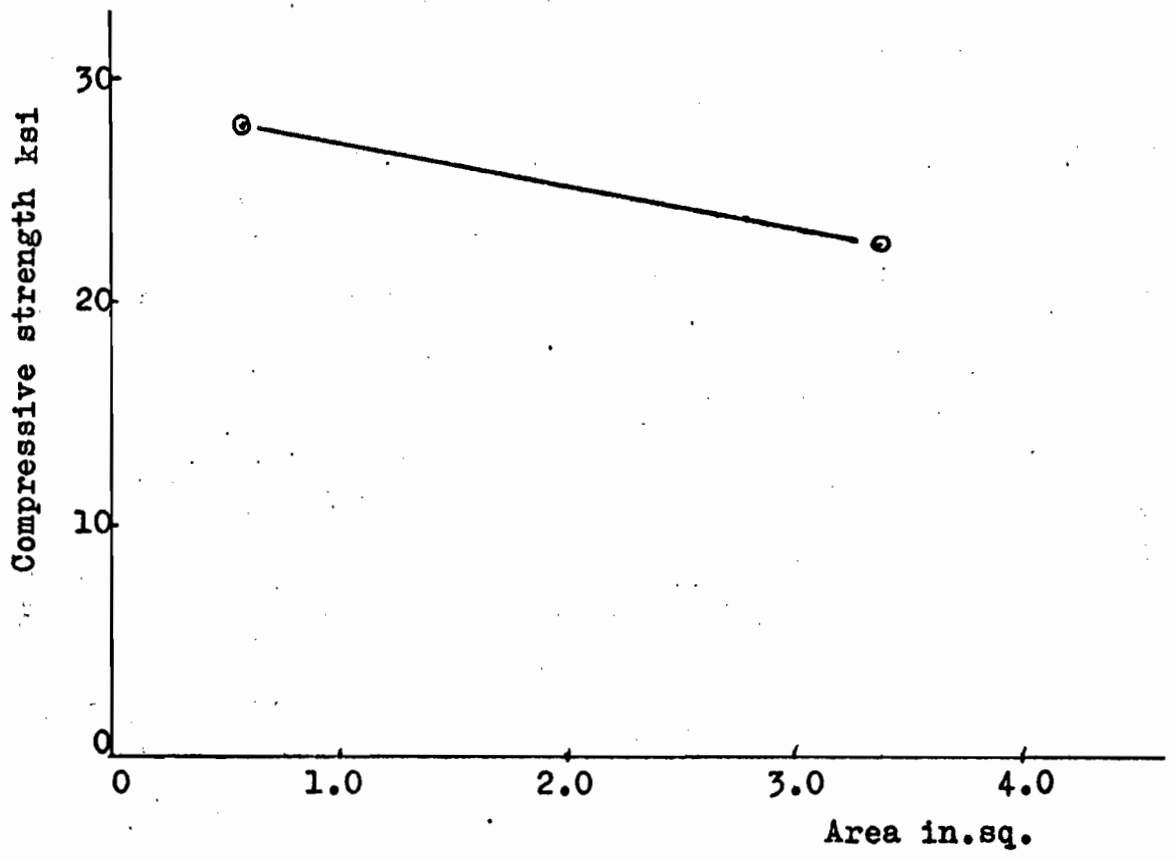

Figure 7-1: Relationship Between Uniaxial Compressive Strength and the Area of Cross-section

crack system will contribute more to failure conditions in the larger specimen than in the smaller one.

(1-3) Effect of end lubrication on uniaxial compressive strength

Specimen No. AB-6 (2-1/8 in. diameter) was tested for the purpose of examining the lateral strain distribution with and without lubricated ends. A very interesting point was confirmed by testing this specimen. With free ends, the load was applied to a maximum value of 45 kips (15,240 psi) without any evidence of failure. The specimen was tested again with lubricated (paraffin) ends and failed at a load of 42 kips (14,400 psi). This shows that the uniaxial compressive strength can be reduced by lubricating the specimen ends.

The reduction of strength by lubrication under uniaxial compression can be explained by the extrusion of the paraffin inducing tensile strain on the ends of the specimen.

(1-4) Elastic constants

The mean value of the modulus of elasticity and Poisson's ratio calculated from 21 specimens of EX-core are 8.39×10^6 psi and 0.148, respectively. The variation between the applied load and the modulus of elasticity, as well as Poisson's ratio, are plotted in the curves of Figure 4-15 and 4-17, respectively. Both of these curves show that increasing the applied load results in increasing both Young's modulus and Poisson's

ratio. These results are in agreement with Hardy's work.(4)

A larger deformation caused by the porosity of rock and the inaccuracy of the pressure gauge was observed in almost all the stress-strain curves at the lower pressure. This results in a low value for Young's modulus.

A comparison of elastic moduli was made by testing the NX-core specimen No. AB-1 which gave a result of 9.28×10^6 psi for Young's modulus and 0.256 for Poisson's ratio. The difference between these and the earlier tests, in addition to inhomogeneity, may be due, in part, to the pressure gauge which is not accurate in the lower range and also to size effect with the larger specimen.

Specimens with hysteresis loops show that the more the cycles, the greater the deformation and the lower the Young's modulus. For the same loop, the higher Young's modulus usually was obtained during the loading phase. Loop effects are not significant on Poisson's ratio. Specimen Nos. X-27, X-31, X-33 and X-36 illustrate these effects. The results are plotted in Figures 4-33, 4-34, 4-35 and 4-36, respectively.

Values of Young's modulus calculated from each individual longitudinal strain gauge and the values of Poisson's ratio from each lateral gauge for specimen No. AB-6, with and without lubricated ends, are given in

Table 7-2 and Table7-3, respectively. For the same specimen, under the same loading conditions, the end lubrication gives a lower mean value for Young's modulus and a higher value for Poisson's ratio, but variations were also obtained with individual strain gauges. This suggests that the determination of elastic constant for rocks needs a precisely defined procedure.

(1-5) Effect of time on strain

Time effect on deformation for this rock type has been shown in the stress-strain curves of Figures 4-37 and 4-38 for specimen No. X-20 and No. X-37, respectively. Both of these curves indicate that the time effect becomes more and more important as the stress is increased. For specimen No. X-37, no time effect was obtained at 14,280 psi but 90 micro in/in. of strain was obtained at 28,530 psi on the longitudinal gauge for a 10 minute time interval. Figures 7-2 and 7-3 give the detailed data of time effect on longitudinal and lateral strain gauges for this specimen.

Axial loading tests on solenhofen limestone, under hydrostatic confining pressure of 10,000 atmospheres, by Griggs,[6] has also shown marked time strains.

(1-6) Lateral deformation

Gramberg and Seldenrath[24] tests on limestone and sandstone have shown that the lateral strain distribution in a stressed cylindrical specimen was affected by the

TABLE 7-2*

Elastic Moduli (Free Ends) Specimen No. AB-6

Load		POISSON'S RATIO													YOUNG'S MODULUS psi x 10^6		
		Lateral Strain Gauges										Average of Lateral Strain Gauges			Longitudinal Strain Gauges		Average of Long. Gauges
kips	Stress psi	#1	#2	#3	#4	#5	#6	#7	#8	#9	#10	1 to 5	6 to 10	1 to 10	#11	#12	11.12
0	0	-	-	-	-	-	-	-	-	-	-	-	-	-	-	-	-
10	3440	0.200	0.200	0.180	0.240	0.160	0.320	0.240	0.380	0.300	0.360	0.196	0.320	0.260	14.3	13.4	13.7
20	6880	0.155	0.155	0.136	0.194	0.194	0.330	0.311	0.359	0.311	0.350	0.171	0.332	0.250	14.0	12.7	13.4
30	10320	0.163	0.156	0.143	0.196	0.221	0.338	0.351	0.357	0.338	0.344	0.175	0.345	0.261	15.0	12.2	13.5
40	13760	0.164	0.164	0.164	0.194	0.227	0.339	0.358	0.362	0.339	0.352	0.181	0.348	0.265	15.7	11.6	13.5
Mean Value		0.171	0.168	0.156	0.206	0.201	0.332	0.315	0.364	0.322	0.351	0.184	0.335	0.259	14.7	12.4	13.5

* Ref. Table 1B-27 - Appendix

TABLE 7-3*

Elastic Moduli (Lubricated Ends) Specimen No. AB-6

Load		POISSON'S RATIO													YOUNG'S MODULUS psi x 10^6		
		Lateral Strain Gauges										Average of Lateral Strain Gauges			Longitudinal Strain Gauges		Average of Long. Gauges
kips	Stress psi	#1	#2	#3	#4	#5	#6	#7	#8	#9	#10	1 to 5	6 to 10	1 to 10	#11	#12	11.12
0	0	-	-	-	-	-	-	-	-	-	-	-	-	-	-	-	-
10	3440	0.230	0.327	0.250	0.307	0.307	0.346	0.385	0.327	0.365	0.346	0.277	0.354	0.315	11.5	15.6	13.2
20	6880	0.296	0.295	0.238	0.304	0.334	0.296	0.314	0.257	0.334	0.295	0.282	0.278	0.284	10.8	14.0	13.0
30	10320	0.280	0.263	0.218	0.268	0.302	0.268	0.275	0.212	0.275	0.268	0.260	0.268	0.267	10.3	13.3	11.6
40	13760	0.296	0.255	0.231	0.282	0.307	0.267	0.263	0.208	0.259	0.271	0.274	0.255	0.264	9.8	12.0	10.8
Mean Value		0.275	0.285	0.234	0.291	0.313	0.295	0.309	0.260	0.308	0.295	0.275	0.289	0.288	10.6	13.7	12.2

* Ref. Table 1B-28 - Appendix

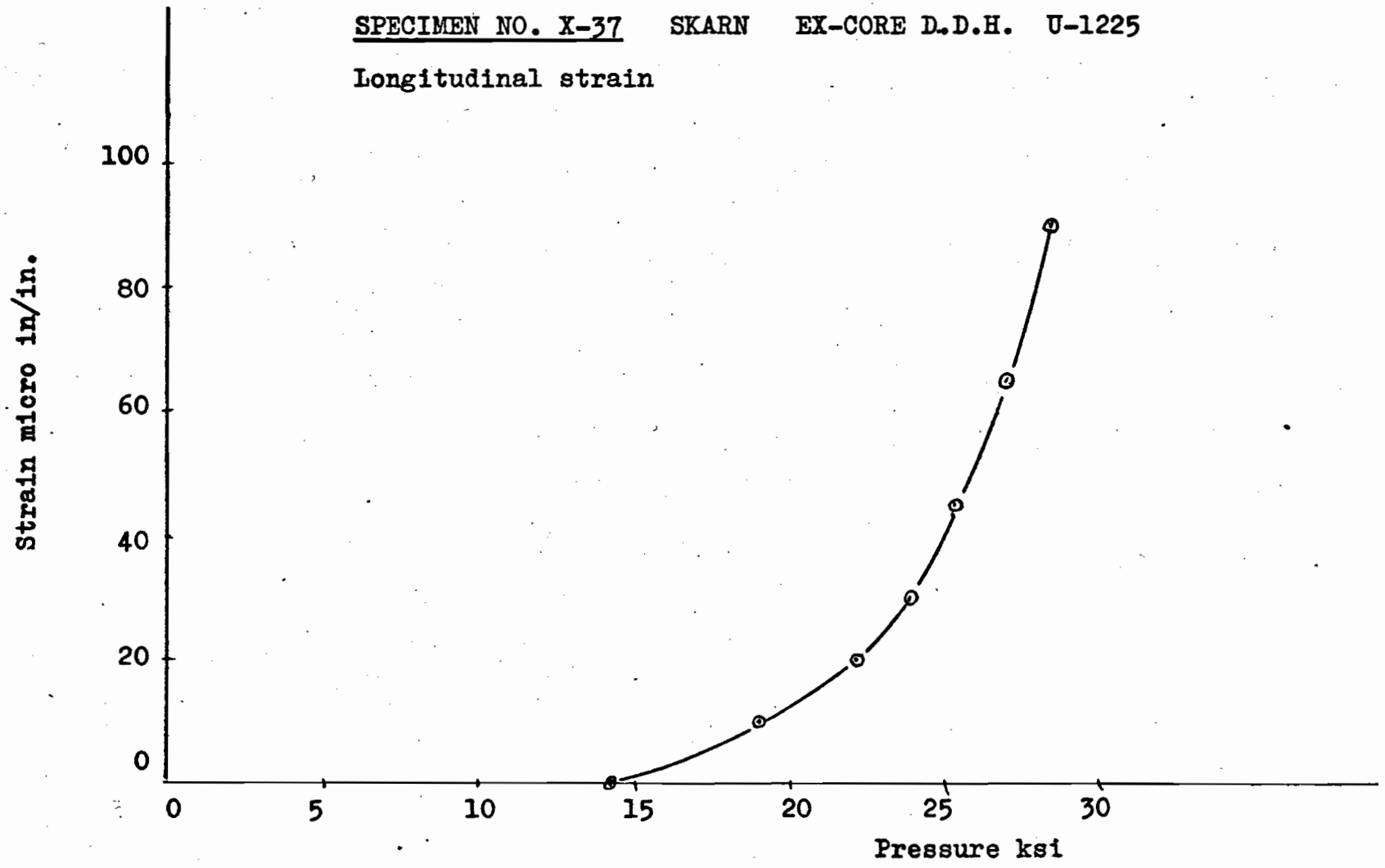

Figure 7-2: Time-strain for 10 Minute Intervals at Different Loading Levels

Ref. Table 1B-21

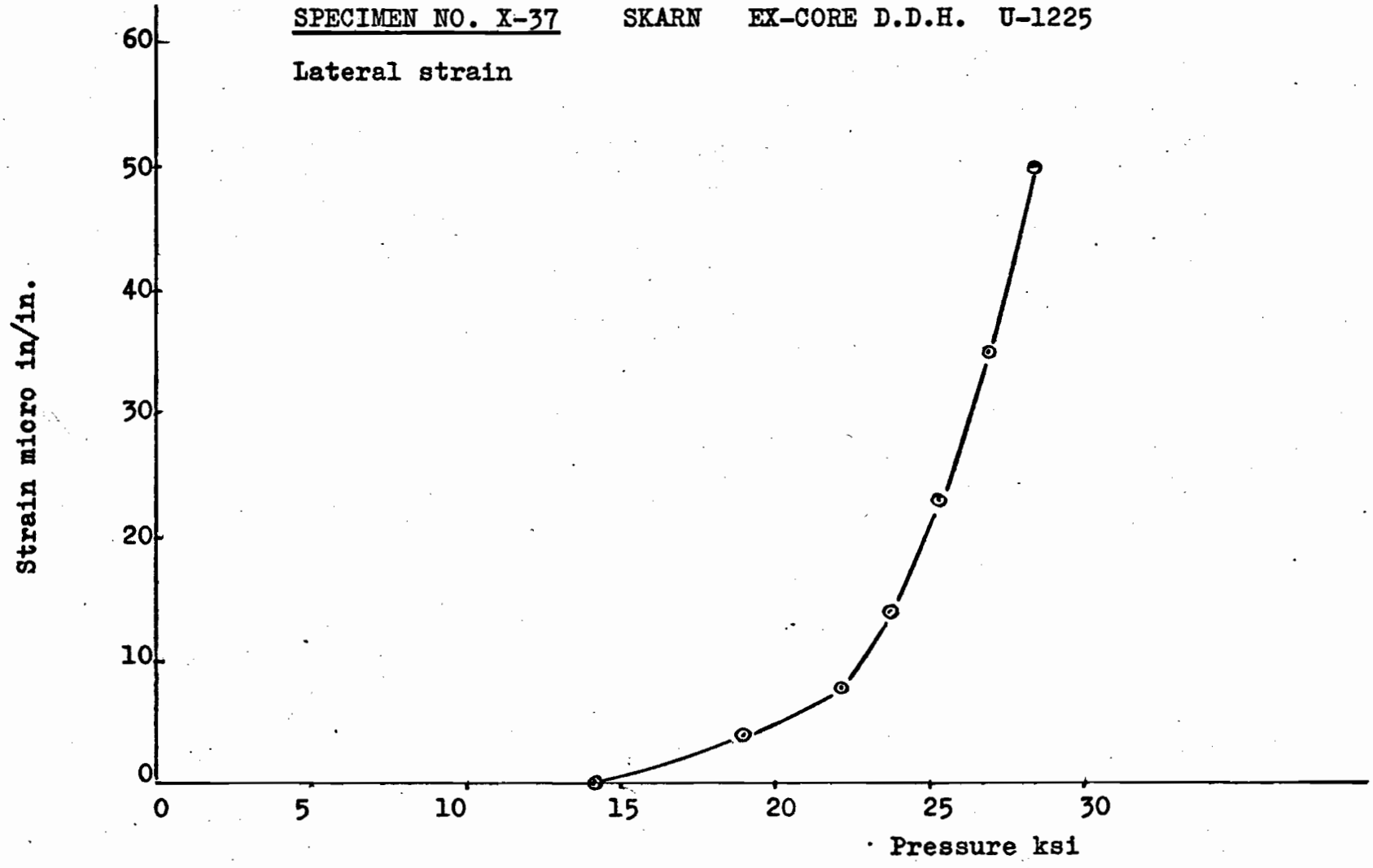

Figure 7-3: Time-strain for 10 Minute Intervals at Different Loading Levels

Ref. Table 1B-21

end conditions. Testing results on skarn, under axial load, also showed the following effects:

NX-core with L/D ratio of 2.5 - the lateral strain distributions for free ends and lubricated ends are shown in Figures 4-40 and 4-42, respectively. For free end specimens the maximum deformations were obtained in strain gauges No. 2 and No. 4 at one quarter and three quarters of the height of the specimen. Strain gauges located in the middle, No. 3 and near the ends, No. 1 and No. 5 give less deformation. The constriction near the ends may be due to the friction between the interface of compression. The larger deformation occurred near the apex of cones developing shear fracture.

For lubricated ends, lateral strain gauges, No. 1 and No. 5, at the top and bottom of the specimen respectively, show more deformation than others and the least deformation was obtained in the middle of the specimen. Tests on other specimens, No. AB-5 and No. AB-6 also show the above characteristics.

The expansion near the ends of specimens can be explained by the extrusion effect of the paraffin between specimen and platen. Tensile failure, no doubt, follows from this effect.

NX-core with different L/D ratios - a comparison was made between L/D ratios greater than 2.5 and also less than 2.0 with and without lubrication. Testing results are plotted in Figures 4-45 and 4-51, respectively. For

free ends and L/D ratio greater than 2.5, the lateral strain distribution is approximately the same as for the 2.5 L/D ratio. For L/D less than 2.0 (Figures 4-49, 4-51), larger deformation was obtained in the middle than at the ends. This suggests that the extension at middle for L/D ratio less than 2.0 is part of the mechanics of cone development referred to earlier.

For lubricated ends, all specimens show a greater extension at the ends than elsewhere over the specimen's height. This agrees with the extrusion principle suggested above.

EX-core with and without lubricated ends - to check the above and also Yu's results[32] specimen SPE-10 (L/D=3.0), Sigma (C) porphyry was tested with 10 strain gauges, five on each side, for both free and lubricated ends. The average value of two corresponding lateral strain gauges for these two cases is shown in Figure 4-52. This figure indicates that, at the same load, lubricated ends give greater deformation for all strain gauges than free ends. Tests on NX-core specimens SPN-2, SPN-5 and skarn specimen No. AB-6 also show the above results (Figures 4-49, 4-50, 4-51 and Figures 4-47, 4-48). This suggests that the reduction on uniaxial compressive strength, as discussed previously, with lubricated ends is due to extrusion of the paraffin, causing tensile failure.

SIGMA PORPHYRY SPECIMEN SPE - 10 EX-CORE

D = 0.876 in. L = 2.71 in. A = 0.603 in. sq. L/D = 3.1

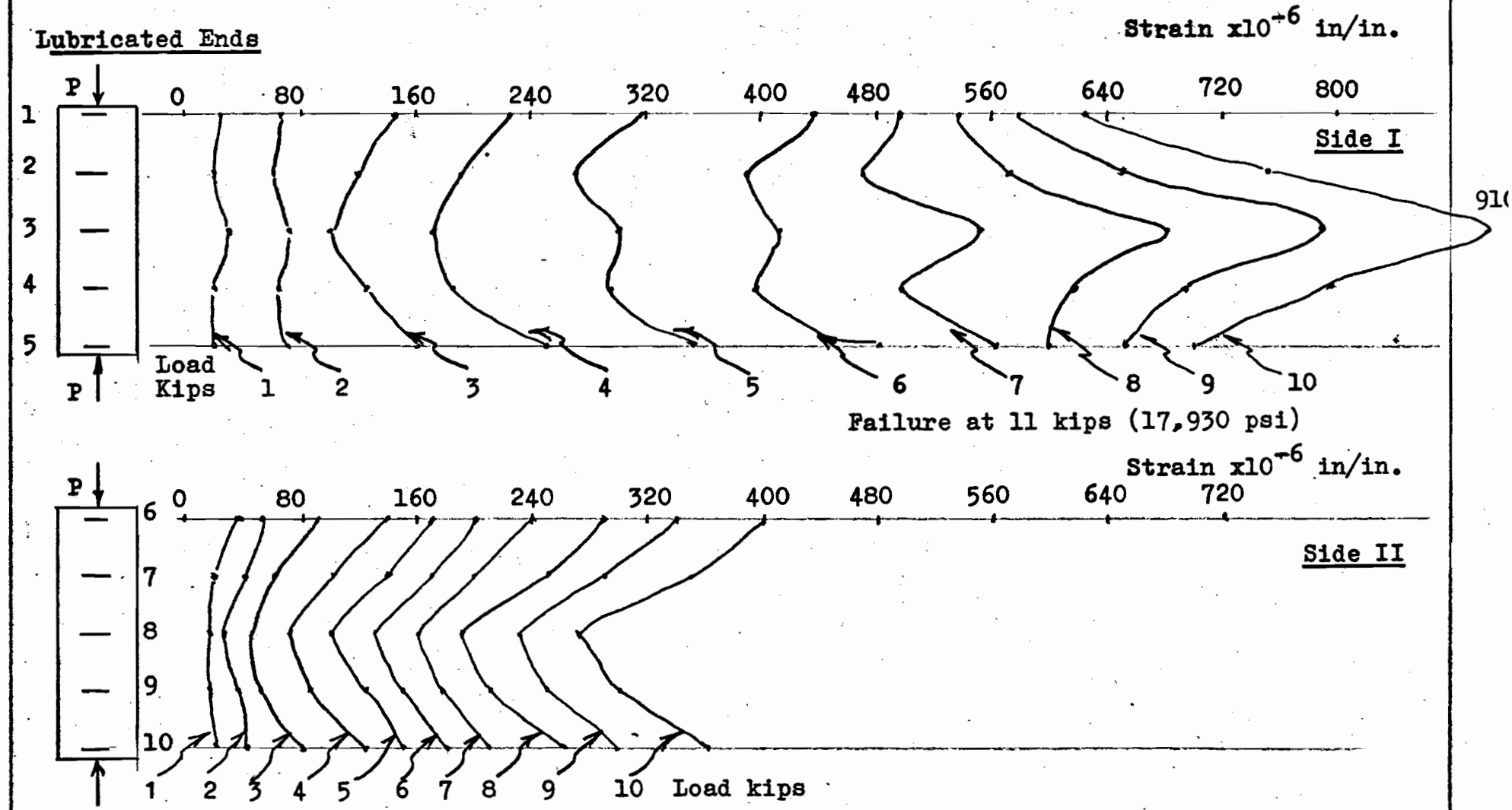

Figure 7-4: Lateral Strain Distribution of Sigma Porphyry Under Uniaxial Compression

Ref. Table 1B-34

SPECIMEN NO. AB-6 NX-CORE U-1474

D = 1.940 in. L = 3.910 in. A = 2.940 in. sq. L/D = 2.10

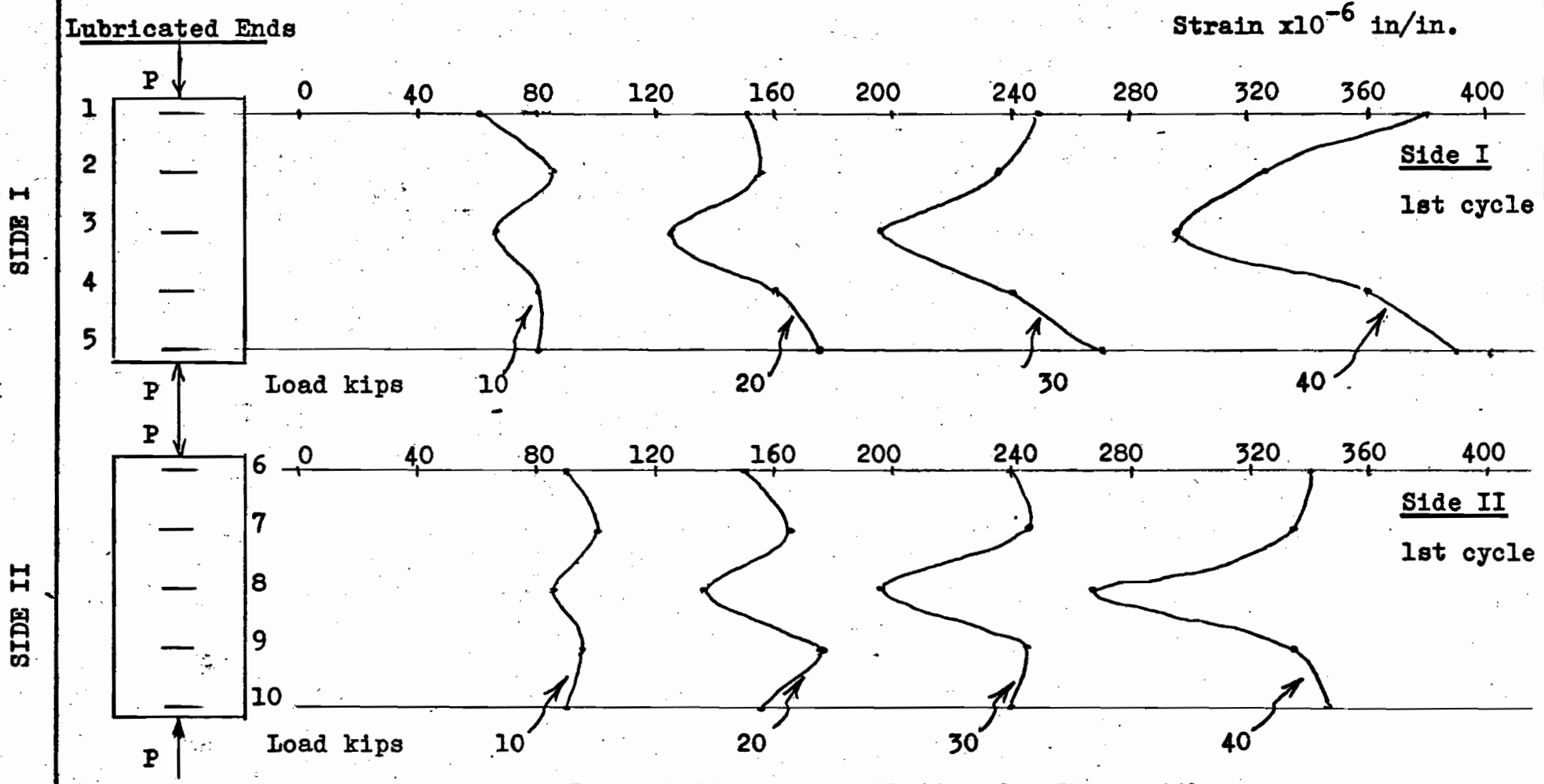

Figure 7-5: Lateral Strain Distribution for Skarn with Lubricated Ends Under Uniaxial Compression

Ref. Table 1B-28

EX-core and NX core with lubricated ends - Figure 7-4 shows the lateral strain distribution for all lateral strain gauges with lubricated ends on EX-core (L/D=3.0), Sigma porphyry. These curves show a great difference in lateral strains between the two sides (strain gauges on Side I; 1, 2, 3, 4, 5, and Side II; 6, 7, 8, 9, 10) at each loading level and increasing the load results in more deformation at mid-height on Side I of the specimen. Specimen No. AB-6, NX-core, (L/D=2.0), skarn, shows the reverse effect (Figure 7-5) for lubricated ends. Lack of parallelism of the ends is an explanation, but the bending effect on EX-core with a larger L/D ratio than the NX-core may also be a factor.

(1-7) Effect of confining pressure on compressive strength

Figure 4-54 shows the testing results on this rock type. Increasing the confining pressure results in an increase of compressive strength. This has also been found by several earlier workers for rocks[6],[21],[22] and coal.[23]

(1-8) Mohr's circle and internal friction angle

The testing results for uniaxial and triaxial compression with an L/D ratio of 2.0 are plotted as Mohr's stress circles in Figure 7-6. Uniaxial tensile strength obtained from pull tests is also plotted. The failure envelope fitted to these results has been drawn perpendicular to the normal stress axis on the tensile side and tangent to the various radii drawn for each

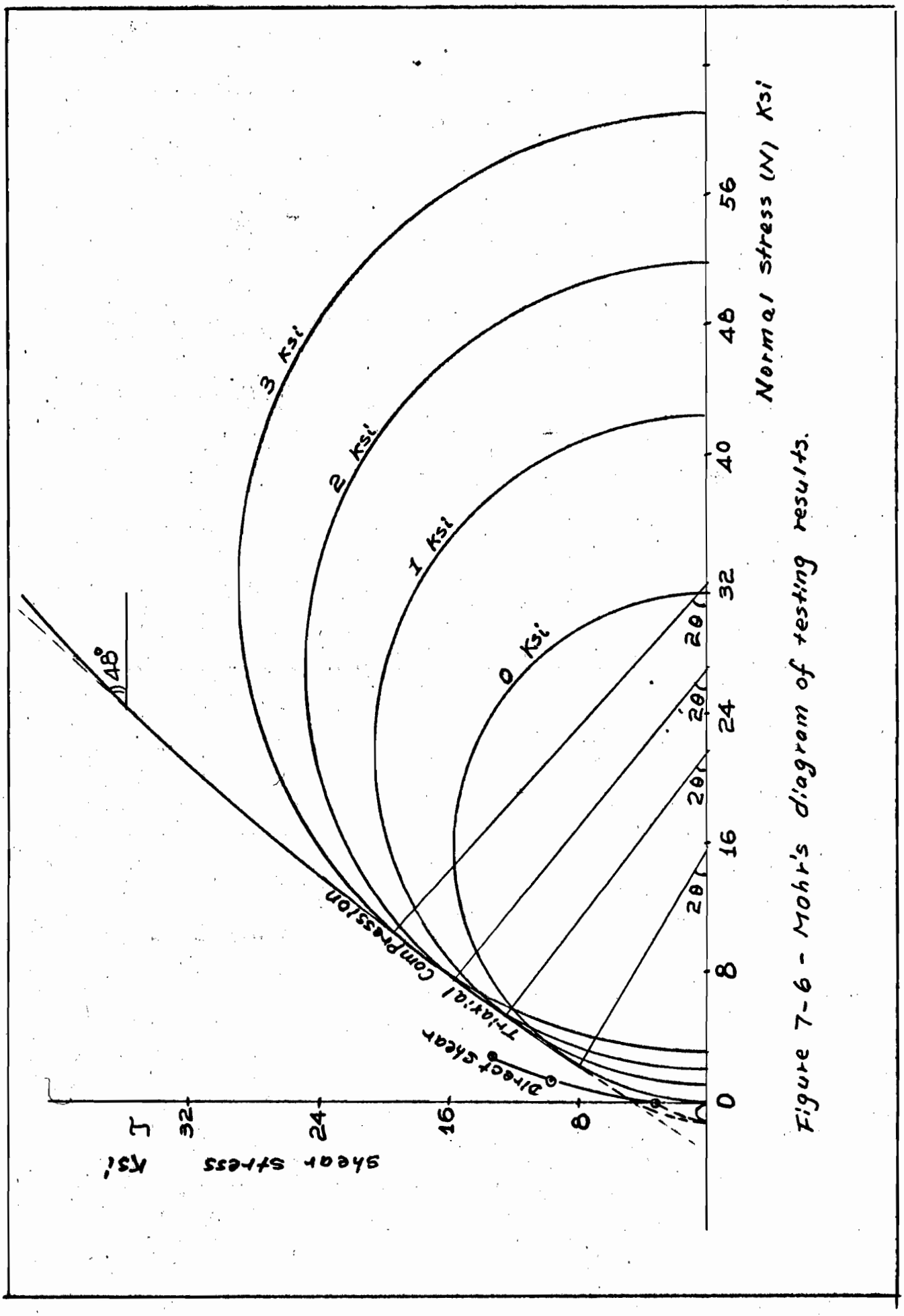

Figure 7-6 - Mohr's diagram of testing results.

circle at an angle of 2θ, where θ is the measured angle of fracture relative to the axis of specimen.

The measured angle of tensile fracture is 12 degrees less than the theoretical fracture angle of 90 degrees to the direction of tensile stress. This may be due to the effect of grips and the inhomogeneity of the specimen. The measured angles of fracture in compression are slightly higher than the angles expected on Mohr's circles. Table 4-3 gives the comparison of theoretical and measured fracture angles. Both of these angles increase with increasing confining pressure, suggesting a curved envelope.

The relationship between the angle of fracture and the angle of internal friction is governed by Mohr's hypothesis and expressed as the following equation:

$$\theta = 45^{\circ} - \frac{\phi}{2} ,$$

where θ = Fracture angle relative to the axis of specimen, degrees.

ϕ = Angle of internal friction, degrees.

The internal friction angle calculated from the average measured fracture angle is 44 degrees. This is lower than the angles shown at the points of failure, but a reasonable approximation with a curved envelope.

A very high value for the angle of internal friction, 77 degrees, was obtained from direct shearing tests. This is attributed to experimental error probably due to the introduction of bending stresses.

(2) Tensile Tests

(2-1) Tensile strength and breaking angle

Pull testing results for clean breaks and doubtful breaks are given in Table 5-1. This table indicates a higher tensile strength and a lower breaking angle for doubtful breaks than for clean breaks.

The lower tensile strength given by clean break specimens can only be explained by the inhomogeneity of the specimens. Unfortunately, there is not sufficient data to give a concentration factor for the effect of the grips. However, the average value for all specimens takes some note of this effect.

The coefficients of variation for clean breaks and doubtful breaks are respectively 8.5% lower and 7.2% higher than for the average value. This probably reflects the effect of the grips, but, in any case, the actual tensile strength for doubtful breaks should be higher than that obtained in the tests. Thus, considering this variation in value, the average value for all tests is the best result for this limited data.

A higher breaking angle was obtained for clean breaks than doubtful breaks.

(2-2) Splitting strength (Brazilian test)

The relationship between t/D ratio and splitting strength for this rock type is given in Table 5-2 and

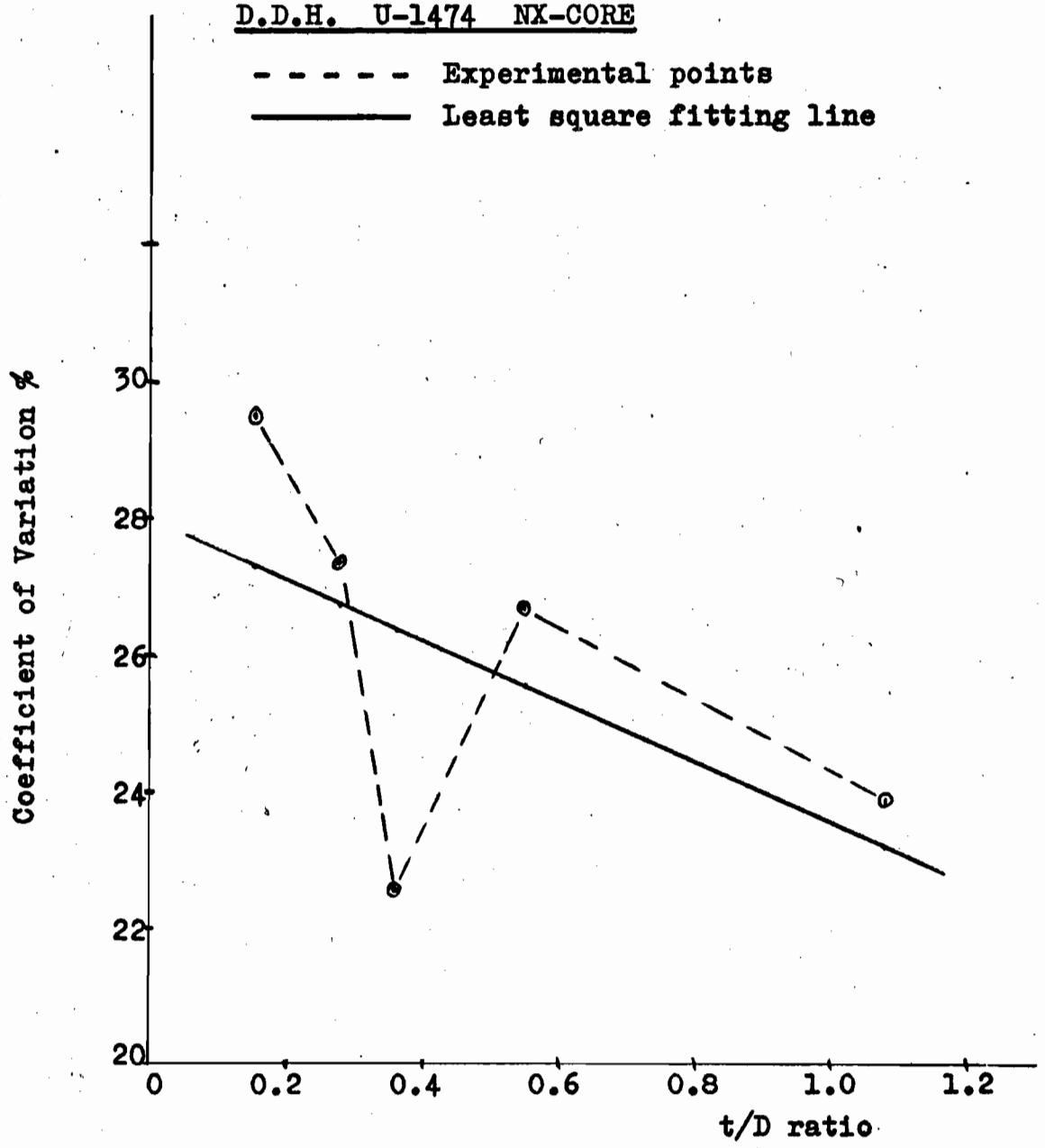

Figure 7-7: Coefficient of Variation as a Function of t/D Ratio

$y = 27.9 - 4.4\ t/D$

Ref. Table 5-2

is shown in Figure 5-11. The mean strength decreases with the increasing of t/D ratio. This result agrees with Evans[13] and Berenbaum's[25] work on coal, but disagrees with Brodie's[14] work on plaster.

The increasing of the t/D ratio causes a decrease of the coefficient of variation. This is shown in Figure 7-7, coefficient of variation (%)=27.9 - 4.4 t/D.

(2-3) Comparison of failure type between uniaxial compression and Brazilian tests

Brazilian test induces a uniform horizontal tensile stress over much of the specimen diameter and also a variable vertical compressive stress acting along the length of the loaded diameter as shown in Figure 7-8. The latter stress rises to an infinite value at the points of contact resulting in large shearing stresses. Therefore, initial failure in shear due to this high compressive stress near the edges is possible. However, Berenbaum and Brodie[14],[25] suggested that the initial failure is due to tension starting at the center of the specimen. Yu[32] actually induced incipient tensile failure of this nature.

Cylindrical specimen of brittle material failing in shear fracture with cones, under uniaxial compression, has been established by Nadai[26] and proved by several investigators[5],[15],[20] and also shown in Figure 4-11 of this thesis.

13 B

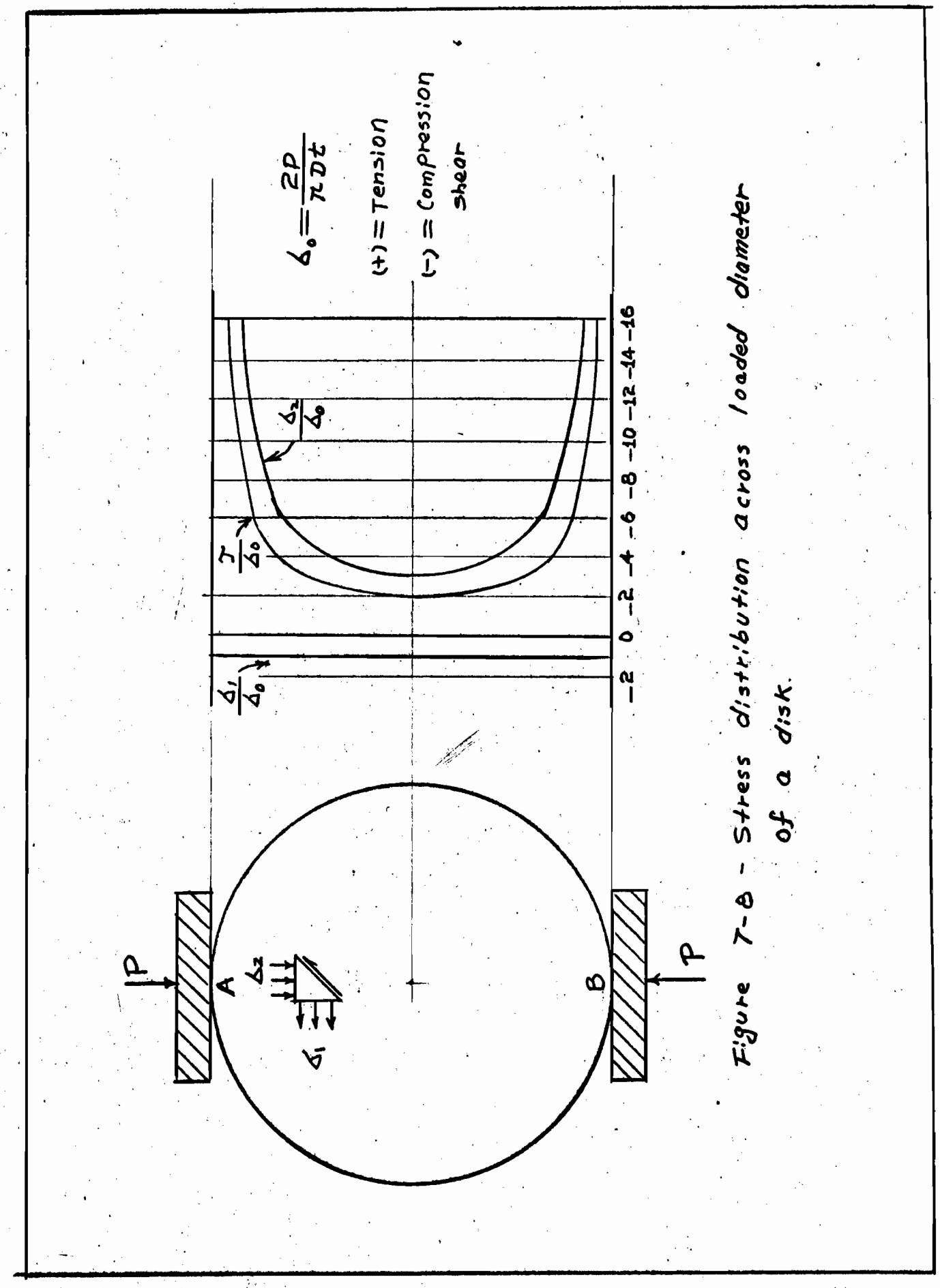

Figure 7-8 - Stress distribution across loaded diameter of a disk.

The mechanisms shown in Figures 4-11 and 5-13 suggest a similarity between uniaxial compression and Brazilian tests. Figure 7-9(a) shows that the specimen under uniaxial load fails in four pieces initially by shear with cones. It is assumed that the tensile stresses due to the pushing of cones (A) are set up along the vertical center line of the specimen to cause tensile failure in the pieces (B). Therefore, shear failure on cones could come first and tensile failure on (B) second. The forming of cones due to the friction between the specimen-platen contacts under uniaxial load also takes place prior to forming of pieces (B).

It is suggested that the above mechanism may be applied to the case of Figure 7-9(b) in Brazilian test. If so, the specimen in case (b) might also fail in two pieces (B) by tension due to the pushing of the initial small failure cones (A) which have a small contact area between the specimen-platen contacts.

Specimens tested for lateral deformation distribution without lubricated ends show that the maximum lateral strain distribution is obtained at the apex of the cones. This means that the failure should start from the apex of the cone.

Unfortunately, this test data is not sufficient to establish the relationship between shear and tension

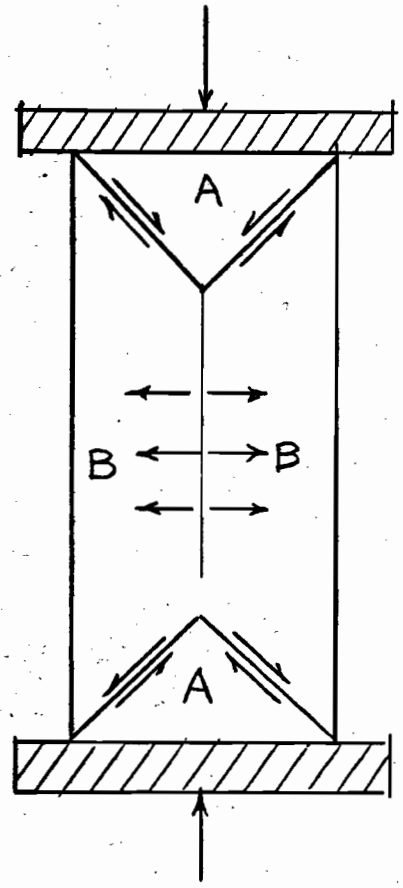

(a). Ref. figure 4-11

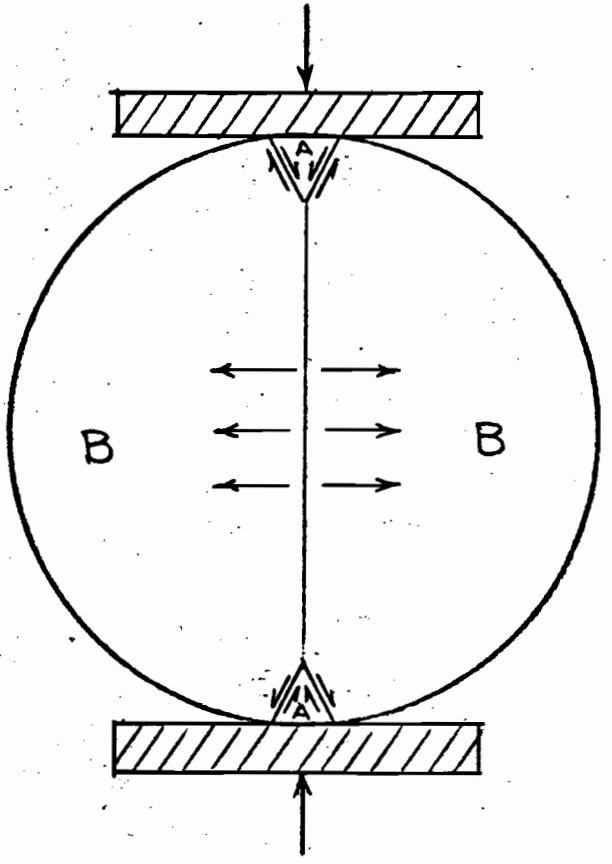

(b) Ref. figure 5-13

Figure 7-9 - Comparison of failure type between Uniaxial Compression and Brazilian Tests

in the Brazilian test. The concensus, with much support, favours this test for a tensile value. This value is usually related to the pull and bending values as indicated later.

(2-4) Flexural strength (Bending test)

The mean flexural strength is decreased with increasing span on bending tests. This relationship is given in Table 5-3 and shown in Figure 5-14.

Table 5-3 also shows that the coefficient of variation increases with increasing length of span (Figure 7-10).

Griffith's theory to explain the size effect on flexural strength and the coefficient of variation is suggested.

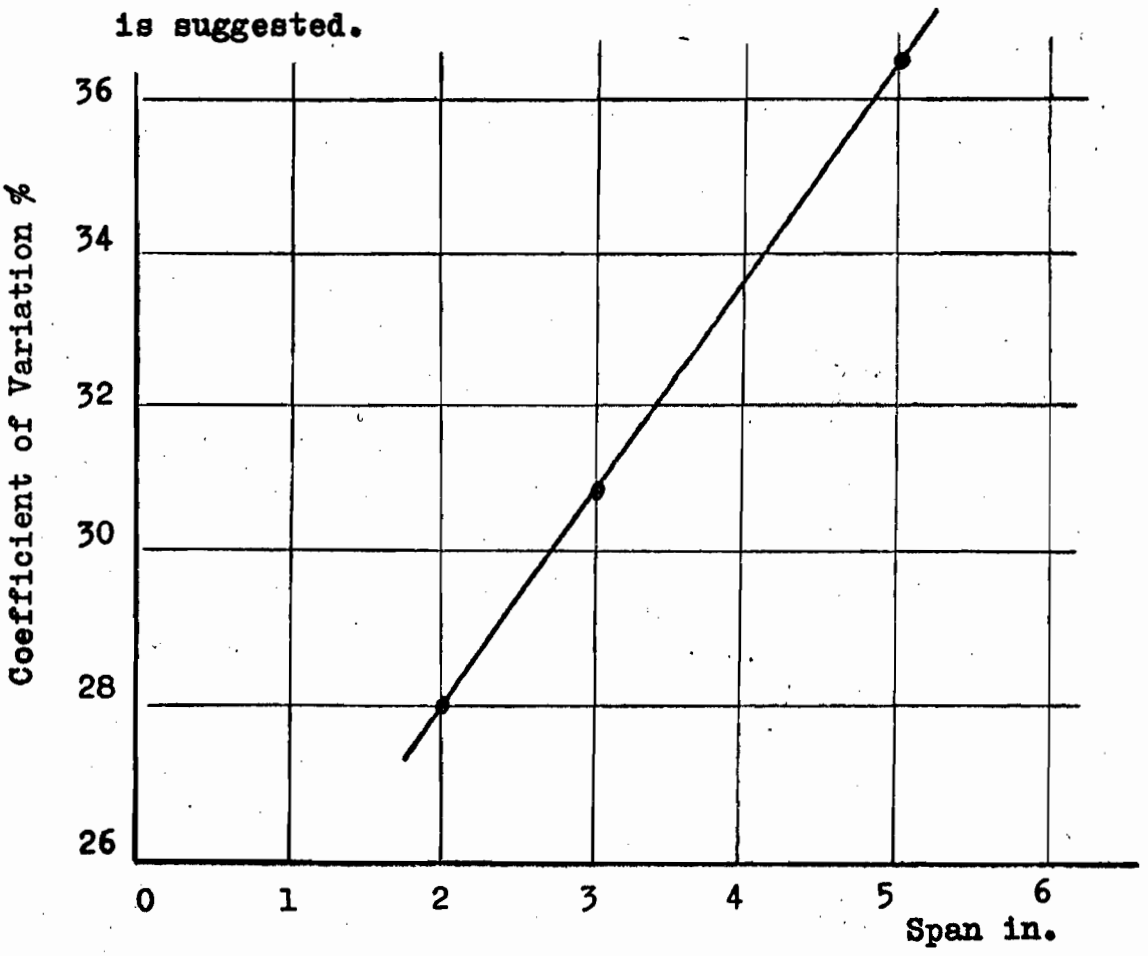

Figure 7-10: Coefficient of Variation and the Lengthsof Span Relationship Re. Table 5-3

(2-5) Reconciliation of tensile results

Wright[27] has suggested that the relationship between tensile strength (T), splitting strength (S_c) and flexural strength (R) for concrete as measured by extension test is, as follows:

$$R \doteqdot 2T, \qquad S_c \doteqdot 1.5T$$

$$T \doteqdot 0.675S_c \doteqdot 0.5R$$

The actual testing results, as shown in Table 7-5, gives a tensile strength of 1,165 psi in pull test for this rock type and the reconciliation is, as follows:

$$T \doteqdot 0.535S_c \doteqdot 0.352R$$

The relationship, in spite of earlier criticism, suggests that the very simple Brazilian test may have a place in estimating tensile strength for rocks.

TABLE 7-5

Reconciliation of Tensile Results

	Tensile Strength T psi	Splitting Strength S_c psi	Flexural Strength R psi
No. of Specimen	39	117	93
Mean Value	1165	2180	3300
Coefficient of Variation	26.9	27.8	31.4
Strength Ratio Relating to Pull Test	1	1.87	2.84

Ref. Table 5-1, 5-2, 5-3.

(3) Shearing Tests

According to Coulomb's equation[28] $J = c + N\tan\phi$, the shearing strength (J) is increased by increasing the normal pressure (N) for cohesive soil and rocks. Early work[29],[30],[31] has shown a diminishing rate of increase in strength with increasing axial pressure. This result is also confirmed for this rock type (skarn), as shown in Figure 6-4.

The cohesion of this rock, as calculated from direct shear test at zero psi axial pressure and as estimated from Mohr's envelope is 3,040 and 4,300 psi, respectively (Figure 7-6). The lower value from direct shear test is mainly due to prior failure in bending which caused failure in more than two planes,

VIII. CONCLUSION

Generally throughout these tests, it was demonstrated that small variations in preparation and testing techniques can result in large variations in results. Within this context the following results and conclusions apply for Gaspe skarn:

(8-1) Strength characteristics

(a) The uniaxial compressive strength with free ends varies from 36.8 to 27.9 ksi as the L/D ratio increases from 0.528 to 2.871 inches, the average value is 31.9 ksi. Ref. Table 4-1, Figure 4-9.

(b) The uniaxial compressive strength can be reduced by lubricating the specimen ends. Ref. specimen No. AB-6.

(c) Shear fracture predominates with free ends and tensile type failure with lubricated ends under uniaxial loading. Ref. Figures 4-11, 4-12.

(d) The triaxial compressive strength increases from 42.4 ksi with 1,000 psi confining pressure to 61.1 ksi with 3,000 psi confinement. Ref. Table 4-3, Figure 4-54.

(e) Grip effects on pull tests should be apparent in the distinction between clean and doubtful breaks. Contrary to expectation, the clean breaks at 1,110 psi are of a

lower value than doubtful breaks at 1,200 psi. Pending further tests, the average value of 1,165 psi is accepted. Ref. Table 5-1.

(f) The splitting strength obtained from the Brazilian test varies from 2,410 to 1,970 psi as the t/D ratio increases from 0.155 to 1.683 inches. The average value is 2,180 psi. Ref. Table 5-2, Figure 5-11.

(g) The flexural strength obtained from the bending test decreases from 3,510 to 3,070 psi with increasing span from 2 to 5 inches, The average value is 3,300 psi. Ref. Table 5-3, Figure 5-14.

(h) The reconciliation of tensile strength between pull, Brazilian and bending tests is, as follows:

$$T \doteqdot 0.535S_c \doteqdot 0.352R$$

where T = Tensile strength, psi.

S_c = Splitting strength, psi.

R = Flexural strength, psi.

(i) Direct shear strength increases from 3,040 to 13,160 psi as the axial pressure on the plane of fracture increases from 0 to 2,534 psi. Ref. Table 6-1, Figure 6-4.

(8-2) Deformation characteristics

(a) Young's modulus and Poisson's ratio each determined from 21 specimens are 8.39×10^6 psi and 0.148, respectively. Reg. Table 4-2. The detailed values for a single specimen are to be noted in Tables 7-2 and 7-3, where a reduction in Young's modulus and an increase in Poisson's ratio are

obtained with lubricated ends.

(b) The loading and unloading cycles on deformation test induce hysteresis loops, the more the loops, the more the deformation and the less the Young's modulus. Ref. Tables 1B-16, 1B-17 and 1B-18.

(c) Time effect on deformation is more significant at higher pressure than lower pressure. Ref. Figures 7-2, 7-3, Table 1B-21.

(d) Lateral strain distribution through a stressed specimen under uniaxial load permits the following observations:

(1) <u>For free ends with L/D ratio less than 2.0</u>
Maximum strain at the middle, minimum strain near the ends were obtained. Ref. Figures 4-49, 4-51.

(2) <u>For free ends with L/D ratio equal 2.5 to 3.0</u>
The greatest deformations were observed at the height of 1/4 and 3/4 on the specimen. Ref. Figures 4-40, 4-45 and 4-52.

(3) <u>For lubricated ends with L/D ratio from 1.9 to 2.7</u>
Maximum deformations near the ends and minimum deformation at the middle of the specimen were obtained in all specimens of NX-core. Ref. Figures 4-42, 4-45, 4-48 and 4-51.

(4) <u>For EX-core with an L/D ratio more than 3.0</u>
Eccentricity and/or bending effects usually occurred on loading the specimens. The lack of parallelism of the specimen ends, resulting in eccentric loading

(Figure 7-4), limits the value of the lateral strain distribution. The solution seems to be better end preparation and perhaps more tests to arrive at a mean value.

BIBLIOGRAPHY

1. Davies, O. L.
   Statistical Methods in Research and Production
   Oliver and Boyd, Ltd., London, 1954.

2. Ford, R. E.
   The Geology of Gaspe Copper Mine
   A Great Canadian Enterprise: Gaspe Copper Limited
   Transections of the Canadian Mining and Metallurgy
   Bulletin, Vol. LXII, 1959, pp. 217-253.

3. Ford, R. E.
   A Brief Summary of the Geology and Mining Procedure
   at Gaspe Copper Mines Limited, 1958.

4. Hardy, H. R., Jr.
   Standardized Procedures for the Determination of the
   Physical Properties of Mine Rock Under Short-Period
   Uniaxial Compression, 1959.

5. Kvapil, R. K.
   Concerning the Theory of Rock Destruction
   Inter. Strata Control Congress, Leipzig, Oct. 1958.

6. Griggs, D. K.
   Deformation of Rocks Under High Confining Pressure
   Journal of Geology, Vol. 44, 1936.

7. Adam, F. D. and Coker, E. G.
   Investigation into the Elastic Constant of Rocks
   Publication 46, Carnegie Institute of Washington
   1906.

8. Zisman, W. A.
   Young's Modulus and Poisson's Ratio with Reference to
   Geophysical Applications, Harvard University, 1933.

9. Windes, S. L.
   Physical Properties of Mine Rock, Part II, R. I. 4727
   Sept. 1950.

10. Obert, L., Windes, S. L. and Duvall, W. I.
    Standardized Tests for Determining the Physical
    Properties of Mine Rock
    USBM R. I. 3891, 1946.

11. Nilsson, S.
The Tensile Strength of Concrete determined by Splitting Tests on Cubes
AIME. RILEM No. 11, 1961.

12. Pomeroy, C. D.
The Tensile Strength of Coal
British Jour. Appl. Physics. Vol. 7, 1956.

13. Evans, I.
The Tensile Strength of Coal
Colliery Engineering, Oct. 1961.

14. Berenbaum, R. and Brodie, I.
The Measurement of Tensile Strength of Brittle Materal
British Jour. Appl. Physics. Vol. 10, 1959.

15. Tun, H.
Elastic and Strength Properties of Elliot Lake Quartzites
McGill Thesis, McGill University, 1961.

16. Brandtzaeg, A.
A Study of the Failure Concrete Under Combined Compressive Stress
Bull. 185, Engrg. Experimental Station, Illinois.

17. Skinner, W. J.
Experiments on the Compressive Strength of Anhydrite
The Engineer, Vol. 207, No. 5377, 1959.

18. Tucker, J.
Effect of Length on the Strength of Compressive Test Specimens
Proc. ASTM, Vol. 45, 1945.

19. Udd, J. E.
The Physical Properties of Elliot Lake Ore Bearing Conglomerate
McGill Thesis, McGill University, 1960.

20. Gill, D. E.
Uniaxial Compression as an Element in a Classification of Rocks
McGill Thesis, McGill University, 1963.

21. Price N. J.
A Study of Rock Properties in Conditions of Triaxial Stress
Proc. of a Conference on Non-Metallic Brittle Materials, 1958.

22. Hoffman, H.
Investigations into Carbonic Rocks Under Triaxial Pressure for the Purpose of Rock Stress Computation
Inter. Strata Control Congress, Leipzig, 1958.

23. Murrel, S. A. F.
The Strength of Coal Under Triaxial Compression
Proc. of a Conference on Non-Metallic Brittle Materials
London, 1958.

24. Gramberg, J. and Seldenrath, Th. R.
Stress-strain Relationship and Breakage of Rocks
Mechanical Properties of Non-Mettalic Brittle Materials
London, 1958.

25. Berenbaum R. and Brodie, I.
The Tensile Strength of Coal
Journal of the Institute of Fuel, Vol. 32, No. 222, 1959.

26. Nadai, A.
Theory of Flow and Fracture of Solids
McGraw Hill, 1950.

27. Wright, P. J. F.
Comments on an Indirect Tensile Test on Concrete Cylinders
Mag. Conc. Res. Vol. 8, No. 22, 1956.

28. Terzaghi, K.
Theoretical Soil Mechanics
John Wiley, 1962.

29. Davies, J. J. L.
Pillars - Applications and Limitations in Underground Mining.
McGill Thesis, McGill University, 1959.

30. Ortlepp, W. D.
An Experimental Investigation into Certain Aspects of Rock Failure.
McGill Thesis, McGill University, 1957.

31. Zahary, G.
A Study of Strength and Deformation Characteristics of a Red Lake Andesite
McGill Thesis, McGill University, 1962.

32. Yu, Y. S.
Physical Properties of a Sigma Porphyry
McGill Thesis, McGill University, 1964.

APPENDIX

APPENDIX

(1) Tables of Compressive Data

A. Uniaxial	1, 2, 3, 4, 5, 6, 7.
B. Deformation	1, 2, 3, to 33.
C. Triaxial	1, 2, 3.

(2) Tables of Tensile Data

A. Pull tests	1, 2, 3.
B. Brazilian tests	1, 2, 3, 4, 5.
C. Bending tests	1, 2, 3.

(3) Tables of Shearing Data

A. Axial pressure	=	0 psi.
B. Axial pressure	=	1267 psi.
C. Axial pressure	=	2534 psi.